Finite size effects and dynamics in one-dimensional integrable systems

Maria Colome-Tatche

Université Paris XI

THÈSE de DOCTORAT de l'UNIVERSITÉ PARIS XI

Spécialité : Physique

présentée par

Maria COLOMÉ TATCHÉ

pour obtenir le titre de

Docteur de l'université Paris XI

Sujet :

Effets de taille finie et dynamique dans les systèmes intégrables unidimensionnels

Soutenue le 17 décembre 2008 devant le jury composé de :

M. Georgy V. SHLYAPNIKOV	Directeur de thèse
M. Nigel COOPER	Rapporteur
M. Alexei M. TSVELIK	Rapporteur
Mme. Isabelle BOUCHOULE	Examinatrice
M. Silvio FRANZ	Président du jury
M. Luis SANTOS	Examinateur

Acknowledgments

First of all, I would like to thank all the people in the Laboratoire de Physique Théorique et Modèles Statistiques for their support over the three years of preparation of my thesis. The positive and dynamical environment in the laboratory has been a great source of inspiration.

In particular, I would like to thank the director Stéphane Ouvry for having hosted me in the laboratory, and Martine Thouvenot and Claudine Le Vaou for all their help in the administrative aspects. A special thank to Vincent Degat: without his computer know-how and patience the development of my thesis would have been much slower. A very warm thanks to the "catalan" section of the LPTMS, Oriol Bohigas and Xavier Campi, with whom I shared very rewarding conversations while being able to communicate in my beloved language. Thanks to Sergey I. Matveenko for our long collaboration and his kindness. I thank Eugène Bogomolny and Oriol Bohigas for sharing with me their passion for chaos. I would also like to thank Patricio Leboeuf and Nicolas Pavloff for all their pertinent advises. I finally want to remember the time shared with Satya Majumdar, Alberto Rosso, Christophe Texier, Marie-Thérèse Commault, Maribel y Pablo and the students of the laboratory.

I would like to thank specially Gora Shlyapnikov for having been my Ph.D. advisor. He has given me the opportunity to work in a wonderful area of research, and to meet a lot of extraordinary people.

I would also like to acknowledge the colleagues that shared office with me, who have always contributed to generate a friendly environment: Dmitry L. Kovrizhin,

Julien Randon-Furling, Rémy Dubertrand, David Papoular and Céline Nadal.

I would like to thank the young members of the "cold-atoms" group. Our conversations have been an infinite source of knowledge for me, and sharing my lunch with them has always been a pleasure. I very specially thank Dimitry M. Gangardt for having initiated me to my research area and for his constant sympathy. I would like to thank very particularly Paolo Pedri and Temo Vekua: without you my thesis would have never been possible. I also want to thank Dmitry S. Petrov for becoming a great collaborator and support.

Many "outsiders" have contributed to my well-being: Leticia, Juanillo, Ximena... and the "magistèriens", of course, my first university colleagues in France who very soon became friends: Justine, Fabio and Steph, Xavier and Marie, Miguel, Marine, FX, Julien, Pascale, Li-hua...

I want to dedicate a very warm thanks to all the friends that I left at home and that I have always missed: Marta, Cristina, Helena, Laura, Clara, Sergi, Montse, María, Mariona... And of course Frank, who has given a meaning to everything.

It is difficult to look behind and determine in which moment the curiosity for science became so relevant for me. However, I would like to thank Roser Castiñeira for having introduced me to the world of research during my high-school years; without that experience I would probably not be here now.

Finally, I would like to thank my family. They have always supported and encouraged me, while keeping a critical eye on me. Thanks to my father for all the discussions about science and other problems, my mother for all her wisdom, and my sister for being unconditionally there. Thanks also to my grandparents and the rest of my family for all their love and support.

Contents

Chapter 1

Introduction

1.1 One dimension

The work presented in this manuscript is devoted to the physics of one-dimensional (1D) systems. 1D systems have often been used as toy models, in an attempt to provide a simplified physical picture of higher-dimensional problems. However, the reduction of dimensionality opens the door to a wide range of new phenomena that do not take place in higher dimensions. These unique properties of 1D systems are primarily related to the unique role of quantum fluctuations, which are so strong in 1D that the intuition based on the free-particle picture and the mean-field theory very often fails, and the effects of strong correlations become important [1, 2].

What, in particular, are the main features that make the 1D systems so different from the systems in two and three dimensions? First of all, in contrast with the 2D and 3D cases, the particles in a 1D configuration can be labelled in a unique way: particle one is at the left of particle two, which is at the left of particle three, and so on. In such a configuration, a particle cannot go around its neighbour but it has to pass through it.

Another peculiar feature of the one-dimensional systems is that they become more interacting the more diluted they are. In the mean-field weakly interacting regime, the interaction energy per particle can be written as $E_{int} \simeq ng$, where

$n = N/L$ is the 1D density and g is the interaction strength. Meanwhile the typical kinetic energy is $E_k \simeq \hbar^2 n^2/m$, since the mean interparticle separation in one dimension is $1/n$. Thus, the ratio of the interaction to kinetic energy is $\gamma \sim g/n$. This is the parameter that characterises the interaction regime in 1D. It increases with decreasing density, showing a related increase in the role of interactions. One-dimensional systems are more strongly interacting the more dilute they are.

One-dimensional systems are characterised by strong thermal fluctuations. This is due to the fact that in one dimension, if the temperature is not zero, disorder is in favour of order. Therefore, in one-dimension ordered phases only exist at zero temperature. If we want to study phase transitions in one dimension we need to look only at the ground state. On the contrary, in higher dimensions phase transitions at higher temperatures occur.

Another striking property of one-dimensional systems is that two-body collisions cannot lead to thermalisation of a gas of identical particles. In order for a system to thermalise one needs a transport process leading to the appearance of a heat flow. In one dimension, when two identical particles collide they only acquire a phase shift (or classically, a time delay). For this reason after such a collision takes place we cannot tell whether the two particles have collided or just have passed through each other. Therefore, the momentum distribution of a 1D ensemble of particles will not be altered by such pair-wise collisions. Thus, in order to reach thermalisation in 1D we need to rely on three-body collisions or many-body processes. In higher dimensions, on the contrary, we cannot determine the outcome of a two-body collision from the knowledge of the two incoming momenta of the particles.

One can use different techniques to study one-dimensional systems. Because of their strong fluctuations the mean field theory, which is of so much utility in two and three dimensions, has a rather limited applicability. This requires the adoption of a different set of techniques. In cases where the system is integrable we can use the exact technique of the Bethe ansatz [3]. Despite its complicated

structure, the Bethe ansatz is a useful exact method that provides results free of uncontrollable approximations, and works for any coupling strengths. Alternative approaches include effective field theory (in particular the bosonisation technique [1, 2]), perturbation theory, as well as numerical methods such as density-matrix renormalisation group [4, 5].

One-dimensional systems are not any more a theoretical artefact, but they are created in the laboratories. Experiments include quasi-one-dimensional organic conductors [6, 7, 8], carbon nanotubes [9, 10, 11], quantum wires [12], quasi-one-dimensional systems made of cold atoms [13], etc. Among these systems, low-dimensional cold gases play a special role. These systems are composed of atoms that have been cooled down to nanokelvin temperatures and trapped into quasi-one-dimensional geometries using magnetic fields or optical lattices. Compared to the systems in solid state physics they present at least three main advantages. First of all, they are clean systems, that is, they are free of impurities, and they are very well isolated systems. Second, their trapping potentials are well known and the interaction between atoms is well understood. Third, many of their parameters can be experimentally tuned, such as the strength of the interaction or the mean interparticle separation. These advantages facilitate an in-depth study of these systems and a more accurate comparison of experiments with theory. Moreover, atomic systems offer different internal degrees of freedom that can lead to states of matter which do not have obvious counterparts in the usual solid-state physics of interacting electrons.

1.2 Integrability

In this manuscript we focus on exactly solvable quantum models. The concept of integrability is not straightforward in quantum theory. In this section we give a short introduction to the notion of integrability in quantum theory, as well as the main procedures that allow us to determine whether a system is integrable or not.

Let us consider the general Hamiltonian for a system of N particles interacting

via the momentum-independent scattering potential v:

$$H = \frac{1}{2}\sum_{j=1}^{N} p_j^2 + \sum_{j=1, j<k}^{N} v(x_k - x_j), \tag{1.1}$$

where x_i and p_i are the coordinates and momenta of the N particles, and we set $\hbar = 1$ and $m = 1$. We will see that in this situation integrability can be viewed as scattering without diffraction, that is, the scattering of any number of particles does not change the set of their momenta [14].

We first consider the scattering of two identical particles. When two identical particles interact via an elastic potential the total momentum and energy are conserved. Hence, after a collision the particles have either interchanged their momenta or retained the same. In the asymptotic region, where all the interparticle separations are larger than the range of the potential, the wave function is that of free particles and it can be written as a product of plane waves. Therefore, after the collision, the wave function is expressed as

$$\begin{aligned} \Psi(x_1, x_2) &= e^{i(k_1 x_1 + k_2 x_2)} - e^{-i\theta(k_1 - k_2) + i(k_2 x_1 + k_1 x_2)} \\ &= \psi(12) e^{i(k_1 x_1 + k_2 x_2)} + \psi(21) e^{i(k_2 x_1 + k_1 x_2)}, \end{aligned} \tag{1.2}$$

where we put $x_1 < x_2$, and $k_1 > k_2$ are the incoming momenta of the particles in the asymptotic region. The function θ is the two-body phase-shift that the particles acquire after scattering on each other, and it can be calculated from the two-body potential v. Due to Galilean invariance it can only depend on the momentum difference $k = k_1 - k_2$, and reversing the collision we see that it is antisymmetric, $\theta(-k) = -\theta(k)$. In the lower line of Eq. (1.2) we write the wave function in a more efficient notation: $\psi(12) = 1$ and $\psi(21) = -e^{-i\theta(k_1 - k_2)}$. We can calculate the wave function in the other sector, where $x_2 < x_1$, using the exchange statistics of the particles, odd for fermions and even for bosons.

Let us consider now the scattering of three particles, $N = 3$, with $x_1 < x_2 < x_3$. In this case, the two conservation laws do not restrict the three momenta to be a rearrangement of the three incoming ones, $k_1 > k_2 > k_3$, and thus the wave

function after the collision can be written as

$$\Psi(x_1,x_2,x_3) = \sum_P \psi(P) e^{i(k_{P1}x_1+k_{P2}x_2+k_{P3}x_3)} + \iiint_{\substack{k_1'<k_2'<k_3' \\ K,Efixed}} dk_1' dk_2' dk_3' S(k_1',k_2',k_3') e^{i(k_1'x_1+k_2'x_2+k_3'x_3)}. \tag{1.3}$$

Here P denotes the permutations of the N momenta over the N particles, similar to equation (1.2), and we have to sum over all the different orderings of the three particles. In the first term of the wave function the 3! amplitudes $\psi(P)$ are determined only considering the scattering between pairs of particles, and like in the case with $N = 2$ we have $\psi(jik) = -\psi(ijk)\exp(-i\theta(k_i - k_j))$. In a more general way we write

$$\psi(P') = -\psi(P) e^{-i\theta(k-k')}, \tag{1.4}$$

where P and P' are two permutations exchanging the momenta k and k'. The construction of the scattering phase factors is such that all different combinations of two-body scattering events leading to the same final rearrangement of the particles have the same phase factor. For example the following two paths lead to the same final order of the three particles:

$$\begin{array}{ccc} \psi(123) & \rightarrow & \psi(213) \rightarrow \psi(231) \\ \downarrow & & \downarrow \\ \psi(132) & \rightarrow & \psi(312) \rightarrow \psi(321). \end{array} \tag{1.5}$$

Following any of the two paths we obtain the same relation between the amplitudes, $\psi(321) = -\psi(123)e^{-i(\theta(k_1-k_2)+\theta(k_2-k_3)+\theta(k_1-k_3))}$.

The first part of the wave function of Eq. (1.3),

$$\Psi(\vec{x}) = \sum_P \psi(P) e^{i\sum_{i=1}^N k_{Pi}x_i}, \tag{1.6}$$

is what constitutes the Bethe ansatz. The second term in the wave function represents the real three-body scattering and is the diffractive part. This part cannot be factorised in terms of collisions involving only two particles, and contains

a spherical portion. The three-body scattering conserves the total momentum K and the total energy E, this restricts the choice of outcoming momenta k'. However, if we want to be able to express the outcoming momenta as a simple permutation of the incoming ones, and thus have the second part of the wave function Eq. (1.3) equal to zero, we need a third quantity to be conserved. If there is diffraction, such independent quantity does not exist. This kind of scattering is precisely what we need in order to get thermalisation in one-dimension. On the contrary, if such a third conserved quantity exists, then the system is very likely to be non-diffractive, since with a third equation of conservation we would probably be able to fix the three outcoming momenta as permutations of the three incoming ones. This reasoning can be generalised to N particles.

Let us now find the meaning of scattering without diffraction in a classical picture. Diffraction is a concept related to waves, and thus to quantum mechanics. However, the classical trajectory of a wave can be obtained as rays of the wave function. In this sense classical mechanics is somewhat analogous to geometrical optics. To see this more clearly consider the scattering of three particles, x_1, x_2 and x_3. Performing the change of coordinates $x = (x_1 - x_3)/\sqrt{2}$, $y = (2x_2 - x_1 - x_3)/\sqrt{6}$, $X = (x_1 + x_2 + x_3)/3$ and integrating out the centre of mass X, we can

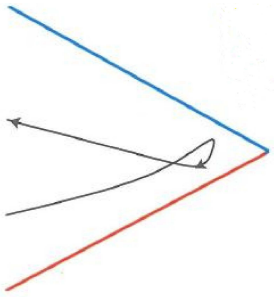

Figure 1.1: Scattering in the plane $x = (x_1 - x_3)/\sqrt{2}$, $y = (2x_2 - x_1 - x_3)/\sqrt{6}$. The straight lines are the boundaries given by the potential and the arrow represents a particular trajectory of three particles (x_1, x_2, x_3) interacting via the potential. Figure from B. Sutherland [14].

plot a classical trajectory of the three particles in the plane (x, y) (Fig. 1.1). If we then take a collection of trajectories that share the same asymptotic momenta but have slightly different initial conditions (the equivalent to a monochromatic light beam) and plot their trajectories under the effect of a given scattering potential, we say that the scattering is non-diffractive if the beam stays collimated and the front is a straight line. Fig. (1.2, top) shows an illustration of such a non-diffractive scattering, while Fig. (1.2, bottom), in contrast, provides an example of the diffractive case. Non diffraction is equivalent in optics to specular reflections from mirrors.

Now we know how to define integrability, but how can we show that a system is integrable? There is no standard procedure for doing so, but there are several methods to determine whether a model is integrable or not. In this manuscript we use the method of "try and see", since it leads to the Bethe ansatz: for a given Hamiltonian, we guess that the solution is non-diffractive everywhere so that the wave-function is assumed to be of the form Eq. (1.6). Then, we check if this form is indeed a solution of the Schrödinger equation for the particular potential. This method is called the Bethe ansatz, and it was first used by Bethe in 1931 to solve the model of the one-dimensional Heisenberg magnet [3].

To show non-integrability, on the contrary, is very easy. All we are required to do is to show the consistency conditions or Yang-Baxter equations (Eq. 1.8) that are necessarily satisfied in systems that show non-diffractive scattering. If these conditions are violated there is no need to try to proof integrability. On the other hand, if these conditions are fulfilled we are still left with the task to proof integrability (since they are necessary conditions but not sufficient). The consistency conditions are easily obtained considering the scattering of three particles on a ring, no matter if they are identical or not. The scattering operator S can be calculated from the potential $v(x_i - x_j)$. The first two particles, with momenta k_1 and k_2, scatter via the two-body scattering operator $S_1(k_1, k_2)$, the next two particles, with momenta k_2 and k_3, scatter via $S_2(k_2, k_3)$, and so on.

Remember that the coefficients of the wave function Eq. (1.6) are charac-

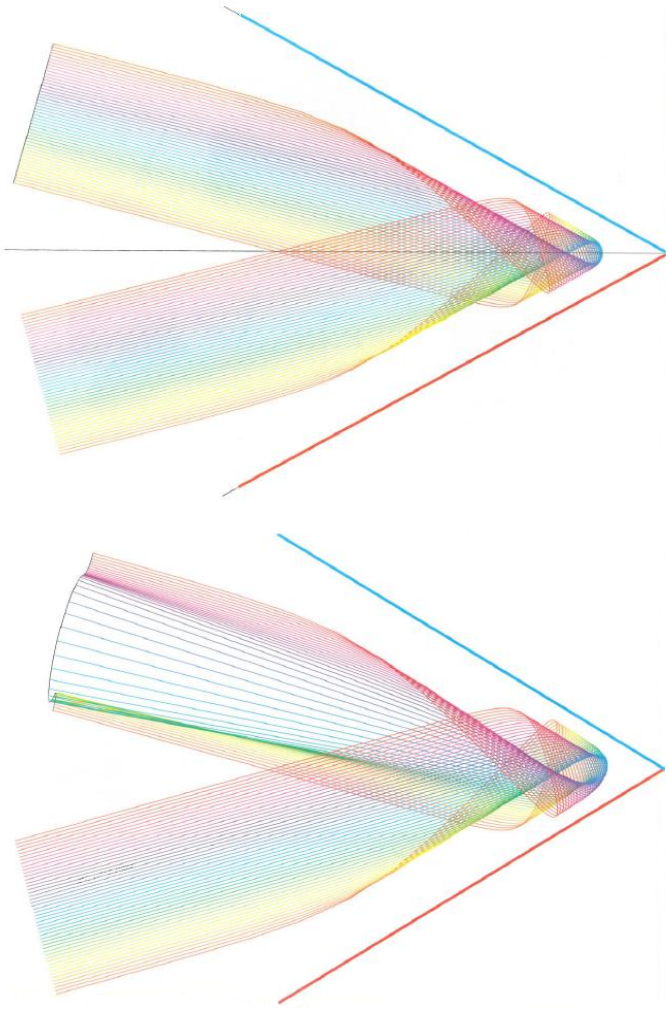

Figure 1.2: Top: non-diffractive scattering in the $x = (x_1 - x_3)/\sqrt{2}$, $y = (2x_2 - x_1 - x_3)/\sqrt{6}$ plane for an integrable potential (inverse-sinh-square or hyperbolic potential). After the scattering the beams stay collimated. Bottom: diffractive scattering in the x, y plane for a non-integrable potential (inverse-cosh-square potential). The wave front is not a straight line after the scattering. Figures from B. Sutherland [14].

terized by the permutation of the particles P. We define now the permutation operator of the i-th pair of particles, α_i: $\alpha_1(123) = (213)$, $\alpha_2(123) = (132)$. Obviously, $\alpha_1\alpha_2\alpha_1 = \alpha_2\alpha_1\alpha_2$, since $(321) = \alpha_1\alpha_2\alpha_1(123) = \alpha_2\alpha_1\alpha_2(123)$; thus $(\alpha_1\alpha_2)^2 = I$. Since the scattering operator also represents permutations among particles, we have a similar equation for the coefficients of the wave function: $\psi(213) = S_1(k_1, k_2)\psi(123)$, $\psi(132) = S_2(k_2, k_3)\psi(123)$, etc. However, there are several different sequences of two-body scattering events that lead to the same set of amplitudes, which is equivalent of saying that there are several sequences of two-body permutations that lead to the same final arrangement of the particles (see Eq. (1.5)). For the permutations of the three particles on the ring we have the equality

$$\begin{aligned}\psi(321) &= S_1(k_2, k_3)S_2(k_1, k_3)S_1(k_1, k_2)\psi(123) \\ &= S_2(k_1, k_2)S_1(k_1, k_3)S_2(k_2, k_3)\psi(123). \end{aligned} \tag{1.7}$$

Since the incoming amplitudes can be arbitrary we have a matrix equation for the consistency of the non-diffractive wave function:

$$S_1(k_2, k_3)S_2(k_1, k_3)S_1(k_1, k_2) = S_2(k_1, k_2)S_1(k_1, k_3)S_2(k_2, k_3). \tag{1.8}$$

In Fig. (1.3) we find a graphical explanation of these consistency conditions, also called Yang-Baxter equations.

Their generalisation to N body systems is straightforward: the permutation group for N particles is generated by the permutation operators α_i, with $i = 1, \ldots, N-1$. They obey the analogous relation

$$(\alpha_j\alpha_k)^{n_{jk}} = I, \tag{1.9}$$

where $n_{jk} = 1$ if $j = k$, $n_{jk} = 3$ if $|j - k| = 1$ and $n_{jk} = 2$ if $|j - k| > 1$. For the case $j = k$ it is evident that $S_j^2 = S_j(k', k)S_j(k, k') = I$, this is the condition of unitarity. For $|j - k| > 1$, the relation Eq. (1.9) implies that scattering of disjoint pairs commute, which is also evident. Finally, for $|j - k| = 1$ we arrive at the consistency conditions Eq. (1.8), with $1 \equiv i$, $2 \equiv j$.

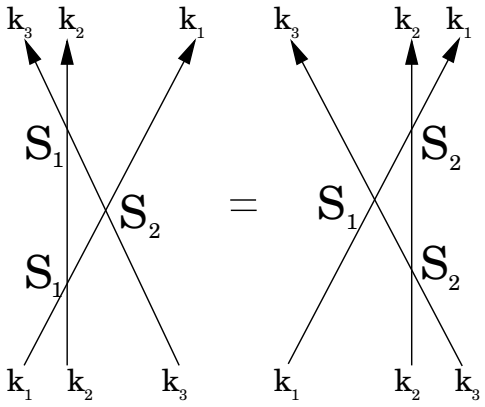

Figure 1.3: Graphical caption of condition Eq. (1.8).

1.3 Bethe ansatz

As we have seen in Section 1.2, the Bethe ansatz is the method of "try and see" that allows us to determine whether a system is integrable or not. Since the present work focus on the Bethe ansatz, it is instructive to provide a more detailed summary of this technique.

We have seen that when the scattering is non-diffractive the wave function is written as a superposition of plane waves, Eq. (1.6). This constitutes the starting point of the Bethe ansatz. Therefore, a system is solvable by the Bethe ansatz if we can prove that the wave-function Eq. (1.6) is an eigenfunction of its Hamiltonian. Although this method can also be applied to certain finite-range interacting models, such as the hyperbolic model [15, 16] and the Calogero-Sutherland model [17, 18, 19, 20, 21, 22, 23, 24], where the solution only has the form of Eq. (1.6) in the asymptotic region, we will consider here only models with short-range interaction, where the asymptotic region is everywhere.

It is indeed easy to understand that in the case of a short-ranged potential, and for a given order of the N particles $0 < x_1 < x_2 < \cdots < x_N < L$, we can treat the particles as free, since they are far away enough from each other not to "feel" the interaction potential. We can then write their wave function

as a superposition of N plane waves, Eq. (1.6). The interaction among them reduces to a scattering condition every time that two particles coincide in space. To summarise: N particles in the sector $0 < x_1 < \cdots < x_N < L$ with Hamiltonian

$$H = \frac{1}{2}\sum_{j=1}^{N} p_j^2 + \sum_{j=1, j<k}^{N} v(x_k - x_j) \tag{1.10}$$

are equivalent to N free particles with wave function

$$\Psi(x) = \sum_{P} \psi(P) e^{i\sum_{j=1}^{N} x_j k_{Pj}} \tag{1.11}$$

and Hamiltonian

$$H = \frac{1}{2}\sum_{j=1}^{N} p_j^2, \tag{1.12}$$

with boundary conditions at vanishing inter-particle separations $x_j \to x_i$.

Consequently, the Hamiltonian reduces to the kinetic energy part, while all the information about the interaction is expressed in terms of two-body scattering. Equation (1.6) can be generalised to include complex momenta which will describe bound states.

Let us now impose boundary conditions on our system. Since the choice of boundary conditions will be irrelevant once we will go to the thermodynamic limit, let us consider periodic boundary conditions. We now allow a particle with momentum p_j to scatter all the other $N-1$ particles and return to its initial position. In the asymptotic region the phase factor after this sequence of two-body scatterings is

$$\prod_{k=1, k\neq j}^{N} e^{-i\theta(p_j - p_k)}. \tag{1.13}$$

Since the particle with momentum p_j is back to its initial position, due to periodic boundary conditions it has also acquired an extra phase $\exp(iLp_j)$. Finally, the periodicity of the wave function requires the total phase to be equal to unity, arriving at the fundamental relation

$$1 = e^{iLp_j} \prod_{k=1}^{N} e^{-i\theta(p_j - p_k)}. \tag{1.14}$$

Taking the logarithm of the previous equation we find

$$p_j L = 2\pi I_j + \sum_{k=1,k\neq j}^{N} \theta(p_j - p_k), \quad j = 1, ...N, \tag{1.15}$$

where I_j are called the quantum numbers. This set of N equations, one for each particle in the system, are the Bethe ansatz equations for the system of N identical particles in a ring of length L. Keeping in mind that now the Hamiltonian of the system contains only the kinetic energy term, and that the eigenfunction is given by a superposition of plane waves (Eq. 1.6), we can calculate very easily the total energy and momentum of the system, given by

$$P = \sum_{j=1}^{N} p_j \qquad \text{and} \qquad E = \frac{1}{2}\sum_{j=1}^{N} p_j^2. \tag{1.16}$$

It is worth noticing that if the asymptotic momentum set contains two equal momenta then the wave-function Eq. (1.6) is equal to zero. This property prevents the formation of a true BEC in one-dimensional systems.

Let us look at the case of bosons interacting via a δ-function potential as an example. This model is called Lieb-Liniger model for the repulsive interaction [25] and McGuire model for the attractive one [26]. The Hamiltonian reads

$$H = \frac{1}{2}\sum_{j=1}^{N} p_j^2 + c \sum_{j=1,j<k}^{N} \delta(x_j - x_k). \tag{1.17}$$

Taking as a solution the symmetric wave-function, integrating the Schrödinger equation across the origin, where the delta potential is located, and imposing the continuity of the wave function, we can write the following condition at the boundaries:

$$\left(\frac{\partial}{\partial x_j} - \frac{\partial}{\partial x_{j+1}}\right)\Psi|_{x_{j+1}-x_j\to 0+} = c\Psi|_{x_{j+1}=x_j}, \tag{1.18}$$

for $j = 1, ..., N-1$. This condition should be fulfilled in order to say that the system is solvable by the Bethe ansatz. Let us show that it is indeed the case.

The $N!$ terms in the linear superposition in the wave-function can be rearranged in pairs of particles that have been interchanged,

$$\Psi = \cdots + \psi(P)e^{i(\cdots + px_j + qx_{j+1} + \cdots)} + \psi(P')e^{i(\cdots + qx_j + px_{j+1} + \cdots)} + \cdots, \tag{1.19}$$

where P and P' are two permutations with only j and $j+1$ interchanged ($Pj = P'(j+1)$, $P(j+1) = P'j$), and $p = k_{Pj}$ and $q = k_{P'j}$. Each pair of terms has to fulfil individually the boundary condition Eq. (1.18) since they are linearly independent. We thus obtain for the amplitudes of the wave function:

$$\frac{\psi(P')}{\psi(P)} = \frac{p-q-ic}{p-q+ic} \equiv -e^{-i\theta(p-q)}, \tag{1.20}$$

which coincides with the expression for the two-body scattering amplitude, or phase factor, for a δ-function potential, which is derived in Appendix A. When two particles collide the wave-function acquires this phase factor. This proofs that the system is solvable by the Bethe ansatz.

Imposing periodic boundary conditions we arrive at the Bethe ansatz equations for the system of interacting bosons:

$$Lp_j = 2\pi I_j - 2\sum_{i=1}^{N} \arctan\left(\frac{p_j - p_i}{c}\right), \tag{1.21}$$

where I_j is a set of N integers (half-odd-integers) for the number of particles N being odd (even). They are called the quantum numbers. Each set I determines a single state. The ground state wave-function corresponds to the Fermi sea, in which all asymptotic momenta lie between $p_1 = -p_F$ and $p_N = p_F$, where p_F is the Fermi momentum. They correspond to the quantum numbers $I_j = \{-\frac{N-1}{2}, -\frac{N-1}{2}+1, \ldots, \frac{N-1}{2}\}$.

In the case where the system is composed of a mixture of different particles the situation is more complicated. In this case, the scattering depends on whether it occurs between two identical particles or two different ones. At the same time, by giving identities to the particles, we open the possibility for transmission and reflection. When writing down the equivalent to the condition Eq. (1.14) we will have to keep this in mind. Examples on how to solve the Bethe ansatz problem for a multicomponent system will be presented in Sections 2.1.3 and 3.1.3 for the two-component Fermi gas with δ-function interaction and for the Hubbard model, respectively.

1.4 Cold atoms

Experiments with ultra-cold atoms have proved to be great means to create one dimensional (or, to be more rigorous, quasi-one dimensional) systems. As it was already pointed out above, in these systems our understanding of properties such as the trapping potential or the interaction between particles is very advanced. At the same time, the experimental parameters can be well controlled. Moreover, the coupling of these systems to the "outside world" can be virtually eliminated. For these reasons, ultra-cold atoms can be used to make nearly perfect models of one-dimensional systems.

In order to have a cloud of ultra-cold atoms that is effectively one-dimensional it has to be trapped into an atom waveguide. The latter is a potential that tightly confines the particle motion in two transverse directions, while leaving it free in the third direction. In order to have a true one-dimensional dynamics in such a configuration all the characteristic energies of the system should be smaller than the energy needed to excite states in the transverse directions. This means that, even though the atom wave function is three-dimensional, it only has dynamics in one of its dimensions. This situation is called quasi-one-dimensional, and the only difference from the purely one-dimensional system is that now the effective one-dimensional interaction between particles depends on the confinement. It is interesting to note that the one-dimensional interaction is independent of the momentum of the particles.

Generally, the trapping potential is modelled by a harmonic potential,

$$V_{\text{ext}}(\vec{r}) = \frac{1}{2}m\omega_{\perp}^2 r^2 + \frac{1}{2}m\omega_z^2 z^2, \tag{1.22}$$

where $r = \sqrt{x^2 + y^2}$. In this configuration, in order to have one-dimensional dynamics we impose $E_c \ll \hbar\omega_{\perp}$, where $\omega_{\perp}$ is the trapping frequency in the transverse direction and E_c is the characteristic energy in the system. If this relation is fulfilled, the transverse motion can be frozen to zero-point oscillations, while keeping the longitudinal motion. In order to reach 1D we thus should have very anisotropic traps, such that the ratio of the longitudinal to transverse trapping frequency is

$\omega_z/\omega_\perp \ll 1$. For trapped fermions or strongly interacting bosons the characteristic energy is the Fermi energy, $E_c = E_F = N\hbar\omega_z/2$, therefore $\omega_z/\omega_\perp \ll 1/N$. For weakly interacting bosons the characteristic energy is $E_c = ng$, therefore the condition that has to be fulfilled is milder. Overall, if the temperature is non-zero, in order to reach the 1D regime it has to fulfil $k_B T \ll \hbar\omega_\perp$.

Such anisotropic traps can be magnetic or optical traps. For magnetic trapping there is need of not axially symmetric magnetic fields. In the case of the Ioffe-Pritchard trap [27], for example, the longitudinal and transversal spring constants can be tuned separately. Another way to create such a trap is using wires on a chip, Fig. (1.4, top) [28, 29, 30]. In this case, the potential is very weak longitudinally along most of its length and becomes very steep at its ends. Experiments performed using these kinds of traps include the formation of dark and bright solitons [31, 32, 33], the one-dimensional Bose-Fermi mixtures [34], studies of the phase and density fluctuations [35, 36, 37, 38], etc.

Optical lattices are also used to generate one-dimensional traps [39], see Fig. (1.4, bottom). Applying counter-propagating laser beams to a cloud of ultra cold atoms one obtains a collection of one-dimensional arrays, organised into a square lattice of tubes. If the lattice is made deep enough such that the tunnelling time

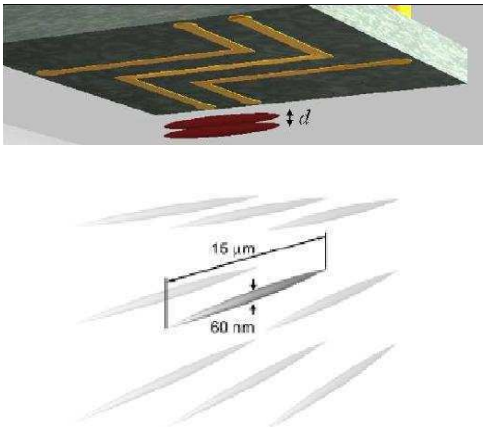

Figure 1.4: Top: two one-dimensional arrays on a chip. Bottom: set of one-dimensional arrays generated by applying a two-dimensional optical lattice.

between tubes is bigger than the typical time of the experiment, then each tube acts as an independent one-dimensional system. These devices permit to reach deeper into the one-dimensional regime, because the transverse length scale of each tube is very small. Optical lattices have been used in experiments in order to study the phase coherence [40] and pair correlations [41], the three-body association [42], the creation of Tonks-Girardeau gas [43, 44], the dipole oscillation damping [45],the creation of confined-induced molecules [46], the p-wave interactions [47] and to study the effects of integrability and thermalisation in one-dimensional systems [48].

If the effective one-dimensional regime is reached, the low-energy scattering properties of the system can be modelled by an effective contact interaction in one dimension $U(z) = g_{1D}\delta(z)$ [49] with the coupling parameter

$$g_{1D} = \frac{-2\hbar^2}{ma_{1D}} = \frac{2\hbar^2 a_{3D}}{ma_\perp^2}\left(1 - C\frac{a_{3D}}{a_\perp}\right)^{-1}, \tag{1.23}$$

where $a_\perp = \sqrt{\hbar/m\omega_\perp}$ is the transverse oscillation length, a_{1D} is the effective 1D scattering length, $C = 1.0326...$ is a numerical parameter and a_{3D} is the three-dimensional scattering length. In order to derive this result, even in the situation where there are no real transverse excitations, it is necessary to take into account virtual excitations of the transverse modes. The one-dimensional interaction is attractive for $g_{1D} < 0$ and repulsive for $g_{1D} > 0$.

By using an external magnetic field the 3D scattering length can be changed continuously [50, 51, 52, 53, 54]. Hence, the one-dimensional interaction strength can take different values. It can in particular be tuned from a repulsive interaction ($g_{1D} > 0$) to an attractive one ($g_{1D} < 0$). In Fig. (1.5) we see g_{1D} and a_{1D} versus the three-dimensional scattering length a_{3D}; the latter can be changed continuously applying a magnetic field and so the sign of the one-dimensional scattering length changes from repulsive to attractive. This phenomenon opens up the possibility to explore experimentally different regimes, and even allows one to change the parameters during an experiment.

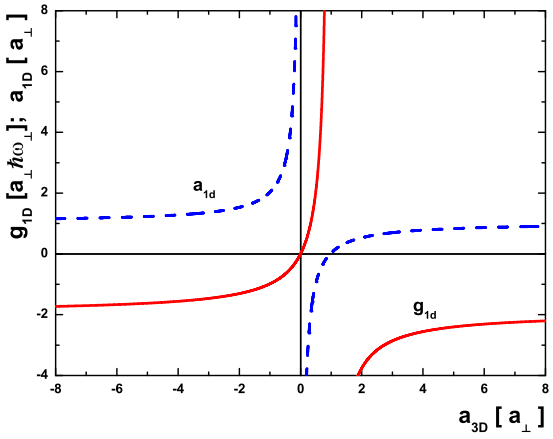

Figure 1.5: Effective one-dimensional coupling constant g_{1D} (solid lines) and effective one-dimensional scattering length a_{1D} (dotted line) versus the three dimensional scattering length. Courtesy of G. Astrakharchik.

1.5 Overview of the thesis

In the following we briefly discuss the contents of this thesis. In the second chapter we present a study on the ground state of a system of two-component fermions in one dimension under harmonic confinement. We begin the chapter with reviewing some of the main properties of the two-component Fermi gas with repulsive δ-function interaction, and give a reminder of the Bethe ansatz solution for its Hamiltonian. Later on this solution is used to calculate the phase diagram of the system in the homogeneous case. Adding a harmonic confinement and using local density approximation we calculate the properties of the system in the trapped configuration. We show that for the harmonically confined case the atoms are distributed in a two-shell structure: the partially polarised phase is located in the inner shell and the fully polarised phase sits at the edges of the trap. The radii of the inner and outer shell are calculated as functions of the polarisation. We calculate the dependence of the magnetisation imbalance on the polarisation, showing that the system always has a finite susceptibility.

In the third chapter we study the finite size effects for the gap of the quasi-particle excitation spectrum in the one-dimensional Hubbard model with on-site attraction. First, as an introduction, we review important known results for the Hubbard model. After that we present a general approach for finding finite size corrections to the ground state energy and to the gap. Two type of corrections to the result of the thermodynamic limit are obtained. First of all, there is a power law correction due to gapless excitations which behaves as $1/N_a$, where N_a is the number of lattice sites. Second, we obtain an exponential correction related to the existence of gapped excitations. In the weakly interacting regime this correction can dominate over the power law correction. We show our numerical simulations which support these analytical results. We finally present a perturbative approach for solving the Bethe ansatz equations in the limiting case of weak interactions.

In chapter four we study the response of a highly excited 1D gas to a periodic modulation of the coupling constant. We calculate the corresponding dynamic structure factors and show that they differ dramatically for the two considered cases: the integrable Lieb-Liniger model and the non-integrable model of a single mobile impurity in a Fermi gas. The non-integrable system is sensitive to excitations with frequencies as low as the mean level spacing, which is exponentially small, whereas the threshold frequency in the integrable case is much larger and scales polynomially with the size of the system. This effect can be used as a probe of integrability for mesoscopic 1D systems, and can be observed experimentally by measuring the heating rate of a parametrically excited gas.

Chapter 2

Two-component repulsive Fermi gas with population imbalance in elongated harmonic traps

2.1 Overview

In this chapter we consider a system of two-component fermions in one dimension under harmonic confinement. The interaction between fermions of different components is symmetric (analogue of the zero-range s-wave interactions in two and three dimensions) and is modelled with a δ-function potential. On the contrary, the scattering between identical fermions is antisymmetric (analogue of the p-wave scattering in two and three dimensions) and the corresponding interaction is omitted in the considered ultra-cold limit.

We study the exact ground state at zero temperature for a two-component 1D Fermi gas with repulsive inter-component interaction. We consider a gas of fermionic atoms, the two components being two different hyperfine states of the same atom, such that they have the same mass m. The two hyperfine states are

labelled by their isospin projections. For simplicity we call them up-spin (↑) and down-spin (↓) particles. We will show that for the harmonically confined case the atoms are distributed in a two-shell structure: the partially polarised phase is located in the inner shell and the fully polarised phase sits at the edges of the trap. The radii of the inner and outer shell are calculated as functions of the polarisation. We calculate the dependence of the magnetisation imbalance on the polarisation, showing that the system always has a finite susceptibility. We begin with reviewing some of the main properties of the system under consideration and give a reminder of the Bethe ansatz solution for the Hamiltonian of the two-component Fermi gas with a delta-function repulsive interaction. This solution is used to calculate the phase diagram of the system in the homogeneous case. Adding a harmonic confinement and using local density approximation we calculate the properties of the system in the trapped configuration. These results are presented in reference [55].

2.1.1 The Hamiltonian

The Hamiltonian of the system under consideration is

$$H = \frac{\hbar^2}{2m}\left(-\sum_{i=1}^{N}\frac{\partial^2}{\partial z_i^2} + c\sum_{i<j}\delta(z_i - z_j)\right) + V_{\text{ext}}(z), \tag{2.1}$$

where c is related to the 1D effective interaction coefficient (Eq. 1.23) by

$$c = \frac{mg_{1D}}{\hbar^2} = \frac{2}{a_{1D}}. \tag{2.2}$$

The first term in the Hamiltonian is the kinetic energy, the second one is the two-body δ-function interaction, and the last one describes the interaction of the particles with the harmonic trapping potential (Eq. 1.22). This model is the dilute limit of the Hubbard model, and the Hamiltonian Eq. (2.1) can be obtained from the Hubbard model Hamiltonian (Eq. 3.1) in the limit of low densities, as it is shown in Appendix B.

As already mentioned in the introduction (Section 1.1), in one dimension the interactions are measured through a dimensionless coupling constant $\gamma = c/n$,

where $n = N/L$ is the density of particles. The limit $\gamma \ll 1$ corresponds to the weakly interacting regime, while $\gamma \gg 1$ stands for the strongly interacting one. Remember that in one dimension the gas becomes more interacting when lowering its density. For two fermions with different isospin projections one finds a bound state in one-dimension for the attractive case ($g_{1D} < 0$), with the binding energy $\epsilon_B = -\hbar^2/ma_{1D}^2$ and with a size $\sim a_{1D}$. For the repulsive case ($g_{1D} > 0$) there is no bound state [49, 56]. We will consider the case with repulsion only.

As pointed out previously, due to the Pauli exclusion principle the delta-function interaction only occurs between particles with opposite isospins. We label the total number of particles by $N = N_\uparrow + N_\downarrow$, where N_σ is the number of particles in each component, $\sigma = \uparrow, \downarrow$.

The Hamiltonian Eq. (2.1) has an obvious symmetry under exchange of up-spin and down-spin particles, $N_\uparrow \leftrightarrow N_\downarrow$. Without loss of generality we can then assume that $N_\downarrow \leq N/2$. We will call the particles with up (down) spin the majority (minority) component.

The model under consideration can be solved analytically in the limiting cases of zero interactions and infinite interactions. The former is the limiting case of free fermions, and the wave-function of the system is a Slater determinant. The latter limit corresponds to the so-called fermionic Tonks-Girardeau regime, and it is a singular limit since the infinite repulsion between fermions mimics the Pauli principle. Therefore, the different fermionic components cannot be differentiated any more. These two limits, free and Tonks-Girardeau, are somehow connected: infinitely interacting two-component fermions behave in a similar way as free one-component fermions.

2.1.2 Excitation spectrum

For the case of repulsive inter-species interactions and in the homogeneous configuration the excitation spectrum of the gas of two-component fermions is described by the fermionic Luttinger Liquid theory [57]. It predicts a two-fold excitation spectrum: there is a linear excitation spectrum for the fluctuations of the total

density (charge), $\epsilon_c(p) = v_c p$, and another linear spectrum for the fluctuations of the density difference (spin), $\epsilon_s(p) = v_s p$. The velocities for each excitation, called charge and spin respectively, are generically not the same. This model is a form of spin-charge separation, which has been verified experimentally in semiconductor quantum wires [58]. In the context of ultra-cold gases in harmonic traps, one can verify the spin-charge separation observing the collective excitation frequencies [59] or by looking at the propagation of wave-packets [60].

For the case with attractive inter-species interaction in the homogeneous configuration the model is explained by the Luther-Emery liquid theory [61]. In this case, the excitation spectrum for the charge part is also linear, $\epsilon_c(p) = v_c p$, but the spin part has a gap in the excitation spectrum : the origin of this gap is the appearance of bound states formed by pairs of fermions with opposite spin. The spectrum in this sector is similar to the one in BCS theory, $\epsilon_s(p) = \sqrt{(\Delta_s/2\hbar)^2 + (v_s p)^2}$. Actually, the two-component spin gas behaves in a similar way as the electron gas in solids. The value of the gap in the spectrum, for weak coupling, has a similar form as the one in the BCS theory, but the prefactor now depends on the interaction, $\Delta_s = 16 E_f/\pi\sqrt{|\gamma|/\pi} exp(-\pi^2/2\gamma)$. In this case, however, the weak coupling is reached at high densities. In the dilute case of strong interaction the gap approaches the value of the two-body bound state energy, $\Delta_s \to \epsilon_B = \frac{\hbar^2 c^2}{4m}$, and thus a pair of fermions can be treated as a bosonic molecule. This gas of molecules behaves like a hard-core Bose gas. Therefore attractive fermions in one dimension evolve from a fermionic Luther-Emery liquid into a gas of repulsive bosons. This evolution is a crossover, not a transition, and is called BEC-BCS crossover [62, 63, 64, 65, 66]. It can be solved exactly using the Bethe ansatz technique [67, 68].

In the case where the system is not perfectly one-dimensional another quantity has to be taken into account, the transverse oscillator length $l_\perp = \sqrt{\hbar/m\omega_\perp}$, which is related to the tightness of the transverse confinement. In this configuration the scattering always exhibits a two-body bound state, irrespectively of the sign of the scattering length. So tuning the scattering length from the negative side to

the positive one by using a Feshbach resonance, the bound pairs of atoms survive. These bound states are called confinement-induced molecules [49, 56, 69, 46, 70]. In order to have a "real" repulsive gas, without the presence of bound states, the atoms should be cooled without interaction ($a = 0$) and after that the repulsive interactions have to be switched on.

For the attractive case the ground state has also been found for the situation with population imbalance, $n_\uparrow \neq n_\downarrow$ [71] (see [72, 73] for the harmonically confined situation). For an applied magnetic field smaller than a critical value, the ground state is a superfluid with equal densities of up and down spins. However, above the critical field $h_c = \Delta_s/2$ the paired ground state is destroyed (Clogston-Chandrasekhar limit) [74, 75]. Inside a harmonic trap, and because the gap becomes larger at low densities, the superfluid phase appears at the edges of the trap while at the centre remains the partially polarised phase. This phase is said to behave like an FFLO state (Fulde-Ferrel-Larkin-Ovchinnikov) [76, 77], having an oscillating superfluid order parameter. The harmonically confined case with population imbalance for the repulsive interactions is

2.1.3 The Bethe ansatz solution

In the homogeneous case, without the harmonic confinement, the Hamiltonian Eq. (2.1) is exactly solvable by the Bethe ansatz. It was solved by C.N. Yang in 1967 [78] using for the first time the technique of the so-called nested Bethe ansatz. Before this solution there were studies by J.M. McGuire [79] who considered the system of only one down-spin particle, $N_\downarrow = 1$, embedded into a system of N up-spin particles, and by Lieb and Flicker [80] who studied the case with two down spins, $N_\downarrow = 2$. Later on, Sutherland generalised Yang's solution to the case with M different species of particles [81].

The starting point of Yang's solution is the Bethe ansatz (see Section 1.3). In a given sector $0 < x_{Q1} < x_{Q2} < \cdots < x_{QN} < L$ the wave function of the system

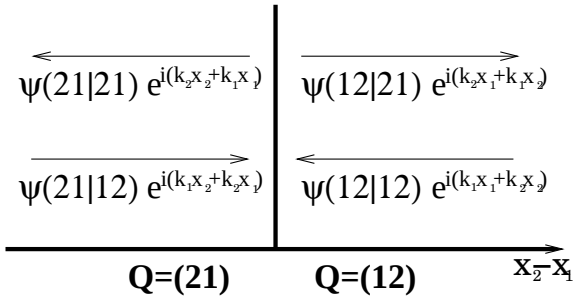

Figure 2.1: Picture of the scattering of two particles with $k_1 > k_2$. The two different regions in space, $Q = (12)$ for $x_2 > x_1$ and $Q = (21)$ for $x_1 > x_2$ are indicated, as well as the incoming and outgoing waves.

can be written as

$$\Psi = \sum_P \psi([Q,P])exp[i(p_{P1}x_{Q1} + \cdots + p_{PN}x_{QN})], \tag{2.3}$$

where $p_1, \ldots, p_N$ are a set of N unequal numbers, and $P = (P1, P2, \ldots, PN)$ gives a permutation of the momenta k. Since now there is a mixture of different types of particles we need to assign each of them an identity. Thus, $Q = (Q1, Q2, \ldots, QN)$ is a permutation of the identity of the particles: x_1 represents particle 1, which is the number j in the line if $Qj = 1$. Then, there are no restrictions on the range of x_i. $\psi([Q,P])$ is a matrix with $N! \times N!$ coefficients, and each of its columns gives a set of $N!$ amplitudes for fixed P and permuting Q.

We have two different types of particles and consequently if there is a scattering process between them there will be reflected and transmitted parts of the wave function. Remember that in the case where all the particles are identical the scattering only generates a phase factor (see Section 1.3). Let us consider first the scattering of two particles in the two regions of space $Q = (1,2)$, which corresponds to $x_2 > x_1$, and $Q = (2,1)$, corresponding to $x_1 > x_2$. They have momenta $k_1 > k_2$, and the wave function of the system is given by Eq. (2.3). The scattering process will be

$$\begin{pmatrix} \psi(Q=(1,2)|P=(2,1)) \\ \psi(Q=(2,1)|P=(2,1)) \end{pmatrix} = \begin{pmatrix} R_{21} & T_{21} \\ T_{21} & R_{21} \end{pmatrix} \begin{pmatrix} \psi(Q=(1,2)|P=(1,2)) \\ \psi(Q=(2,1)|P=(1,2)) \end{pmatrix}, \tag{2.4}$$

in Fig. (2.1) we find a graphical picture of this process. In the case of a δ-function interaction, the transmission and reflection amplitudes are given by (see Appendix A)

$$R(\Delta k) = \frac{-ic}{\Delta k + ic}, \quad T(\Delta k) = \frac{\Delta k}{\Delta k + ic}, \tag{2.5}$$

and the scattering operator (in the reflection-diagonal representation) is

$$S(\Delta k) = \begin{pmatrix} R(\Delta k)\ T(\Delta k) \\ T(\Delta k)\ R(\Delta k) \end{pmatrix} = R(\Delta k) + T(\Delta k)\hat{P}, \tag{2.6}$$

where $\hat{P}$ is the operator that permutes two particles. One can easily verify that a solution of Eq. (2.4) is given by

$$\begin{aligned} &\psi(1,2|1,2) = k_1 - \lambda - ic/2; \qquad \psi(2,1|1,2) = -(k_2 - \lambda + ic/2); \\ &\psi(1,2|2,1) = -(k_2 - \lambda - ic/2); \quad \psi(2,1|2,1) = k_1 - \lambda + ic/2, \end{aligned} \tag{2.7}$$

where λ is an auxiliary variable.

Let us have a look now at the 3-body case. The wave function is given by equation (2.3) with $3! \times 3!$ different coefficients $\psi(Q|P)$. The relation between the coefficients $\psi(Q|123)$ and $\psi(Q|213)$ is given by the $3! \times 3!$ scattering operator $S_{21}^{12} = R_{21}\mathbb{I} + T_{21}P^{12}$, where $R_{21} = \frac{-ic}{k_2 - k_1 + ic}$, $T_{21} = \frac{k_2 - k_1}{k_2 - k_1 + ic}$ and P^{12} is the operator that permutes particles 1 and 2:

$$\begin{pmatrix} \psi(123|123) \\ \psi(132|123) \\ \psi(321|123) \\ \psi(213|123) \\ \psi(231|123) \\ \psi(312|123) \end{pmatrix} = \begin{pmatrix} R_{21} & 0 & 0 & T_{21} & 0 & 0 \\ 0 & R_{21} & 0 & 0 & 0 & T_{21} \\ 0 & 0 & R_{21} & 0 & T_{21} & 0 \\ T_{21} & 0 & 0 & R_{21} & 0 & 0 \\ 0 & 0 & T_{21} & 0 & R_{21} & 0 \\ 0 & T_{21} & 0 & 0 & 0 & R_{21} \end{pmatrix} \begin{pmatrix} \psi(123|213) \\ \psi(132|213) \\ \psi(321|213) \\ \psi(213|213) \\ \psi(231|213) \\ \psi(312|213) \end{pmatrix}. \tag{2.8}$$

There are five other scattering relations for the rest of the coefficients.

In general, for arbitrary N, the scattering operator is a $N! \times N!$ operator acting on the $N!$ vector of amplitudes in the following way:

$$\begin{pmatrix} \psi(Q^1|P) \\ \psi(Q^2|P) \\ \psi(Q^3|P) \\ \vdots \\ \psi(Q^{N!}|P) \end{pmatrix} = (R_{ji}\mathbb{I} + T_{ji}\hat{P}^{ij}) \begin{pmatrix} \psi(Q^1|P') \\ \psi(Q^2|P') \\ \psi(Q^3|P') \\ \vdots \\ \psi(Q^{N!}|P') \end{pmatrix}, \tag{2.9}$$

where $Q^1 = (1, 2, 3, \cdots, N)$, $Q^2 = (2, 1, 3, \cdots, N)$, and so on, are the permutation for the identities of the particles; and $P = (1, \cdots, i, \cdots, j, \cdots, N)$ and $P' = (1, \cdots, j, \cdots, i, \cdots, N)$ are two different permutations for the momenta. The operator $\hat{P}^{ij}$ is the $(N! \times N!)$-dimensional permutator of particles i and j. One can verify that the scattering operator $S_{ij}^{ab} = R_{ij} + T_{ij}\hat{P}^{ab}$ fulfils the Yang-Baxter conditions (1.8):

$$\begin{aligned} S_{ij}^{ab} S_{ji}^{ab} &= 1 \\ S_{jk}^{ab} S_{ik}^{bc} S_{ij}^{ab} &= S_{ij}^{bc} S_{ik}^{ab} S_{jk}^{bc}. \end{aligned} \tag{2.10}$$

Thus, knowing the coefficients $\psi(Q^i|P)$ in the sector P all the rest are uniquely determined by the scattering. In the N-body case, the relation between the coefficients of the wave function Eq. (2.3) following from Eq. (2.9) is

$$\psi(Q|P) = R_{l+1,l}\ \psi(Q|P(l, l+1)) + T_{l+1,l}\ \psi(Q(l, l+1)|P(l, l+1)), \tag{2.11}$$

where $P(l, l+1)$ and $Q(l, l+1)$ are the permutations interchanging the elements l and $l+1$, and $R_{l+1,l} = \frac{-ic}{k_{P(l+1)} - k_{Pl} + ic}$ and $T_{l+1,l} = \frac{k_{P(l+1)} - k_{Pl}}{k_{P(l+1)} - k_{Pl} + ic}$.

Let us assume that, for the case of three particles, particles 1 and 2 have spin up and particle 3 has spin down. Then the antysymmetry under permutation of two identical fermions leads to the relations $\psi(123|P) = -\psi(213|P)$, $\psi(321|P) = -\psi(312|P)$ and $\psi(132|P) = -\psi(231|P)$. Therefore we need to determine only 6×3 coefficients:

$$\Phi(1|P) = \epsilon_P \psi(312|P), \quad \Phi(2|P) = \epsilon_P \psi(231|P), \quad \Phi(3|P) = \epsilon_P \psi(123|P), \tag{2.12}$$

where $\Phi(y|P)$ is the amplitude of the wave function with the down-spin particle at position y and ϵ_P is the sign of the permutation P. Hence the relations between the coefficients Φ are:

$$\begin{aligned} &\Phi(y|P) = \Phi(y|P(l, l+1)), \text{ if } y \neq l, l+1, \\ &\Phi(l|P) = \tilde{R}_{P(l+1),Pl}\ \Phi(l|P(l, l+1)) + \tilde{T}_{P(l+1),Pl}\ \Phi(l+1|P(l, l+1)), \\ &\Phi(l+1|P) = \tilde{R}_{P(l+1),Pl}\ \Phi(l+1|P(l, l+1)) + \tilde{T}_{P(l+1),Pl}\ \Phi(l|P(l, l+1)), \end{aligned} \tag{2.13}$$

where the new transmission and reflexion coefficients are $\tilde{R}_{l+1,l} = -R_{l+1,l}$ and $\tilde{T}_{l+1,l} = T_{l+1,l}$. The change of sign in $\tilde{R}$ is due to the new permutation symmetry of the particles: the antisymmetry under exchange of identical fermions is already taken into account in the definition of Φ. A solution to equations (2.13) is:

$$\begin{aligned}
\Phi(1;P) &= A\ (k_{P2} - \lambda - ic/2)(k_{P3} - \lambda - ic/2), \\
\Phi(2;P) &= A\ (k_{P1} - \lambda + ic/2)(k_{P3} - \lambda - ic/2), \\
\Phi(3;P) &= A\ (k_{P1} - \lambda + ic/2)(k_{P2} - \lambda + ic/2),
\end{aligned} \tag{2.14}$$

where A is a coefficient. One can easlily generalise to the case with N particles and one down spin, $M = 1$:

$$\Phi(y;P) = A\ F_P(y,\lambda), \quad F_P(y,\lambda) = \prod_{j=1}^{y-1}(k_{Pj} - \lambda + ic/2) \prod_{l=y+1}^{N}(k_{Pl} - \lambda - ic/2). \tag{2.15}$$

For a general number of particles N and a general number of down spins M we have to consider the amplitudes $\Phi(y_1, y_2, \ldots, y_M|P)$, where $y_1 < y_2 < \cdots < y_M$ are the positions of the down-spin particles along the chain. The relations among these amplitudes are:

$$\begin{aligned}
&\Phi(y_1, y_2, \ldots, y_M|P) = \Phi(y_1, y_2, \ldots, y_M|P(l, l+1)), \quad \text{for } y_\alpha \neq l, l+1; \\
&\Phi(y_1, y_2, \ldots, y_M|P) = R_{l,l+1}\Phi(y_1, y_2, \ldots, y_\alpha, \ldots, y_M|P(l, l+1)) + \\
&\quad T_{l,l+1}\Phi(y_1, y_2, \ldots, y_\alpha + 1, \ldots, y_M|P(l, l+1)), \quad \text{for } y_\alpha = l \text{ and } y_\alpha \neq l+1; \\
&\Phi(y_1, y_2, \ldots, y_M|P) = R_{l,l+1}\Phi(y_1, y_2, \ldots, y_\alpha, \ldots, y_M|P(l, l+1)) + \\
&\quad T_{l,l+1}\Phi(y_1, y_2, \ldots, y_\alpha - 1, \ldots, y_M|P(l, l+1)), \quad \text{for } y_\alpha \neq l \text{ and } y_\alpha = l+1; \\
&\Phi(y_1, y_2, \ldots, y_M|P) = \Phi(y_1, y_2, \ldots, y_M|P(l, l+1)), \quad \text{for } y_\alpha = l \text{ and } y_\alpha = l+1.
\end{aligned} \tag{2.16}$$

A solution to these equations is given by the generalised Bethe ansatz:

$$\Phi(y_1, y_2, \ldots, y_M|P) = \sum_R A(R)\ F_P(y_1, \lambda_{R1})F_P(y_2, \lambda_{R2}) \ldots F_P(y_M, \lambda_{RM}), \tag{2.17}$$

where R is the permutation of the M down-spin particles. Using the relations Eq. (2.16) with $R' = R(\alpha, \alpha+1)$ and $P' = P(y_\alpha, y_\alpha + 1)$, we can write

$$A(R)\ F_P(y_\alpha, \lambda_{R\alpha})F_P(y_\alpha + 1, \lambda_{R(\alpha}+1)) + A(R')\ F_P(y_\alpha, \lambda_{R(\alpha+1)})F_P(y_\alpha + 1, \lambda_{R\alpha}) =$$

$$A(R)\ F_{P'}(y_\alpha, \lambda_{R\alpha}) F_{P'}(y_\alpha + 1, \lambda_{R(\alpha}+1)) + A(R')\ F_{P'}(y_\alpha, \lambda_{R(\alpha+1)}) F_{P'}(y_\alpha + 1, \lambda_{R\alpha}),$$

therefore,

$$A(R)(\lambda_{R(\alpha+1)} - \lambda_{R\alpha} - ic) + A(R')(\lambda_{R\alpha} - \lambda_{R(\alpha+1)} - ic) = 0. \tag{2.18}$$

This condition is satisfied by

$$A(R) = \epsilon_R \prod_{j<l} (\lambda_{Rj} - \lambda_{Rl} - ic). \tag{2.19}$$

The wave function (2.17) is the solution to the Hamiltonian of the problem, Eq. (2.1).

We will now impose periodic boundary conditions. Let us first look at the case with two particles only. In this case $\Psi(x_1 + L, x_2) = \Psi(x_1, x_2)$ with $x_1 + L > x_2$ ($Q = (2, 1)$) for the l.h.s and $x_1 < x_2$ ($Q = (1, 2)$) for the r.h.s.:

$$\begin{aligned} \Psi(x_1 + L, x_2) &= \psi(21, 12) e^{ix_1k_2 + ix_2k_1} e^{iLk_2} + \psi(21, 21) e^{ix_1k_1 + ix_2k_2} e^{iLk_1} = \\ &= \Psi(x_1, x_2) = \psi(12, 12) e^{ix_1k_1 + ix_2k_2} + \psi(12, 21) e^{ix_1k_2 + ix_2k_1}. \end{aligned} \tag{2.20}$$

We also have $\Psi(x_1, x_2 + L) = \Psi(x_1, x_2)$, with $x_2 + L > x_1$ ($Q = (1, 2)$) for the l.h.s and $x_2 < x_1$ ($Q = (2, 1)$) for the r.h.s.,

$$\begin{aligned} \Psi(x_1, x_2 + L) &= \psi(12, 12) e^{ix_1k_1 + ix_2k_2} e^{iLk_2} + \psi(12, 21) e^{ix_1k_2 + ix_2k_1} e^{iLk_1} = \\ &= \Psi(x_1, x_2) = \psi(21, 12) e^{ix_1k_2 + ix_2k_1} + \psi(21, 21) e^{ix_1k_1 + ix_2k_2}. \end{aligned} \tag{2.21}$$

We therefore have for the scattering process:

$$\begin{aligned} \begin{pmatrix} \psi(1,2|1,2) \\ \psi(2,1|1,2) \end{pmatrix} e^{ik_2L} &= \begin{pmatrix} T & R \\ R & T \end{pmatrix} \begin{pmatrix} \psi(1,2|1,2) \\ \psi(2,1|1,2) \end{pmatrix}; \\ \begin{pmatrix} \psi(1,2|2,1) \\ \psi(2,1|2,1) \end{pmatrix} e^{ik_1L} &= \begin{pmatrix} 0 & 1 \\ 1 & 0 \end{pmatrix} \begin{pmatrix} R & T \\ T & R \end{pmatrix}^{-1} \begin{pmatrix} \psi(1,2|2,1) \\ \psi(2,1|2,1) \end{pmatrix}. \end{aligned} \tag{2.22}$$

Equations (2.22) tell us that after scattering around the ring and returning to its initial position a particle acquires a phase $\exp ik_jL$.

In the case with N particles the periodic boundary condition reads for the wave function $\Psi(x_N - L, x_1, \ldots, x_{N-1}) = \Psi(x_1, x_2, \ldots, x_N)$. Therefore for each of the

coefficients of this wave function we have $\Psi(Q|P)\ exp(ik_{PN}L) = \Psi(Q'|P')$, with $Q=(Q1, Q2, \ldots, QN)$ and $Q'=(QN, Q1, \ldots, Q(N-1))$; and $P=(P1, P2, \ldots, PN)$ and $P'=(PN, P1, \ldots, P(N-1))$. After scattering of one particle with the $N-1$ others it will return to its initial position with an extra phase $\lambda_j = \exp(ip_jL)$. In terms of the function Φ we can write

$$\Phi(y_1, y_2, \ldots, y_M; P)e^{ik_{PN}L} = \Phi(y_1+1, y_2+1, \ldots, y_M+1; PN, P1, \ldots, P(N-1)),$$
$$\Phi(y_1, y_2, \ldots, y_{M-1}, N+1; P) = \Phi(1, y_1, y_2, \ldots, y_{M-1}; P). \tag{2.23}$$

We have two different situations, for $y_M = N$ and for $y_M \neq N$. Let us first take into account the case with $y_M \neq N$. Using the solution of the wave function Eq. (2.17) we have the relation

$$e^{ik_{PN}L} = \prod_{\alpha=1}^{M} \frac{k_{PN} - \lambda_\alpha + ic/2}{k_{PN} - \lambda_\alpha - ic/2}. \tag{2.24}$$

In the case $y_M = N$, using the equation above we get

$$\Phi(y_1, \ldots, N; P) \prod_{\alpha=1}^{M} \frac{k_{PN} - \lambda_\alpha + ic/2}{k_{PN} - \lambda_\alpha - ic/2} = \Phi(1, y_1+1, \ldots, y_{M-1}+1; P'), \tag{2.25}$$

where $P' = (PN, P1, P2, \ldots, P(N-1)$. This relation is satisfied by

$$A(R) = A(RM, R1, \ldots, R(M-1)) \prod_{j=1}^{N} \frac{k_{Pj} - \lambda_{RM} - ic/2}{k_{Pj} - \lambda_{RM} + ic/2}; \tag{2.26}$$

substituting the expression for $A(R)$ we get the second relation

$$\prod_{j=1}^{N} \frac{k_j - \lambda_{RM} + ic/2}{k_j - \lambda_{RM} - ic/2} = -\prod_{\alpha=1}^{M} \frac{\lambda_{RM} - \lambda_\alpha - ic}{\lambda_{RM} - \lambda_\alpha + ic}. \tag{2.27}$$

Taking the logarithm of equations (2.24) and (2.27) we have

$$p_jL = 2\pi I_j - 2\sum_{\beta=1}^{N_\downarrow} \arctan\left(\frac{p_j - \lambda_\beta}{c/2}\right), \tag{2.28}$$
$$\pi J_\alpha - \sum_{j=1}^{N} \arctan\left(\frac{p_j - \lambda_\alpha}{c/2}\right) = \sum_{\beta=1}^{N_\downarrow} \arctan\left(\frac{\lambda_\alpha - \lambda_\beta}{c}\right).$$

These two equations are the Bethe ansatz equations for a system of N fermions with M down-spin particles. When taking the logarithm, care has to be taken to add $2\pi in$ terms, with n being an integer. Taking this into account, we see that the N numbers I_j are integer for even number of down-spin particles and half-odd-integer for odd number of down-spin particles, $I_j \equiv \left(\frac{N_\downarrow}{2}\right) \mathrm{mod}(1)$; and the set of $N_\downarrow$ numbers J_α are integers if the combination $N - N_\downarrow$ is an odd number, or half-odd-integers if it is even, $J_\alpha \equiv \left(\frac{N-N_\downarrow+1}{2}\right) \mathrm{mod}(1)$. The energy reads:

$$E = \frac{\hbar^2}{2m} \sum_{j=1}^{N} p_j^2, \tag{2.29}$$

where L is the length of the system; the total momentum is $P = \sum_{j=1}^{N} p_j = 2\pi \left(\sum I_j + \sum J_\alpha\right)/L$.

Thus an eigenstate of the Hamiltonian Eq. (2.1) is characterized by a set of N density quantum numbers I_j, $(j = 1, \ldots, N)$, and $N_\downarrow$ spin quantum numbers J_α, $(\alpha = 1, \ldots, N_\downarrow)$, which define a set of N quasi-momenta p_j and $N_\downarrow$ spin rapidities λ_α: they satisfy the set of Bethe ansatz coupled equations. The ground state, for N even and $N_\downarrow$ odd, is given by the set of quantum numbers $I_j = \left\{-\frac{N-1}{2}, \ldots, \frac{N-1}{2}\right\}$ and $J_\alpha = \left\{-\frac{N_\downarrow-1}{2} \ldots, \frac{N_\downarrow-1}{2}\right\}$. If we want to construct the ground state for a different combination of N and $N_\downarrow$ other than even/odd we will not be able to satisfy $\sum I_j = 0$ and $\sum J_\alpha = 0$ and the ground state will have a current.

Taking the thermodynamic limit $N \to \infty$ and $L \to \infty$, keeping $n = N/L$ and $n_\downarrow = N_\downarrow/L$ constant, we define the densities of p and λ as $\rho(p) = L^{-1}\frac{\partial I}{\partial p}$ and $\sigma(\lambda) = L^{-1}\frac{\partial J}{\partial \lambda}$. Then the Bethe ansatz equations become:

$$\begin{aligned}
\rho(p) &= \frac{1}{2\pi} + \frac{1}{\pi} \int_{-B}^{B} \frac{2}{1 + 4(p-\lambda)^2} \sigma(\lambda) d\lambda, \\
\sigma(\lambda) &= \frac{1}{\pi} \int_{-Q}^{Q} \frac{2}{1 + 4(p-\lambda)^2} \rho(p) dp \\
&\quad - \frac{1}{\pi} \int_{-B}^{B} \frac{1}{1 + 4(\lambda - \lambda')^2} \sigma(\lambda') d\lambda',
\end{aligned} \tag{2.30}$$

where we have rescaled all the parameters by c: $\lambda = \lambda/c$, $p = p/c$, $B = B/c$, $Q = Q/c$. The cut-offs B and Q are determined by fixing the number of particles

of the system

$$\frac{n}{c} = \int_{-Q}^{+Q} \rho(p)dp; \ \frac{n_\downarrow}{c} = \int_{-B}^{+B} \sigma(\lambda)d\lambda. \tag{2.31}$$

The expression for the energy reads

$$E(n,s) = \frac{\hbar c^3}{2m} \int_{-Q}^{Q} p^2 \rho(p)dp; \tag{2.32}$$

and the magnetisation is defined as $s = n_\uparrow - n_\downarrow$. The coupling strength is controlled by the parameter $\gamma^{-1} = n/c$, Eq. (2.31), the weak coupling regime corresponding to $n/c \gg 1$, and the strong coupling one to $n/c \ll 1$.

2.2 Phase diagram

We now construct the ground state phase diagram of the system under consideration. This is done by analysing the integral equations that determine the distribution of Bethe ansatz roots in the ground state, Eq. (2.30). The different phases are identified by considering the integration boundaries Q and B as control parameters, and the phase diagram is given as a function of the chemical potential μ and the magnetic field h. Since there is a coexistence of two components we can rewrite the total chemical potential and magnetic field as

$$\mu = \frac{\mu_\uparrow + \mu_\downarrow}{2} \quad h = \frac{\mu_\uparrow - \mu_\downarrow}{2}, \tag{2.33}$$

where $\mu_{\uparrow,\downarrow}$ are the chemical potentials relative to each component.

For two-component fermions with repulsive δ-function interactions three phases appear: a balanced phase, where the number of up and down spin particles is the same, $n_\uparrow = n_\downarrow$ or equivalently the magnetisation is zero, $s = 0$; a fully polarised phase for which the density of spin-down particles vanishes and there is only majority component, $n_\downarrow = 0$, or equivalently $n_\uparrow = n = s$; and a partially polarised phase, that contains an imbalanced mixture of up and down spins $0 < s < n$. Next, we calculate the boundaries between the three phases.

2.2.1 Balance

In the balanced phase the number of up spin particles equals the number of down spin ones, and so the magnetisation is zero, $s = 0$. Note that the system under consideration is gapless, therefore any applied magnetic field breaks the balance between up and down spins. Consequently, the balanced phase exists only without the presence of an external magnetic field. Thus in the (h, μ) plane the balanced phase is located at the line $h = 0$. The border between this phase and the partially polarised one is the line $h = 0$ for any chemical potential μ.

2.2.2 Saturation

The saturation line in the phase diagram is the one below which the systems becomes fully polarised. This happens when the number of down-spin particles becomes zero, $n_\downarrow = 0$, which is equivalent to $s = n$. We want to calculate the border between the partially polarised phase and the fully polarised one. There is a small parameter in this limit, $n - s \sim 0$, which in the Bethe ansatz equations (2.31) translates to $B \sim 0$.

In order to calculate the magnetic field and the chemical potential at saturation we can follow two different schemes. In the first one we will calculate the magnetic field and the chemical potential from the Bethe ansatz equations (2.30), and after doing so we will take the saturation limit. In the second approach, we will calculate directly the expression for the energy close to saturation and then, taking its derivatives, we obtain the magnetic field and chemical potential at saturation.

In the first approach, we write the expressions for the chemical potential and magnetic field from Eq. (2.32) as:

$$\begin{aligned} h &= \frac{\partial E(n,s)/L}{\partial s} = \frac{\hbar^2 c^3}{2m}\frac{\partial}{\partial s}\int_{-Q}^{Q} p^2 \rho(p) dp = \\ &= \frac{\hbar^2 c^3}{2m}\left(\frac{\partial}{\partial Q}\int_{-Q}^{Q} p^2\rho(p)dp\,\frac{\partial Q}{\partial s} + \frac{\partial}{\partial B}\int_{-Q}^{Q} p^2\rho(p)dp\,\frac{\partial B}{\partial s}\right); \\ \mu &= \frac{\partial E(n,s)/L}{\partial n} = \frac{\hbar^2 c^3}{2m}\frac{\partial}{\partial n}\int_{-Q}^{Q} p^2 \rho(p) dp = \end{aligned}$$

$$= \frac{\hbar^2 c^3}{2m}\left(\frac{\partial}{\partial Q}\int_{-Q}^{Q} p^2\rho(p)dp\,\frac{\partial Q}{\partial n} + \frac{\partial}{\partial B}\int_{-Q}^{Q} p^2\rho(p)dp\,\frac{\partial B}{\partial n}\right). \qquad (2.34)$$

From the equations for the number of particles, Eq. (2.31), we can obtain the derivatives of the density of particles n and the magnetisation s with respect to the cut-offs Q and B in the limit $B = 0$:

$$\begin{aligned}
\left.\frac{\partial n}{\partial Q}\right|_{B=0} &= \frac{c}{\pi}; \quad \left.\frac{\partial n}{\partial B}\right|_{B=0} = \frac{4c}{\pi^3}\arctan^2(2Q);\\
\left.\frac{\partial s}{\partial Q}\right|_{B=0} &= \frac{c}{\pi}; \quad \left.\frac{\partial s}{\partial B}\right|_{B=0} = \arctan(2Q)\left(\frac{4c}{\pi^3}\arctan(2Q) - \frac{4c}{\pi^2}\right), \qquad (2.35)
\end{aligned}$$

and by inverting the Jacobian, the derivatives of Q and B with respect to n and s become:

$$\begin{aligned}
\left.\frac{\partial Q}{\partial n}\right|_{B=0} &= -\frac{\pi}{c}\left(\frac{\arctan(2Q)}{\pi} - 1\right); \quad \left.\frac{\partial Q}{\partial s}\right|_{B=0} = \frac{1}{c}\arctan(2Q);\\
\left.\frac{\partial B}{\partial n}\right|_{B=0} &= \frac{\pi^2}{4\arctan(2Q)}; \qquad \left.\frac{\partial B}{\partial s}\right|_{B=0} = -\frac{\pi^2}{4c\arctan(2Q)}. \qquad (2.36)
\end{aligned}$$

On the other hand, in this particular limit the derivatives of the energy Eq. (2.32) are

$$\begin{aligned}
\left.\frac{\partial E(n,s)/L}{\partial Q}\right|_{B=0} &= \frac{\hbar^2 c^3}{2m}\frac{Q^2}{\pi};\\
\left.\frac{\partial E(n,s)/L}{\partial B}\right|_{B=0} &= \frac{\hbar^2 c^3}{2m}\frac{\arctan(2Q)}{\pi^3}(2Q - \arctan(2Q)). \qquad (2.37)
\end{aligned}$$

Combining equations (2.34), (2.36) and (2.37) we obtain the values of the magnetic field and chemical potential at saturation:

$$\begin{aligned}
h_s &= 2\epsilon_B\left(\frac{Q_0^2}{\pi}\arctan(2Q_0) - \frac{Q_0}{2\pi} + \frac{\arctan(2Q_0)}{4\pi}\right),\\
\mu_s &= -h + 2\epsilon_B Q_0^2, \qquad (2.38)
\end{aligned}$$

where $\epsilon_B = \hbar^2 c^2/4m$ is the binding energy and $Q_0 = n\pi/c$ is the Fermi momentum. Note that the saturation line crosses the point $(0, 0)$, which is a consequence of the fact that there is no gap in the excitation spectrum of the system.

For the strongly interacting regime, where $Q_0 \to 0$ or equivalently $h \ll \epsilon_B$, the chemical potential tends to zero as

$$\frac{h_s}{\epsilon_B} = \frac{8Q^3}{3\pi}; \qquad \frac{\mu_s}{\epsilon_B} = -\frac{8Q^3}{3\pi} + 2Q^2$$
$$\Rightarrow \frac{\mu_s}{\epsilon_B} = -\frac{h_s}{\epsilon_B} + 2\left(\frac{3\pi}{8}\frac{h_s}{\epsilon_B}\right)^{2/3}. \tag{2.39}$$

For the weakly interacting regime we have $Q_0 \to \infty$ or equivalently $h \gg \epsilon_B$, in this case the chemical potential diverges:

$$\frac{h_s}{\epsilon_B} = Q^2 - \frac{2Q}{\pi} + \frac{1}{4} - \frac{1}{6\pi Q}; \qquad \frac{\mu_s}{\epsilon_B} = Q^2 + \frac{2Q}{\pi} - \frac{1}{4} + \frac{1}{6\pi Q}$$
$$\Rightarrow \frac{\mu_s}{\epsilon_B} = \frac{h_s}{\epsilon_B} + \frac{4}{\pi}\sqrt{\frac{h_s}{\epsilon_B}} + \left(\frac{4}{\pi^2} - \frac{1}{2}\right). \tag{2.40}$$

An alternative approach to calculate the magnetic field and chemical potential at saturation involves an expansion of the energy in the small parameter $(n-s)$. In order to calculate the magnetic field and chemical potential we should know the energy up to the first order in $(n-s)$. We compute it up to the second order, which allows us to also compute also the magnetic susceptibility in this regime.

From equations (2.30) and (2.31) we can eliminate the density of rapidities $\sigma(\lambda)$ using the relation

$$\int_{-B}^{B} f(\lambda)\sigma(\lambda)d\lambda = f(\lambda^*)\int_{-B}^{B}\sigma(\lambda)d\lambda,\ -B < \lambda^* < B, \tag{2.41}$$

and we obtain an equation for the number of particles and for the energy:

$$\frac{E(n,s)}{L} = \frac{\hbar^2 c^3}{2m}\left(\frac{Q^3}{3\pi} + \frac{n-s}{c}\frac{1}{2\pi}\int_{-Q}^{Q}\frac{2p^2}{1+4p^2}dp\right) =$$
$$= \frac{\hbar^2 c^3}{2m}\left[\frac{Q^3}{3\pi} + \frac{(n-s)}{c}\frac{1}{2\pi}\left(Q - \frac{1}{2}\arctan(2Q)\right)\right], \tag{2.42}$$
$$Q = \frac{n\pi}{c} + \frac{n-s}{c}\frac{1}{\pi}\arctan(2Q). \tag{2.43}$$

We can solve the equation for Q up to second order in $(n-s)$ making a Taylor expansion:

$$Q = Q_0 + \left.\frac{\partial Q}{\partial(n-s)}\right|_0 \frac{n-s}{c} + \frac{1}{2!}\left.\frac{\partial^2 Q}{\partial(n-s)^2}\right|_0 \frac{(n-s)^2}{c^2} + \cdots. \tag{2.44}$$

Taking the derivatives in $(n-s)$ from equation (2.43) we obtain for Q:

$$Q = Q_0 - \frac{n-s}{c}\arctan(2Q_0) + \frac{(n-s)^2}{c^2}\frac{\arctan(2Q_0)}{1+4Q_0^2}. \tag{2.45}$$

Then we can calculate the energy from equation (2.42) substituting the expression for Q. Taking the derivatives with respect to s and m we obtain for the magnetic field and chemical potential at saturation:

$$\begin{aligned} h_s &= 2\epsilon_B\left(\frac{Q_0^2}{\pi}\arctan(2Q_0) - \frac{Q_0}{2\pi} + \frac{\arctan(2Q_0)}{4\pi}\right), \\ \mu_s &= -h + 2\epsilon_B Q_0^2, \end{aligned} \tag{2.46}$$

which are again equations (2.38). The two approaches are equivalent, but the second one allows us to calculate in a straightforward way the susceptibility at saturation, taking the second derivative of the energy with respect to the magnetisation:

$$\chi_s^{-1} = \left.\frac{\partial^2 E(n,s)}{\partial s^2}\right|_{s=n} = \frac{2\epsilon_B}{c}\left(\frac{2Q_0}{\pi}\arctan^2(2Q_0)\right). \tag{2.47}$$

We see that the susceptibility only diverges in the limit of the empty band ($Q_0 = 0$) and in the limit of infinite interaction, and remains finite otherwise.

We finally want to compare the results of the mean-field approximation with the exact ones. In the mean field approach we can write the energy of the ground state for a two-component Fermi gas as $E(n_\uparrow, n_\downarrow) = gn_\uparrow n_\downarrow + \hbar^2/2m(n_\uparrow^3 + n_\downarrow^3)\pi^2/3$. Taking the derivatives of the energy with respect to the total density n and the magnetisation s we obtain in this approximation

$$\frac{h_s}{\epsilon_B} = Q^2 - \frac{2Q}{\pi}; \qquad \frac{\mu_s}{\epsilon_B} = Q^2 + \frac{2Q}{\pi}, \tag{2.48}$$

which is the same result as equation (2.40), up to a constant value. Therefore, we see how the mean-field approach gives a reasonable approximation for the weakly interacting regime in one dimension.

This phase transition is of the commensurate-incommensurate type, since the system goes from a non-gapped phase to a phase containing a gap in the excitation

spectrum. All the calculations have been performed for the case with a fixed number of particles, which in experiments with ultra-cold atoms is more relevant than the case with a fixed chemical potential. In this case one does not expect any divergence due to the flat band, since the constraint of a fixed number of particles does not allow the system to populate all the states available at the bottom of the band when approaching saturation. In other words, the van Hove singularity is not present and so we do not expect a divergence of the magnetic susceptibility at saturation.

2.2.3 Vacuum

The vacuum corresponds to the absence of any particles, $n = 0$. Consider first the inequality $n_\downarrow < n_\uparrow$, which means that unless we consider the balanced case, we first reach $n_\downarrow = 0$ rather than $n_\uparrow = 0$. We are therefore concerned with the situation where $n_\uparrow$ becomes zero, which is equivalent to imposing the chemical potential for the majority component to become zero, $\mu_\uparrow = 0$. Thus, in the chemical potential versus magnetic field phase diagram the boundary for the vacuum state (μ_v) corresponds to:

$$\mu_\downarrow = \frac{h + \mu_v}{2} = 0 \longrightarrow \mu_v = -h. \tag{2.49}$$

The vacuum line Eq. (2.49) never crosses the saturation line Eq. (2.38), meaning that there is no boundary between the partially polarised phase and the vacuum, except for the case of balance. This implies that for any imbalance the system cannot have a direct transition from the partially polarised phase to the vacuum without crossing the fully polarised phase.

2.2.4 Results

The phase diagram of the system is presented in Fig. (2.2). We can recognise here the different phases of the system. The balanced phase exists only at the boundary $h = 0$ and thus is not present in the plot. The partially polarised phase appears between the balanced one and the fully polarised one. The border between the partially polarised phase and the fully polarised one is the saturation

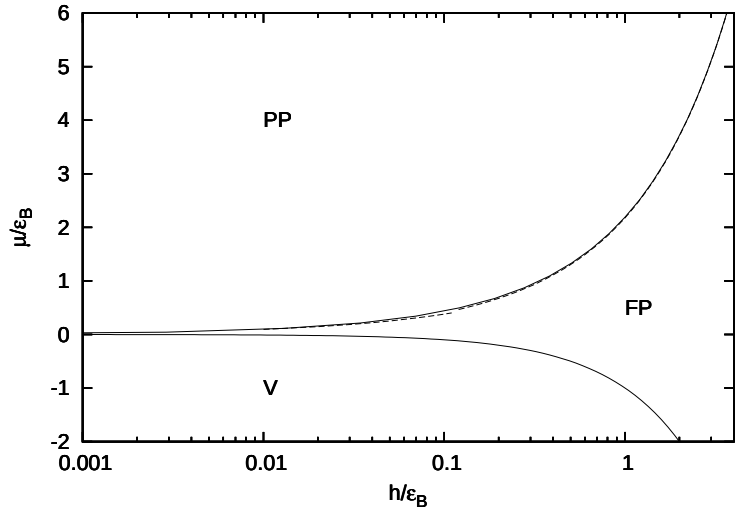

Figure 2.2: Phase diagram in the plane μ/ϵ_B and h/ϵ_B. The partially polarised phase (PP), fully polarised phase (FP) and vacuum (V) are displayed. The dashed lines correspond to the asymptotes discussed in the text.

line Eq. (2.38), and the dashed lines in the plot are the asymptotes discussed above, Eq. (2.39) and (2.40). Finally, the vacuum phase is also displayed. Note that there is no boundary between the partially polarised phase and the vacuum. We also note that the saturation line crosses the point $(h = 0, \mu = 0)$ giving evidence for the absence of a gap in the system.

2.3 Trapped density profiles

We consider now the system in an external trapping potential. We take the trapping potential as a harmonic potential, $V_{ext} = m\omega_z^2 z^2/2$, because this is the case in most experimental set-ups. Under these circumstances the system is non-homogeneous, and therefore is not exactly solvable any more. Despite this fact, using the theory of the local density approximation (see Appendix C), in certain cases we can approximate very well the features of the cloud in the inhomogeneous

configuration. This allows us to write the local equilibrium conditions

$$\mu_\uparrow(n_\uparrow(z), n_\downarrow(z)) = \mu_\uparrow^0 - V_{ext}, \quad \mu_\downarrow(n_\uparrow(z), n_\downarrow(z)) = \mu_\downarrow^0 - V_{ext}. \tag{2.50}$$

In order to be able to apply the local density approximation treatment we need the size of the cloud to be much bigger than the characteristic length of the potential $a_z = \sqrt{\hbar/m\omega_z}$.

We have a system of two-components that we label by their spin indices, and we define the total chemical potential and the magnetic field as

$$\begin{aligned} \mu(n_\uparrow(z), n_\downarrow(z)) &= \frac{\mu_\uparrow(n_\uparrow(z), n_\downarrow(z)) + \mu_\downarrow(n_\uparrow(z), n_\downarrow(z))}{2} \\ h(n_\uparrow(z), n_\downarrow(z)) &= \frac{\mu_\uparrow(n_\uparrow(z), n_\downarrow(z)) - \mu_\downarrow(n_\uparrow(z), n_\downarrow(z))}{2}, \end{aligned} \tag{2.51}$$

where $n_{\uparrow,\downarrow}(z)$ is the local density of each of the two atomic components. Therefore, the chemical potential and the magnetic field depend on the position z through the local densities. Since we consider the two components as being two different hyperfine states of the same atom, the external potential acts in the same way on both, $\mu_{\uparrow,\downarrow} = \mu_{\uparrow,\downarrow}^0 - \frac{1}{2}m\omega_z^2 z^2$. We can rewrite the chemical potential and magnetic field as

$$\mu(n_\uparrow(z), n_\downarrow(z)) = \mu^o - \frac{1}{2}m\omega_z^2 z^2, \qquad h(n_\uparrow(z), n_\downarrow(z)) = h^o, \tag{2.52}$$

where μ^o and h^o have been defined as $\mu^0 = (\mu_\uparrow^o + \mu_\downarrow^o)/2$ and $h^0 = (\mu_\uparrow^o - \mu_\downarrow^o)/2$. We see from Eq. (2.52) that the local magnetic field $h(z)$ is kept constant inside the trap, while the local chemical potential $\mu(z)$ decreases as we approach the boundaries of the cloud. In Fig. (2.3) the vertical arrow in the phase diagram follows the variation of the local chemical potential and local magnetic field inside the trap, and at the origin they take the values $h(0) = h^o$, $\mu(0) = \mu^o$.

The total number of particles, $N = N_\uparrow + N_\downarrow$, and the total magnetisation $S = N_\uparrow - N_\downarrow$, like in Eq. (C.10) from the Appendix C, are the two conserved quantities that fix the value of the normalisation constants μ^o and h^o, i.e. the value of the chemical potential and magnetic field in the centre of the trap. In the trapped configuration they are given by

$$N = \int_{-R}^{R} n(z)dz \qquad \text{and} \qquad S = \int_{-R}^{R} s(z)dz. \tag{2.53}$$

In order to calculate the density profiles we solve numerically Eqs. (2.52) for a given pair μ^o and h^o, i.e. for a fixed total number of particles and imbalance, with z ranging from $z = 0$ in the centre of the cloud to $z = R_{out}$ at the edges. For convenience, we define the dimensionless quantities $\tilde{z} = z a_{1D}/\sqrt{2}a_z^2$, $\tilde{n} = n/c$, $\tilde{s} = s/c$, and

$$N\frac{a_{1D}^2}{a_z^2} = 2\sqrt{2}\int_{-\tilde{R}}^{\tilde{R}} \tilde{n}(\tilde{z})d\tilde{z}, \qquad S\frac{a_{1D}^2}{a_z^2} = 2\sqrt{2}\int_{-\tilde{R}}^{\tilde{R}} \tilde{s}(\tilde{z})d\tilde{z}. \tag{2.54}$$

Numerically, we start by fixing N and S, i.e. B and Q, and we solve the Bethe ansatz equations (2.30) in the centre of the trap. In this way we obtain the normalisation constants μ^o and h^o. Then, we start moving towards the edges of the trap, by lowering the chemical potential $\mu = \mu^o - m\omega_z^2 z^2/2$ and making sure that we keep $h(z) = h^o$ constant, i.e. following the arrow in Fig. (2.3).

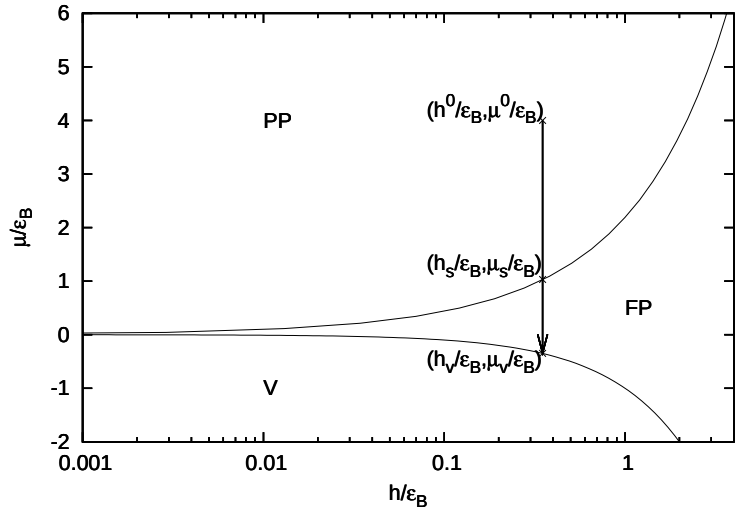

Figure 2.3: Phase diagram in the plane μ/ϵ_B and h/ϵ_B. The arrow follows the variation of $h(z)$ and $\mu(z)$ inside of the trap. Since $h(z)$ is constant the arrow is a vertical line. In the centre of the trap $h = h^0$ and $\mu = \mu^0$, when the line crosses the saturation line $h = h_s$ and $\mu = \mu_s$, given by Eq. (2.38), and when the arrow crosses the vacuum line $h = h_v$ and $\mu = \mu_v$, given by Eq. (2.49).

For each position z we solve the Bethe ansatz equations and thus calculate the corresponding total density $n(z)$, density of up-spin particles $n_\uparrow(z)$, density of down-spin particles $n_\downarrow(z)$, magnetisation $s(z)$, etc. The density profiles for two different values of the polarisation $P = (N_\uparrow - N_\downarrow)/N$ are shown in Fig. (2.4).

We can understand the density profile as follows: when moving along the trap, the chemical potential difference $h(z)$ remains constant while the chemical potential $\mu(z)$ decreases parabolically and so does the one-dimensional local density. The interaction strength $\gamma(z) = c/n(z)$ increases while we move away from the centre of the cloud, since it is inversely proportional to the one-dimensional local density. This explains why moving from the centre of the trap towards the edges of the cloud we find two different phases: at the centre we have an imbalanced mixed phase for any magnetic field h, while at the edges, where the two species become more repulsive, we find a fully polarised phase. We can see that there always exists a "slice" of fully polarised phase between the partially polarised phase and the vacuum. Since the system is gapless any applied magnetic field leads to the appearance of magnetisation and to the presence of a mixture of up and down spins, $s \neq 0$.

In three dimensions, the density profiles at a weak interaction strength present a similar qualitative structure [82]. However, when increasing the interaction strength in three dimensions a symmetry breaking occurs, driven by the competition between the repulsive interaction energy and the kinetic energy. As a result, the phase separation occurs: the minority component is pushed to the edges of the trap while the majority component accommodates in the centre. In one dimension we can calculate the limit of infinite inter-species interaction exactly by means of the exact mapping onto a fermionic Tonks-Girardeau gas (two-component Fermi gas with hard-core inter-species interaction) for which the density profile is known to be equivalent to that of $N = N_\uparrow + N_\downarrow$ bosons with Tonks-Girardeau point-like interaction [83, 84]. Therefore we expect no phase-separation in this limit in the one-dimensional configuration, which is consistent with our numerical calculations.

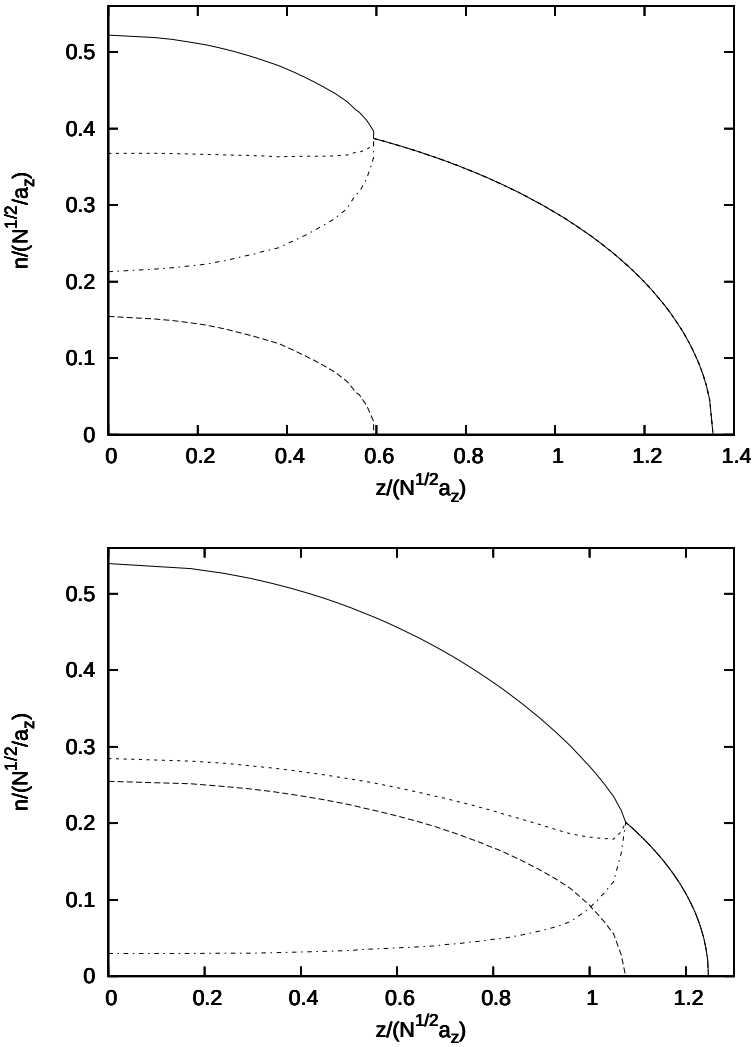

Figure 2.4: Density profile for polarisation $P = 0.7$ (top) and $P = 0.15$ (bottom) for $N(a_{1D}^2/a_z^2) = 1$. The solid line is the total density $n(z)/(\sqrt{N}/a_z)$, the dotted line is the density of up spins $n_\uparrow(z)/(\sqrt{N}/a_z)$, the dashed line is the density of down spins $n_\downarrow(z)/(\sqrt{N}/a_z)$ and the dashed-dotted line is the magnetisation $m(z)/(\sqrt{N}/a_z)$. We can see the two shells: the inner one contains an imbalanced mixture of up and down spins, while the external shell is fully polarised.

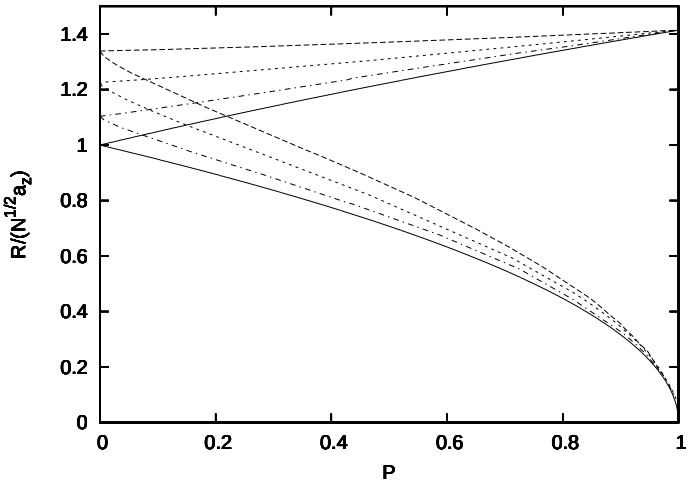

Figure 2.5: Radius of the inner (inferior line) and the outer (superior line) shells; for $N(a_{1D}^2/a_z^2) = \infty$ (solid line), $N(a_{1D}^2/a_z^2) = 10$ (dashed-dotted line), $N(a_{1D}^2/a_z^2) = 1$ (dotted line) and $N(a_{1D}^2/a_z^2) = 0.1$ (dashed line).

2.3.1 Size of the cloud

We can calculate the radii of the two shells of the cloud, similar to Eq. (C.10) from Appendix C. From Fig. (2.3) we see that the radius of the inner shell is determined by the point where the value of the the chemical potential coincides with the saturation line, $\mu(R_{in}) = \mu_s = \mu^o - m\omega_z^2 R_{in}^2/2$. Therefore we have

$$\frac{a_{1D}}{a_z^2} R_{in} = \sqrt{2\left(\frac{\mu^o}{\epsilon_B} - \frac{\mu_s}{\epsilon_B}\right)}. \tag{2.55}$$

Similarly the radius at the boundary of the cloud is given by the crossing of the vacuum line, $\mu(R_{out}) = \mu_v = \mu^o - m\omega_z^2 R_{out}^2/2$,

$$\frac{a_{1D}}{a_z^2} R_{out} = \sqrt{2\left(\frac{\mu^o}{\epsilon_B} - \frac{\mu_v}{\epsilon_B}\right)}. \tag{2.56}$$

Fig. (2.5) displays the variation of the radii of the inner and outer shells versus the polarisation P for different values of the coupling strength. We see that for a

fully polarised system, $P = 1$, the radius of the inner shell vanishes and the radius of the outer shell takes the value $\sqrt{2N}a_z$, which is the Thomas-Fermi radius for the cloud of N free fermions. In the other limit, where $P = 0$, the radii of the inner and the outer shells coincide, since the number of up-spin and down-spin atoms is the same.

We now discuss two limiting cases, namely $c = 0$ and $c = \infty$, for which we know an exact analytical result. In the case of free fermions, $c = 0$, we can treat the two clouds as being independent and we have to calculate the radius of each cloud following the theory of free fermions in a harmonic trap. The energy in this situation reads

$$E = \sum_{k=-k_F}^{k_F} \frac{\hbar^2 k^2}{2m} = \frac{L}{2\pi}\frac{\hbar^2}{2m}\int_{-k_F}^{k_F} k^2 dk = \frac{L}{3\pi}\frac{\hbar^2 k_F^3}{2m}, \tag{2.57}$$

where the Fermi momentum k_F is given by counting the number of available states

$$N = \frac{L}{2\pi}\int_{-k_F}^{k_F} dk \Rightarrow \frac{N}{L} = n = \frac{k_F}{\pi} \Rightarrow k_F = n\pi. \tag{2.58}$$

Applying the local density approximation condition Eq. (C.3) for a harmonic potential $V(x) = m\omega_z x^2/2$, and with $\mu = \partial E/\partial N = \hbar^2 k_F^2/2m$, we find

$$\begin{aligned} \frac{\hbar^2 k_F^2(x)}{2m} + V(x) = \mu_o \Rightarrow k_F(x) = \sqrt{\frac{2m}{\hbar^2}(\mu_o - V(x))} \Rightarrow \\ n(x) = \frac{1}{\pi}\sqrt{\frac{2m}{\hbar^2}(\mu_o - \frac{1}{2}mx^2\omega_z^2} = \sqrt{\frac{2\mu_o m}{\pi^2\hbar^2}}\left(1 - \frac{m\omega_z^2}{2\mu_o}x^2\right)^{1/2} \Rightarrow \\ n(x) = n(0)\left(1 - \frac{x^2}{R_{TF}^2}\right)^{1/2}. \end{aligned} \tag{2.59}$$

Here $n(x)$ is the so-called Thomas-Fermi profile, and the Thomas-Fermi radius is defined as $R_{TF}^2 = 2\mu_o/m\omega_z^2$. The density in the centre of the cloud is given by $n(0) = \sqrt{2\mu_o m/\pi^2\hbar^2}$. Using the known result for the chemical potential inside the harmonic trap, $\mu = N\omega_z\hbar$, the Thomas-Fermi radius can be expressed in a more convenient way as $R_{TF}^2 = 2Na_z^2$, where $a_z^2 = \hbar/m\omega_z$ is the characteristic length of the potential. In terms of the polarisation $P = (N_\uparrow - N_\downarrow)/N$, the Thomas-Fermi

radii for each component are given by

$$\frac{R_\uparrow}{\sqrt{N}a_z} = \sqrt{1+P}, \qquad \frac{R_\uparrow}{\sqrt{N}a_z} = \sqrt{1-P}. \tag{2.60}$$

They are plotted in Fig. (2.5) as solid lines.

The limit of infinitely repulsive fermions, $c = \infty$, is a singular limit, since the infinite repulsion between fermions mimics the Pauli principle, and the two-component cloud of fermions can be imaged as the cloud of $N = N_\uparrow + N_\downarrow$ spin-less fermions. This limit is called the fermionic Tonks-Girardeau regime. In this case the two species of fermions cannot be distinguished from each other any more, and the density profile of the mixture is equivalent to that of N Tonks-Girardeau bosons trapped in the same potential [84]. Therefore there is just one shell in the density profile. The radius of the cloud is thus given by the Tomas-Fermi radius

$$\frac{R}{\sqrt{N}a_z} = \sqrt{2} \tag{2.61}$$

for any value of the polarisation. As we can see, the numerical results shown in Fig. (2.5) agree with these two limiting results.

2.3.2 Magnetic field versus polarisation

We finally calculate the behaviour of the magnetic field versus the polarisation for different values of the interaction strength and for a fixed number of particles, shown in Fig. (2.6). The onset of magnetisation occurs at $h = 0$, which is consistent with the absence of a gap in the system: for any applied magnetic field the system acquires polarisation. We observe that the slope of the magnetisation at the onset of polarisation is linear. This slope is sensitive to the rate at which the gas polarises. The slope remains close to a constant throughout the regime $0 < h < h_s$, showing that the polarisability of the system (the capacity of the system to polarise) is very weakly affected by extra imbalanced particles. Even though there is a discontinuity in the slope of the polarisation versus the magnetic field at the saturation point, from the value of the susceptibility at saturation, Eq. (2.47) we do not expect a divergence of the magnetic susceptibility at saturation.

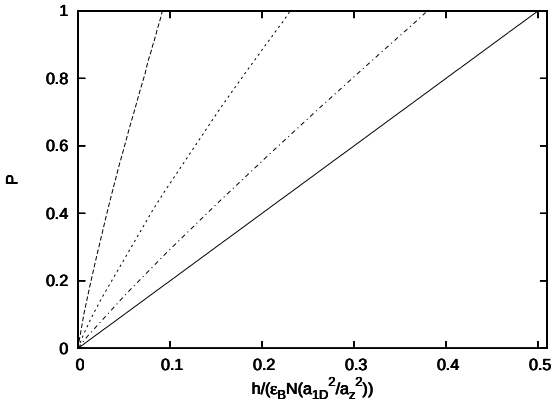

Figure 2.6: Phase diagram in the plane P and h/ϵ_B; for $N(a_{1D}^2/a_z^2) = \infty$ (solid line), $N(a_{1D}^2/a_z^2) = 10$ (dashed-dotted line), $N(a_{1D}^2/a_z^2) = 1$ (dotted line) and $N(a_{1D}^2/a_z^2) = 0.1$ (dashed line).

In the limit of free fermions, where $c = 0$, the magnetic field versus the polarisation can be calculated very easily. In this case, the energy can be simply written as $E = (N_\uparrow \mu_\uparrow + N_\downarrow \mu_\downarrow)/2$, where again the chemical potential is given by $\mu = N\omega_z\hbar$. Taking the derivative with respect to $S = N_\uparrow - N_\downarrow$ we find the variation of the magnetic field versus the polarisation

$$h = \frac{\partial E}{\partial S} = \hbar\omega_z \frac{N_\uparrow - N_\downarrow}{2} \Rightarrow \frac{h}{\epsilon_B} = \frac{N_\uparrow - N_\downarrow}{2} \frac{a_{1D}^2}{a_z^2} = N \frac{a_{1D}^2}{a_z^2} \frac{P}{2}, \tag{2.62}$$

which is independent of a_{1D}. It is displayed in Fig. (2.6) as a solid line.

2.4 Conclusions

In conclusion in this chapter we have calculated the ground state phase diagram for a system of two-component fermions interacting via a repulsive δ-function interaction. For the homogeneous case we give the exact result for the ground-state phase diagram in terms of the chemical potential and magnetic field. We see that four phases appear: the balanced phase, the fully polarised phase, the partially polarised phase and the vacuum. The boundaries between the phases, as

well as the susceptibility at saturation, are calculated analytically.

Next, we consider the harmonic trapping potential, which leads to inhomogeneities in the system. Applying the local density approximation we calculate numerically the density profiles of the cloud in the trap. For any imbalance we observe the emergence of a two-shell structure: the partially polarised phase is located at the centre of the trap, while the fully polarised phase appears at the edges. We find that there is no direct transition from the partially polarised phase to the vacuum. We compute the radii of the two shells for different values of the imbalance in relative concentrations of up-spin and down-spin particles, finding a perfect agreement with the limiting cases of free fermions and fermionic Tonks-Girardeau regime (hard-core fermions). We also calculate the magnetic field versus polarisation.

This model is experimentally accessible. Present techniques allow to cool fermionic atoms till the temperature needed to reach quantum degeneracy [85, 86, 87]; then using radio-frequency pulses it is possible to prepare spin mixtures of the atoms in two different spin states, for example for ^{40}K one can select the two hyperfine states $|F = 9/2, m_F = -9/2\rangle$ and $|F = 9/2, m_F = -7/2\rangle$, with different concentrations. Adiabatically superposing a 2D optical lattice leads to arrays of nearly identically parallel 1D traps.

Chapter 3

Finite size effects for the gap in the excitation spectrum of the one-dimensional Hubbard model

3.1 Overview

The Hubbard model describes a system of itinerant interacting particles on a lattice and it has long been important in solid state physics. In this model, one visualises the electrons in a narrow energy band hopping between the Wannier states of neighbouring lattice sites, and with on-site interaction. In the frame of ultra-cold atomic physics this model is essential for the description of a two-component Fermi gas in the lattice. The Hubbard model is the lattice version of the two-component Fermi gas in the continuum with short-range interactions, discussed in Chapter 2. The Hamiltonian in the latter case can be obtained form the Hubbard Hamiltonian for a small filling factor (see appendix B).

In this chapter we study the finite size effects for the gap of the quasiparticle excitation spectrum in the one-dimensional Hubbard model with on-site attrac-

tion. First, as an introduction, we review important known results for the Hubbard model. After that we present a general approach for finding finite size corrections to the ground state energy and to the gap. Two type of corrections to the result of the thermodynamic limit are obtained. First of all, there is a power law correction due to gapless excitations which behaves as $1/N_a$, where N_a is the number of lattice sites. Second, we obtain an exponential correction related to the existence of gapped excitations. In the weakly interacting regime this correction can become important compared to the power law correction. We show our numerical simulations which support these analytical results. We finally present a perturbative approach for solving the Bethe ansatz equations in the limiting case of weak interactions.

The literature devoted to the Hubbard model is so extensive that it would be impossible to give an exhaustive compendium in this Thesis. We will however try to present some of the main results that will be useful for the consistency of the calculations. For an in-depth review on the subject, see for example [88, 89].

3.1.1 Hamiltonian: the Hubbard model

The Hamiltonian of the one-dimensional Hubbard model has the form

$$H = -t \sum_{\sigma=\uparrow,\downarrow;j=1}^{N_a} (c^\dagger_{\sigma,j} c_{\sigma,j+1} + c^\dagger_{\sigma,j+1} c_{\sigma,j}) + U \sum_{j=1}^{N_a} n_{j,\uparrow} n_{j,\downarrow} \tag{3.1}$$

where N_a is the number of lattice sites, t is the amplitude of hopping between neighbouring sites, and U is the on-site interaction, that can be attractive ($U < 0$) or repulsive ($U > 0$). $c^\dagger_{i,\sigma}$ and $c_{i,\sigma}$ are the creation and annihilation operators of a particle with spin projection σ, and $n_{j,\sigma} = c^\dagger_{j,\sigma} c_{j,\sigma}$. We impose periodic boundary conditions, $c_{L+1,\sigma} = c_{1,\sigma}$, and the Hamiltonian is invariant under cyclic permutations of lattice sites.

The operators c and $c^\dagger$ are fermionic operators and they satisfy the anticommutation relations

$$\begin{aligned} \{c_{i,\sigma}, c_{j,\sigma'}\} &= \{c^\dagger_{i,\sigma}, c^\dagger_{j,\sigma'}\} = 0, \\ \{c_{i,\sigma}, c^\dagger_{j,\sigma'}\} &= \delta_{ij}\delta_{\sigma\sigma'}, \end{aligned} \tag{3.2}$$

for all $i = 1, \ldots, L$ and $\sigma = \uparrow, \downarrow$. The empty state (vacuum state) of the Hilbert space is defined by

$$c_{i,\sigma}|0\rangle = 0, \qquad i = 1, \ldots, N_a;\ \sigma = \uparrow, \downarrow . \tag{3.3}$$

The creation operator $c^\dagger_{i,\sigma}$ generates the space of states for the Hubbard model acting on the vacuum:

$$|i, \sigma\rangle = c^\dagger_{i,\sigma}|0\rangle \longrightarrow |\vec{x}, \vec{\sigma}\rangle = c^\dagger_{x_N,\sigma_N} \ldots c^\dagger_{x_1,\sigma_1}|0\rangle. \tag{3.4}$$

Here $\vec{x} = \{x_1, \ldots, x_N\}$ and $\vec{\sigma} = \{\sigma_1, \ldots, \sigma_N\}$, where the x_i are the lattice sites, $x_i \in \{x_1, \ldots, x_N\}$, and $\sigma_i = \{\uparrow, \downarrow\}$. The states $|\vec{x}, \vec{\sigma}\rangle$ are called Wannier states and they form a basis of the space of states of the Hubbard model. We understand them as states where particles with spin projection σ_i occupy the lattice sites x_i.

Each site has four available states: the empty state $|0\rangle$, the spin-up state $c^\dagger_{i,\uparrow}|0\rangle$, the spin-down state $c^\dagger_{i,\downarrow}|0\rangle$, and the doubly occupied state $c^\dagger_{i,\uparrow}c^\dagger_{i,\downarrow}|0\rangle$. Since due to the Pauli exclusion principle electrons with the same spin projection cannot occupy the same site, we have $(c^\dagger_{i,\sigma})^2 = 0$. Thus, the dimension of the Hilbert space is 4^{N_a}.

The operator $n_{i,\sigma} = c^\dagger_{i,\sigma}c_{i,\sigma}$ is the local particle number operator because

$$n_{i,\sigma}|\vec{x}, \vec{\sigma}\rangle = \sum_{j=1}^{N} \delta_{i,x_j}\delta_{\sigma,\sigma_j}|\vec{x}, \vec{\sigma}\rangle. \tag{3.5}$$

Therefore, $n_{i,\sigma}|\vec{x}, \vec{\sigma}\rangle = |\vec{x}, \vec{\sigma}\rangle$ if the site i is occupied by the σ spin, and is equal to zero otherwise. It satisfies $[n_{i,\sigma}, c^\dagger_{j,\sigma'}] = \delta_{ij}\delta_{\sigma\sigma'}c^\dagger_{j,\sigma'}$, and $n_{i,\sigma}|0\rangle = 0$. The quantities

$$N_\uparrow = \sum_j c^\dagger_{j,\uparrow}c_{j,\uparrow}, \qquad N_\downarrow = \sum_j c^\dagger_{j,\downarrow}c_{j,\downarrow}, \tag{3.6}$$

are the total number of up-spin particles and down-spin particles respectively, and the total number of particles is $N = N_\uparrow + N_\downarrow$.

In order to have a deeper understanding of the Hubbard model Hamiltonian, let us look at the two limiting cases, $t = 0$ and $U = 0$. In the $U = 0$ case the

Hamiltonian is called the tight-binding Hamiltonian and it can be replaced by an effective Hamiltonian, H_{at}, for each single atom localized on a lattice site. This is possible when the eigenfunction of each single atom is very small at distances of the order of the lattice spacing, and thus the lattice sites can be treated independently. The Hamiltonian is translationally invariant and therefore it can be diagonalized by a discrete Fourier transformation:

$$H = -2t \sum_{k=0}^{L-1} \sum_{\sigma} \cos(\Phi k) \tilde{n}_{k,\sigma}, \tag{3.7}$$

where $\tilde{c}^{\dagger}_{k,\sigma} = \frac{1}{\sqrt{L}} \sum_{j=1}^{L} \exp(i\Phi kj) c^{\dagger}_{j,\sigma}$ and $c^{\dagger}_{j,\sigma} = \frac{1}{\sqrt{L}} \sum_{k=0}^{L-1} \exp(-i\Phi kj) \tilde{c}^{\dagger}_{k,\sigma}$, for $k = 0, \ldots, L-1$ and $j = 1, \ldots, L$, respectively. We put $\Phi = 2\pi/N_a$. The Fourier transformation leaves the anticommutation relations (3.2) invariant, and $\tilde{n}_{k,\sigma} = \tilde{c}^{\dagger}_{k,\sigma} \tilde{c}_{k,\sigma}$. This Hamiltonian is diagonal in the basis of Bloch states,

$$|\vec{q}, \vec{\sigma}\rangle = \tilde{c}^{\dagger}_{k_N,\sigma_N} \ldots \tilde{c}^{\dagger}_{k_1,\sigma_1} |0\rangle, \tag{3.8}$$

which are eigenstates of the lattice momentum operator with $\vec{q} = \{q_1, \ldots, q_N\} = \Phi\ (k_1, \ldots, k_N)$. Thus, they represent states with a definite momentum but delocalised in space. The tight binding Hamiltonian acts on this basis as

$$H|\vec{q}, \vec{\sigma}\rangle = -2t \sum_{j=1}^{N} \cos(q_j) |\vec{q}, \vec{\sigma}\rangle, \tag{3.9}$$

describing non-interacting particles with a cosine dispersion of width $4t$.

Let us look now at the other limit, $t = 0$. In this case the Hamiltonian contains only the density part, which is diagonal in the Wannier basis of states:

$$\begin{aligned}
\sum_{j=1}^{L} n_{j,\uparrow} n_{j,\downarrow} |\vec{x}, \vec{\sigma}\rangle &= \sum_{i,j=1}^{N} \delta_{x_i,x_j} \delta_{\uparrow,\sigma_i} \delta_{\downarrow,\sigma_j} |\vec{x}, \vec{\sigma}\rangle = \\
&= \sum_{1 \le i < j \le N} \delta_{x_i,x_j} (\delta_{\uparrow,\sigma_i} \delta_{\downarrow,\sigma_j} + \delta_{\downarrow,\sigma_i} \delta_{\uparrow,\sigma_j}) |\vec{x}, \vec{\sigma}\rangle = \\
&= \sum_{1 \le i < j \le N} \delta_{x_i,x_j} (\delta_{\uparrow,\sigma_i} + \delta_{\downarrow,\sigma_i})(\delta_{\uparrow,\sigma_j} + \delta_{\downarrow,\sigma_j}) |\vec{x}, \vec{\sigma}\rangle = \\
&= \sum_{1 \le k < l \le N} \delta_{x_k,x_l} |\vec{x}, \vec{\sigma}\rangle.
\end{aligned} \tag{3.10}$$

This limit is called the atomic limit since it describes particles localised in lattice sites $x_1, \dots x_N$.

The two parts of the Hubbard Hamiltonian, the tight-binding part and the density part, do not commute with each other, and the Hamiltonian cannot be diagonalised neither in the Wannier basis nor in the Bloch basis. Therefore, the physics of the model can be understood as the competition between the two effects: one tends to delocalise the particles while the other one tries to localise them. The parameter that measures the relative contribution of the two terms is

$$u = \frac{U}{4t}, \tag{3.11}$$

and it represents the dimensionless coupling constant for the Hubbard model.

3.1.2 Symmetries

The Hubbard model has certain symmetries which are worth pointing out since they will be used in the following discussion. One of these symmetries is the particle-hole symmetry. Let us divide the lattice into two sub-lattices, such that the nearest neighbours of a particle in sub-lattice A belong always to sub-lattice B. Then we perform the following transformation for the spin operators

$$\begin{aligned} a^\dagger_{i,\sigma} &= c_{i,\sigma}, \quad a_{i,\sigma} = c^\dagger_{i,\sigma} && \text{for } i \in A \\ a^\dagger_{i,\sigma} &= -c_{i,\sigma}, \; a_{i,\sigma} = -c^\dagger_{i,\sigma} && \text{for } i \in B, \end{aligned} \tag{3.12}$$

which transforms the vacancies into occupied sites and vice-versa. This is why this transformation is called the particle-hole symmetry. Under this transformation the Hamiltonian remains unchanged up to terms equivalent to one-body fields, i.e. the chemical potential, but the numbers of particles change in the following way:

$$N_\uparrow \to N_a - N_\uparrow, \qquad N_\downarrow \to N_a - N_\downarrow. \tag{3.13}$$

We can also exchange particles by holes only for one type of particles, for example for the spin up:

$$\begin{aligned} a^\dagger_{i,\uparrow} &= c_{i,\uparrow}, \quad a_{i,\uparrow} = c^\dagger_{i,\uparrow} && \text{for } i \in A \\ a^\dagger_{i,\uparrow} &= -c_{i,\uparrow}, \; a_{i,\uparrow} = -c^\dagger_{i,\uparrow} && \text{for } i \in B, \end{aligned} \tag{3.14}$$

while $c_{i,\downarrow}$ remains unchanged. In this case the sign of the interaction will be reversed, $U \to -U$. Like before we also obtain extra one-body fields which can be absorbed in the chemical potential. Under this transformation the Hamiltonian for attraction transforms into the one for repulsion and vice-versa. For the number of particles we have the following relation

$$N_\uparrow \to N_a - N_\uparrow, \qquad N_\downarrow \to N_\downarrow. \tag{3.15}$$

The Hamiltonian of the Hubbard model also has the obvious $SU(2)$ symmetry under exchange of up-spin and down-spin particles. There are further symmetries, but I will not mention them here because they are irrelevant for the subsequent discussion.

For the ground state energy, the discussed symmetries are catalogued in the following way:

$$\begin{aligned} E_{N_a}(N_\uparrow, N_\downarrow; U) &= -(N_a - N_\uparrow - N_\downarrow)U + E_{N_a}(N_a - N_\uparrow, N_a - N_\downarrow; U) \\ &= N_\uparrow U + E_{N_a}(N_\uparrow, N_a - N_\downarrow; -U) \\ &= N_\downarrow U + E_{N_a}(N_a - N_\uparrow, N_\downarrow; -U) \end{aligned} \tag{3.16}$$

where $E_{N_a}(N_\uparrow, N_\downarrow; U)$ is the ground state energy for a system with $N_\uparrow$ up-spins and $N_\downarrow$ down-spins in a lattice with N_a lattice sites and interaction strength U. These symmetries tell us that it is sufficient to work in a determined sector of the space of parameters, since then the results can be extended to the other ones using relations Eq. (3.16). Therefore, without loss of generality, we can assume $N_\downarrow \leq N_\uparrow$ and $U > 0$.

3.1.3 The Bethe ansatz solution

The Hubbard Model is exactly solvable in one dimension. It was first solved in 1968 by E.H. Lieb and F.Y. Wu [90] using the Bethe ansatz technique. They reduced the problem to solving a set of algebraic equation known as the Lieb-Wu equations. The derivation of these equations is done for the case of the model with repulsion and is very similar to the one for fermions in the continuum with

short-rang interactions that was presented in Section 2.1.3. The energy for the case with attraction can be calculated using Eq. (3.16).

The lattice sites for a one-dimensional system can be labelled consecutively from 1 to N_a. In this case we have spin-up and spin-down particles: the down-spins are located in sites $x_1, \ldots, x_{N_\downarrow}$ and the up-spin in $x_{N_\downarrow+1}, \ldots, x_N$. We define $\Psi(x_1, \ldots, x_{N_\downarrow} | x_{N_\downarrow+1}, \ldots, x_N)$ as the eigenfunction of the system for this particular order of up and down spins. Then, the Hamiltonian (3.1) acts on Ψ in the following way:

$$\begin{aligned} \hat{H}\Psi &= -\sum_{i=1}^{N} \sum_{s=\pm 1} \Psi(x_1, \ldots, x_{i+s}, \ldots, x_N) + 4u \sum_{i<j} \delta(x_i - x_j) \Psi(x_1, \ldots, x_N) \\ &= E\Psi(x_1, \ldots, x_N), \end{aligned} \tag{3.17}$$

where $\delta(x_i - x_j) = 1$ for $x_i = x_j$ and is zero otherwise. The operators of particles with the same spin projection anticommute with each other, and we thus need Ψ to be antisymmetric in the first $N_\downarrow$ coordinates and in the last $(N - N_\downarrow)$ ones. Applying the Bethe ansatz we write the wave function Ψ as

$$\Psi(x_1, \ldots, x_{N_\downarrow} | x_{N_\downarrow+1}, \ldots, x_N) = \sum_P \psi(Q, P) e^{i \sum_{j=1}^{N} k_{Pj} x_{Qj}}, \tag{3.18}$$

for $x_{Q1} \leq x_{Q2} \leq \ldots \leq x_{QN}$. P and Q are two permutations of the numbers $1, \ldots, N$: $P = (P1, \ldots, PN)$ and $Q = (Q1, \ldots, QN)$. The momenta $k = k_1, \ldots, k_N$ are a set of N unequal numbers, and the total energy and momentum are given by

$$E = -2 \sum_{j=1}^{N} \cos(k_j) \qquad K = \sum_{j=1}^{N} k_j. \tag{3.19}$$

The coefficients $\psi(Q, P)$ can be regarded as the components of a $N! \times N!$ matrix. These coefficients have to be antisymmetric under exchange of the spin-up particles and under exchange of spin-down ones. In order to determine the values of these coefficients we have to look at the two-body scattering process,

similar to Eq. (2.9):

$$\begin{pmatrix} \psi(Q^1|P) \\ \psi(Q^2|P) \\ \psi(Q^3|P) \\ \vdots \\ \psi(Q^{N!}|P) \end{pmatrix} = (R_{ji}\mathbb{I} + T_{ji}\hat{P}^{ij}) \begin{pmatrix} \psi(Q^1|P') \\ \psi(Q^2|P') \\ \psi(Q^3|P') \\ \vdots \\ \psi(Q^{N!}|P') \end{pmatrix}, \tag{3.20}$$

where $P = (1, \cdots, i, \cdots, j, \cdots, N)$ and $P' = (1, \cdots, j, \cdots, i, \cdots, N)$ are two permutations of the momenta. The reflection and transmission coefficients are calculated from the Hubbard model Hamiltonian (see Appendix A):

$$\begin{aligned} R(\sin(k_n) - \sin(k_m)) &= \frac{-2iu}{\sin(k_n) - \sin(k_m) + 2iu}, \\ T(\sin(k_n) - \sin(k_m)) &= \frac{\sin(k_n) - \sin(k_m)}{\sin(k_n) - \sin(k_m) + 2iu}, \end{aligned} \tag{3.21}$$

where we used Eq. (3.11). The scattering operator fulfills the Yang-Baxter equations (1.8).

Note that equations (3.20) and (3.21) are the same as those for the two-component fermions in the continuum with δ-function interaction, Eqs. (2.9) and (2.5), except for the different dispersion relation, which implies the replacement of k by $\sin k$. We can therefore write the ansatz for the wave-function in the same way as in Section 2.1.3:

$$\psi(y_1, y_2, \ldots, y_{N_\downarrow}|P) = \epsilon_{Q,P} \sum_R A_R F_P(\lambda_{R1}, y_1) F_P(\lambda_{R2}, y_2) \cdots F_P(\lambda_{RN_\downarrow}, y_{N_\downarrow}), \tag{3.22}$$

where we labelled the positions of the down-spin particles by $1 \leq y_1 < y_2 < \ldots y_{N_\downarrow} \leq N$, and $\epsilon_{Q,P}$ is the sign of the permutations Q and P. It takes care of the antisymmetry under interchange of the $N_\downarrow$ down-spin particles and interchange of the $N_\uparrow$ up-spin ones. With this ansatz we find

$$\begin{aligned} F(y, \lambda) &= \prod_{j=1}^{y-1} (\sin(k_{Pj}) - \lambda + iu) \prod_{l=y+1}^{N} (\sin(k_{Pl}) - \lambda - iu), \\ A_R &= \epsilon_R \prod_{j<l} (\lambda_{Rj} - \lambda_{Rl} - 2iu). \end{aligned} \tag{3.23}$$

Here λ_i is a set of $N_\downarrow$ different auxiliary variables. Applying periodic boundary conditions we get the Bethe ansatz equations

$$e^{ik_j N_a} = \prod_{\beta=1}^{N_\downarrow} \frac{\sin(k_j) - \lambda_\beta + iu}{\sin(k_j) - \lambda_\beta - iu}$$

$$\prod_{j=1}^{N} \frac{\lambda_\alpha - \sin(k_j) + iu}{\lambda_\alpha - \sin(k_j) - iu} = -\prod_{\beta=1}^{N_\downarrow} \frac{\lambda_\alpha - \lambda_\beta + 2iu}{\lambda_\alpha - \lambda_\beta - 2iu}, \tag{3.24}$$

and taking the logarithm of these equations we get

$$\sum_{j=1}^{N} 2\arctan\frac{\lambda_\alpha - \sin k_j}{u} = 2\pi J_\alpha + \sum_{\beta=1}^{M} 2\arctan\frac{\lambda_\alpha - \lambda_\beta}{2u}, \quad \alpha = 1, ...M, \tag{3.25}$$

$$N_a k_j = 2\pi I_j - \sum_{\beta=1}^{M} 2\arctan\frac{\sin k_j - \lambda_\beta}{u}, \quad j = 1, ...N. \tag{3.26}$$

These are the Bethe ansatz equations for the Hubbard model, also called Lieb-Wu equations. When taking the logarithms one has to add a constant $2\pi in$ term, with n being integer. The quantum numbers I_j are integers (half-odd integers) for even (odd) $N_\downarrow$, $I = \frac{N_\downarrow}{2}$ (mod 1); and the quantum numbers J_α are integers (half-odd integers) for odd (even) $N - N_\downarrow$, $J = \frac{N - N_\downarrow + 1}{2}$ (mod 1). The total momentum can be written as $K = 2\pi/N_a(\sum I_j + \sum J_\alpha)$. For the ground state the quantum numbers I_j and J_α are consecutive half-odd integers and integers, respectively, centred around the origin:

$$J_\alpha = \{-\frac{N_\downarrow - 1}{2}, ..., -1, 0, 1, ..., \frac{N_\downarrow - 1}{2}\},$$
$$I_j = \{-\frac{N-1}{2}, ..., -\frac{1}{2}, \frac{1}{2}, ..., \frac{N-1}{2}\}. \tag{3.27}$$

The choice of these quantum numbers for the ground state implies that N is even and $N_\downarrow$ is odd. If we want to construct the ground state for a different combination we will not be able to satisfy $\sum I_j = 0$ and $\sum J_\alpha = 0$, and the ground state will have a current.

In the thermodynamic limit, when $N \to \infty$ and $N_a \to \infty$ keeping the density $n = N/L$ constant, we can define the density of momenta k and the density of

rapidities λ as $\rho(k) = L^{-1}\frac{\partial I}{\partial k}$ and $\sigma(\lambda) = L^{-1}\frac{\partial J}{\partial \lambda}$, respectively. Then, the Bethe ansatz equations become

$$\sigma(\lambda) + \frac{1}{\pi}\int_{-B}^{B} \frac{2u}{4u^2 + (\lambda - \lambda')^2}\sigma(\lambda')d\lambda' = \frac{1}{\pi}\int_{-Q}^{Q} \frac{u}{u^2 + (\lambda - \sin k)^2}\rho(k)dk, \quad (3.28)$$

$$\rho(k) = \frac{1}{2\pi} + \frac{\cos k}{\pi}\int_{-B}^{B} \frac{u}{u^2 + (\lambda - \sin k)^2}\sigma(\lambda)d\lambda, \quad (3.29)$$

where the constants B and Q are given by fixing the filling factor n and the down-spin density $n_\downarrow$,

$$\frac{N}{N_a} = n = \int_{-Q}^{Q}\rho(k)dk, \qquad \frac{N_\downarrow}{N_a} = n_\downarrow = \int_{-B}^{B}\sigma(\lambda)d\lambda. \quad (3.30)$$

The energy in the thermodynamical limit is given by

$$E = -2N_a\int_{-Q}^{Q}\rho(k)\cos k dk. \quad (3.31)$$

In the case of a half-filled band, and for a ground state without magnetisation, for which $N = N_a$, $N_\downarrow = N_\uparrow = N/2$, or equivalently $B = \infty$, $Q = \pi$, equations (3.28) and (3.29) can be solved exactly using Fourier transform, and we can express the densities of momenta and rapidities as

$$\rho(k) = \frac{1}{2\pi} + \frac{\cos k}{2\pi}\int_0^\infty \frac{\cos(\omega \sin k)e^{-\omega u}}{\cosh \omega u}J_0(\omega)d\omega, \quad (3.32)$$

$$\sigma(\lambda) = \frac{1}{2\pi}\int_0^\infty \frac{\cos \omega\lambda}{\cosh \omega u}J_0(\omega)d\omega. \quad (3.33)$$

Using these expressions the energy in this case reads

$$E_{N_a}\left(\frac{N_a}{2}, \frac{N_a}{2}; U\right) = -4N_a\int_0^\infty \frac{J_0(\omega)J_1(\omega)d\omega}{\omega\left(1 + \exp\left(\frac{\omega U}{2}\right)\right)}, \quad (3.34)$$

where J_0 and J_1 are Bessel functions.

The results obtained above are valid for all $U > 0$. They can be written for the case $U < 0$ using the symmetry relations (3.16) for the energy. In the case of attraction the momenta of some particles becomes complex, which is the sign of the formation of bound states. In particular, the Bethe ansatz equations change

in the following way: the equations for the λ's remain unchanged, while the set of N momenta k is replaced by another set in which $N - 2N_\downarrow$ momenta are real and $2N_\downarrow$ momenta are complex [91]. The real k satisfy the same Bethe ansatz equation as in the repulsive case, Eq. (3.26), while the complex momenta are coupled in pairs (k^+, k^-) that satisfy:

$$\sin k_\alpha^+ = \lambda_\alpha + iu + O\left(e^{-L}\right), \qquad \sin k_\alpha^- = \lambda_\alpha - iu + O\left(e^{-L}\right), \tag{3.35}$$

and therefore can be calculated with exponential accuracy from the value of the λ's, Eq. (3.25) [91, 71].

3.1.4 The excitation spectrum

The simplest excitations for the ground state of the Hubbard model are single particle excitations: we can add a particle to the ground state and create a "particle" excitation or remove a particle from it and create a "hole" excitation. The excited states of the Hubbard model are combinations of particle-hole excitations for the ground state. Their energy is the sum of the contributions of the particle excitations and the hole ones.

For the model with repulsion at half filling there is a gap for excitations that carry charge, while spin excitations are gapless. Away from half filling both spin and charge excitations are gapless. For the model with attraction, which can be obtained from the repulsive model using the relations (3.16), the low lying excitations are gapless charge excitations and gapped spin excitations.

Let us start with the repulsive model at half filling. The half filled ground state is characterized by the set of integers (3.27), with $N = N_a$ and $N_\downarrow = N_a/2$. We first consider a spin excitation, that leaves the total number of particles unchanged but decreases the number of down spins by one, $N_\downarrow = N_a/2 \to N_a/2 - 1$, and increases the number of up spins by one, $N_\uparrow = N_a/2 \to N_a/2 + 1$. The quantum numbers become (remember that $I = \frac{N_\downarrow}{2}$ (mod 1) and $J = \frac{N - N_\downarrow + 1}{2}$ (mod 1)):

$$J_\alpha = -\frac{Na}{4}, \ldots, \frac{Na}{4} - s - 1, \frac{Na}{4} - s + 1, \ldots, \frac{Na}{4} - r - 1, \frac{Na}{4} - r + 1, \ldots,$$

$$\frac{Na}{4}-1,\frac{Na}{4},\quad 0\le r<s\le\frac{N_a}{2};$$
$$I_j=-\frac{N_a-2}{2},\ldots,\frac{N_a-2}{2},\frac{N_a}{2}. \tag{3.36}$$

We see that there are two holes in the distributions of J, each of them being called spinon. The total momentum for this state is $K=2\pi/N_a(r+s)$, while the energy of this excitation is obtained by solving the Bethe ansatz equations for this particular combination of quantum numbers [88]:

$$\begin{aligned}\Delta E &= \epsilon(\lambda_r)+\epsilon(\lambda_s), \qquad \text{with}\\ \epsilon(\lambda) &= \frac{1}{2u}\int_{-\pi}^{\pi}dk\ \cos^2 k\ \mathrm{sech}\left[\frac{\pi(\lambda_r-\sin k)}{2u}\right].\end{aligned} \tag{3.37}$$

The change in momentum can be rewritten as

$$K=q(\lambda_r)+q(\lambda_s),\ \text{with}\ q(\lambda)=2\pi\int_{\lambda}^{\infty}dx\int_{-\pi}^{\pi}\frac{dk}{2\pi}\frac{1}{4u}\mathrm{sech}\left[\frac{\pi(x-\sin k)}{2u}\right]. \tag{3.38}$$

From equations (3.37) and (3.38) one can calculate the group velocity for the spin excitations,

$$v_s=2\frac{I_1\left(\frac{\pi}{2u}\right)}{I_0\left(\frac{\pi}{2u}\right)}, \tag{3.39}$$

where I_0, I_1 are modified Bessel functions.

Let us now turn to the charge excitations, for which $N=N_a-1$ and $N_\downarrow=N_a/2-1$. The quantum numbers are given by

$$\begin{aligned}J_\alpha &= -\frac{N_a/2-1}{2},\ldots,\frac{N_a/2-1}{2}-s-1,\frac{N_a/2-1}{2}-s+1,\ldots,\frac{N_a/2-1}{2}\\ I_j &= -\frac{N_a}{2}+1,\ldots,\frac{N_a}{2}-r-1,\frac{N_a}{2}-r+1,\ldots,\frac{N_a}{2}-1,\frac{N_a}{2}.\end{aligned} \tag{3.40}$$

There is a hole in the distribution of I_j called holon and a hole in the distribution of J_α called spinon. The total momentum of this state is $K=2\pi/N_a[r+s-(N_a-2)/4]$. Solving the Bethe ansatz equations for this distributions of I_j and J_α we find for the energy of this excitation

$$\Delta E=2u+2\cos k_r+4\int_0^{\infty}\frac{J_1(\omega)\cos(\omega\sin k_r)}{\omega\left(e^{2u\omega}+1\right)}d\omega, \tag{3.41}$$

the difference in momentum can be reexpressed as

$$\Delta K = q(\lambda_s) + 2\pi \int_{k_r}^{\pi} \rho(k)dk - \frac{\pi}{2}. \tag{3.42}$$

The charge excitation spectrum possesses a gap since there is a non-zero minimum value of ΔE. This minimum takes place at the points $k_r = \pm\pi$, $\lambda_s = \pm\infty$. Therefore, the energy gap of charge excitations in the half-filled state is

$$\Delta = 2u - 2 + 4 \int_0^{\infty} \frac{J_1(\omega)d\omega}{\omega\left(1 + e^{2\omega u}\right)} \tag{3.43}$$

which is the so-called Lieb-Wu gap [90].

One can also think of the Lieb-Wu gap as the difference in energy in the ground state when adding and removing a particle, which can be rewritten as $\Delta = (\mu_+ - \mu_-)$, with

$$\mu_+ = E\left(M+1, M; U\right) - E\left(M, M; U\right),\ \mu_- = E\left(M, M; U\right) - E\left(M-1, M; U\right), \tag{3.44}$$

where we put $M = N_a/2$. Here the mean-field effects have been compensated adding an extra particle and removing it.

The value of the gap is positive for all $U > 0$, and the half-filled state is an insulator state. The insulating nature of the half-filled ground state in the repulsive Hubbard model is driven entirely by interactions, since there is no band gap in the excitation spectrum of the Hubbard model. This type of insulator is called Mott insulator. From the expression for the gap (3.43) it follows that

$$\lim_{u \to 0} \Delta = 0. \tag{3.45}$$

One then can conclude that the ground state for the half-filled band is insulating for any non-zero U, and conducting for $U = 0$. That is to say, there is no Mott transition for non-zero U.

In the case of less than half-filled band for the model with repulsion we see that $\mu_+ = \mu_-$, using the relations (3.16). Therefore, there is no gap in the spectrum.

In the case for the model with attraction at half filling, using relations (3.16), we see that the value of the gap, this time in the spin sector, takes the same form

as the one for the charge sector in the case with repulsion. However, in order to compute the value of the gap far from the half-filled case we have to follow another strategy. The general expression for the energy of the gap in this case reads

$$\Delta = \mu_+ - \mu_-, \tag{3.46}$$

$$\mu_+ = E_{N_a}(N_\uparrow + 1, N_\downarrow; U) - E_{N_a}(N_\uparrow, N_\downarrow; U), \tag{3.47}$$

$$\mu_- = E_{N_a}(N_\uparrow, N_\downarrow; U) - E_{N_a}(N_\uparrow - 1, N_\downarrow; U). \tag{3.48}$$

Some values of the gap out of half-filling have been obtained in some limiting cases, for example by Krivnov and Ovchinnikov [92] in the cases close to half filling and close to zero filling, or by Larkin and Sak [93] for all fillings but in the case of small interaction.

3.1.5 Conformal field theory and finite size corrections

One-dimensional models that have a critical point at zero temperature have correlation functions that decay asymptotically as powers of the distance, due to scale invariance. This critical behaviour does not depend on the details of the microscopic theory, but belongs to a universality class of critical theories. Lorentz invariant systems with critical points at zero temperature are conformally invariant [94, 95, 96, 97]. These systems belong to a class of universality that is determined by a single dimensionless number, the central charge c of the underlying Virasoro algebra. The finite size corrections to the energy of the ground state in these models have then the structure [94, 95, 96, 97]

$$E_0 - L\epsilon_0 = -\frac{\pi}{6N_a} vc + o\left(\frac{1}{L}\right), \tag{3.49}$$

where E_0 is the ground state energy for the system of size N, and ϵ_0 is the ground state density of energy in the thermodynamic limit, v is the Fermi velocity and c is the conformal charge. This result holds for periodic boundary conditions. For the energy of the low-lying excited states the following formula holds for the finite size corrections [98]

$$E_n^{N^+,N^-} - E_0 = \frac{2\pi v}{N_a}(x_n + N^+ + N^-) + o\left(\frac{1}{L}\right), \tag{3.50}$$

where N^+ and N^- are two non-negative integers and x_n is the scaling dimension of the scaling operators. Thus, for a conformally invariant system, if we are interested in determining the power law $1/N$ corrections to the thermodynamic energy we should know the Fermi velocity v, the central charge c of the theory and the scaling dimensions of the operators.

Consider the situation of free fermions on a lattice ($U = 0$), this simple example is useful to get an intuition about the origin of the $1/N_a$ structure. The energy spectrum is given by $E = -2t\sum\cos(k_j)$, with $k_j = 2\pi n_j/N_a$. We consider a lowest energy particle-hole excitation on top of the the ground state. The excess of energy due to this excitation is $\Delta E = -2t\left(\cos\left(\frac{2\pi}{N_a}(\frac{N}{2}+1)\right) - \cos\left(\frac{2\pi}{N_a}\frac{N}{2}\right)\right) \simeq 2t\sin\left(\frac{\pi N}{N_a}\right)\sin\left(\frac{2\pi}{N_a}\right)$. Using the definition of the sound velocity we write the variation of energy as $\Delta E \simeq \frac{2\pi}{N_a}v$, which is the conformal correction for $c = 1$.

For a system with several critical degrees of freedom with different Fermi velocities, the concept of conformal invariance is not directly applicable. This is the case of the Hubbard model, because generally both the charge and the spin degrees of freedom are critical (gapless) and have different sound velocities. There are two particular cases where there is only one critical excitation. This is the case at half-filling where only one mode is critical, and the case with a strong magnetic field where the spin-density waves have a gap.

The finite size conformal corrections to the energy of the repulsive Hubbard model at half filling, where the charge mode possesses a gap, were determined by Woynarovich and Eckle [99]. The central charge is equal to one, $c = 1$, and the scaling dimensions of the scaling operators in the critical spin sector are $x_s = S^2/2$, where S is the magnetisation of the corresponding excited state. The Fermi velocity is given by Eq. (3.39). Woynarovich and Eckle calculated the finite size corrections for the Hubbard model, which are equal to

$$\begin{aligned} E_0 - L\epsilon_0 &= -\frac{\pi v_s}{6N_a}\left(1 + 0.3433\frac{1}{\ln^3(N_a I_0(\pi/2u))} + \cdots\right), \\ E_s - L\epsilon_0 &= \frac{\pi S^2 v_s}{N_a}\left(1 - \frac{1}{2}\frac{1}{\ln(N_a I_0(\pi/2u))} + \cdots\right). \end{aligned} \tag{3.51}$$

Away from half filling the system is no longer conformally invariant, because

the two degrees of freedom are critical and have different sound velocities. It is however possible to treat the two sectors as being described by two independent conformal theories. Even though these two contributions are not independent, because the scaling dimensions in both sectors depend on the state of both Fermi seas, they can nonetheless be treated as such, and one obtains:

$$E_0 - L\epsilon_0 = -\frac{\pi}{6N_a}v_c - \frac{\pi}{6N_a}v_s. \tag{3.52}$$

This situation has been studied by Woynarovich [100] who found that the validity of Eq. (3.52) requires the number of particles and the filling to meet several special conditions.

3.2 Finite size effects in the energy of the gap

In this section we develop a technique for solving the Bethe ansatz equations of the Hubbard model in the situation where the system is finite. Later, we will use these results to calculate the finite size corrections for the ground state energy and the gap. This will allow us to access the finite size corrections in the gapped sector of the spectrum, which are believed to be non-universal and cannot be calculated using conformal field theory. Finally we present the numerical results and show their agreement with our predictions.

3.2.1 General approach

In order to calculate the finite size corrections to the energy and to the gap of the Hubbard model from the Bethe ansatz equations we follow the scheme proposed by de Vega and Woynarovich [101]. This scheme consists of writing the Bethe ansatz equations (3.26) and (3.25) in the form:

$$\begin{aligned} Z^s(\lambda) \;&=\; \frac{1}{N_a}\sum_j^N \frac{1}{\pi}\arctan\frac{\lambda-\sin k_j}{u} - \frac{1}{N_a}\sum_\beta^M \frac{1}{\pi}\arctan\frac{\lambda-\lambda_\beta}{2u}, \\ Z^s(\lambda_\alpha) &= \frac{J_\alpha}{N_a}; \end{aligned}$$

$$Z^c(k) = \frac{k}{2\pi} + \frac{1}{N_a}\sum_{\alpha}^{M}\frac{1}{\pi}\arctan\frac{\sin k - \lambda_\alpha}{u},$$
$$Z^c(k_j) = \frac{I_j}{N_a}. \tag{3.53}$$

We then define the densities of momenta k and rapidities λ for a finite size system as

$$\sigma_N(\lambda) \equiv \frac{dZ^s}{d\lambda} = \frac{1}{2\pi N_a}\sum_{j=1}^{N}K_1(\lambda - \sin k_j) - \frac{1}{2\pi N_a}\sum_{\beta=1}^{M}K_2(\lambda - \lambda_\beta),$$
$$\rho_N(k) \equiv \frac{dZ^c}{dk} = \frac{1}{2\pi} + \frac{1}{N_a}\frac{\cos k}{2\pi}\sum_{\alpha=1}^{M}K_1(\sin k - \lambda_\alpha), \tag{3.54}$$

where $K_1(x) = 2u/(u^2+x^2)$, and $K_2 = 4u/(4u^2+x^2)$. The densities satisfy the relations:

$$\int_{\Lambda_-}^{\Lambda_+}\sigma_N(\lambda)d\lambda = \frac{M}{N_a}, \quad \int_{Q_-}^{Q_+}\rho_N(k)dk = \frac{N}{N_a}, \tag{3.55}$$

where $Q_\pm$, $\Lambda_\pm$ are determined from the equations

$$Z^c(Q_+) = \frac{I_+}{N_a} = \frac{I_{max}+1/2}{N_a}; \;\; Z^s(\Lambda_+) = \frac{J_+}{N_a} = \frac{J_{max}+1/2}{N_a}. \tag{3.56}$$

We define the functions X_N,

$$X_N^c(k) = \frac{1}{N_a}\sum_{j=1}^{N_a}\delta(k-k_j) - \rho_N(k), \tag{3.57}$$

$$X_N^s(\lambda) = \frac{1}{N_a}\sum_{\alpha=1}^{N_a/2}\delta(\lambda-\lambda_\alpha) - \sigma_N(\lambda), \tag{3.58}$$

that will allow us to write an integral equation for the densities at a finite N:

$$\sigma_N(\lambda) = \frac{1}{2\pi}\int_{Q_-}^{Q_+}K_1(\lambda-\sin k)\rho_N(k)dk - \frac{1}{2\pi}\int_{\Lambda_-}^{\Lambda_+}K_2(\lambda-\mu)\sigma(\mu)d\mu$$
$$+\frac{1}{2\pi}\int_{Q_-}^{Q_+}K_1(\lambda-\sin k)X_N^c(k)dk - \frac{1}{2\pi}\int_{\Lambda_-}^{\Lambda_+}K_2(\lambda-\mu)X_N^s(\mu)d\mu, \tag{3.59}$$
$$\rho_N(k) = \frac{1}{2\pi} + \frac{1}{2\pi}\int_{\Lambda_-}^{\Lambda_+}K_1(\sin k-\lambda)\cos k\;\sigma_N(\lambda)d\lambda$$
$$+\frac{1}{2\pi}\int_{\Lambda_-}^{\Lambda_-}\cos k K_1(\sin k-\lambda)X_N^s(\lambda)d\lambda. \tag{3.60}$$

The finite size corrections to the ground state energy, which are the difference between the energy in the thermodynamic limit and the energy for the finite system, are given by

$$\delta E_N = E_N - E_{\infty,N} = -2N_a \int_{Q_-}^{Q_+} \rho_N(k) \cos k \, dk + 2N_a \int_{Q_-}^{Q_+} \rho_{\infty,N}(k) \cos k \, dk, \tag{3.61}$$

where we put $E_N \equiv E_{N_a}(N-M, M, |U|)$.

3.2.2 Corrections

We now calculate the finite size corrections to the energy of the gap, Δ, in the Hubbard model with attraction:

$$2\Delta = E_{N_a}(N_\uparrow + 2, N_\downarrow, U) + E_{N_a}(N_\uparrow - 2, N_\downarrow, U) - 2E_{N_a}(N_\uparrow, N_\downarrow, U), \tag{3.62}$$

with $N_\uparrow = N_\downarrow = N_a/2 = M$. This definition of the gap is convenient since it conserves the parity of N, $N_\uparrow$ and $N_\downarrow$. Using the symmetry relations Eq. (3.16) it can be rewritten through the energies of the repulsive model:

$$\begin{aligned} 2\Delta = {} & 2|U| + E_{N_a-2}(M-2, N_a-M, |U|) + E_{N_a-2}(N_a-M-2, M, |U|) \\ & - 2E_{N_a}(M, N_a-M, |U|). \end{aligned} \tag{3.63}$$

For the half-filled case ($N = 2M = N_a$), Eq. (3.63) takes the form:

$$\Delta = |U| + E_{N_a-2}(N_a/2, N_a/2-2, |U|) - E_{N_a}(N_a/2, N_a/2, |U|). \tag{3.64}$$

Therefore, in order to calculate the finite size corrections to the gap energy we have to calculate $E_{N_a}(N_a/2, N_a/2; |U|)$ and $E_{N_a}(N_a/2, N_a/2-2; |U|)$.

In the first case we have $N = N_a$ and $N_\uparrow = N_\downarrow = N_a/2 = M$, and the quantum numbers Eq. (3.27) for the ground state are

$$\begin{aligned} J_\alpha &= \{-\frac{M-1}{2}, ..., -1, 0, 1, ..., \frac{M-1}{2}\}, \\ I_j &= \{-\frac{N-1}{2}, ..., -\frac{1}{2}, \frac{1}{2}, ..., \frac{N-1}{2}\}. \end{aligned} \tag{3.65}$$

Therefore, from Eq. (3.56) we have

$$J_{max} = \frac{N_a/2-1}{2} \rightarrow J_+ = \frac{N_a}{4}, \rightarrow Z_s(\infty) = \frac{N}{2N_a} - \frac{M}{2N_a} = \frac{1}{4}, \rightarrow \Lambda_+ = \infty,$$
$$I_{max} = \frac{N_a-1}{2}, \rightarrow I_+ = \frac{N_a}{2}, \rightarrow Z_c(Q_+) = \frac{1}{2}, \rightarrow Q_+ = \pi. \tag{3.66}$$

We re-write the equations (3.59) and (3.60) for $N = N_a$:

$$\sigma_{N_a}(\lambda) = \frac{1}{2\pi}\int_{-\pi}^{\pi} K_1(\lambda - \sin k)\rho_{N_a}(k)dk - \frac{1}{2\pi}\int_{-\infty}^{\infty} K_2(\lambda-\mu)\sigma_{N_a}(\mu)d\mu$$
$$+ \frac{1}{2\pi}\int_{-\pi}^{\pi} K_1(\lambda - \sin k)X^c_{N_a}(k)dk - \frac{1}{2\pi}\int_{\infty}^{\infty} K_2(\lambda-\mu)X^s_{N_a}(\mu)d\mu, \tag{3.67}$$
$$\rho_{N_a}(k) = \frac{1}{2\pi} + \frac{1}{2\pi}\int_{-\infty}^{\infty} K_1(\sin k - \lambda)\cos k \;\; \sigma_{N_a}(\lambda)d\lambda$$
$$+ \frac{1}{2\pi}\int_{-\infty}^{\infty} \cos k \;\; K_1(\sin k - \lambda)X^s_{N_a}(\lambda)d\lambda, \tag{3.68}$$

with the quantities $X^s_{N_a}$ and $X^c_{N_a}$ defined from Eqs. (3.57) and (3.58),

$$X^c_{N_a}(k) = \frac{1}{N_a}\left[\sum_{j=1}^{N_a}\delta(k-k_j)\right] - \rho_{N_a}(k), \tag{3.69}$$

$$X^s_{N_a}(\lambda) = \frac{1}{N_a}\left[\sum_{\alpha=1}^{N_a/2}\delta(\lambda-\lambda_\alpha)\right] - \sigma_{N_a}(\lambda). \tag{3.70}$$

The solution of the Bethe ansatz equations is known in the thermodynamic limit, Eqs. (3.32) and (3.33). Integrating the density of momenta $\rho(k)$ in Eq. (3.32) over dk we obtain

$$Z^c_{N_a}(k) = \frac{k}{2\pi} + \frac{1}{2\pi}\int_0^{\infty}\frac{\sin(\omega\sin k)e^{-\omega u}}{\omega\cosh\omega u}J_0(\omega)d\omega. \tag{3.71}$$

Next, we consider the situation for $N = N_a - 2$, $N_\uparrow = N_a/2$, and $N_\downarrow = N_a/2 - 2$. We should remove two particles from the system with $N = N_a$ or add two holes with momenta $k_h = \{k_1, k_{N_a}\}$ and spin rapidities $\lambda_h = \{\lambda_1, \lambda_{N_a/2}\}$ in order to satisfy the conditions $Q_\pm = \pm\pi$ and $\Lambda_\pm = \pm\infty$. The Bethe ansatz equations in the discrete case read

$$\sum_{j=1}^{N_a} 2\arctan\frac{\lambda_\alpha - \sin k_j}{u} = 2\pi J_\alpha + \sum_{\beta=1}^{N_a/2} 2\arctan\frac{\lambda_\alpha - \lambda_\beta}{2u} \tag{3.72}$$

$$+\sum_{k_h} 2\arctan\frac{\lambda_\alpha-\sin k_h}{u}-\sum_{\lambda_h} 2\arctan\frac{\lambda_\alpha-\lambda_h}{2u},\quad \alpha=1,...N_a/2,$$

$$N_a k_j = 2\pi I_j - \sum_{\beta=1}^{N_a/2} 2\arctan\frac{\sin k_j-\lambda_\beta}{u}+\sum_{\lambda_h} 2\arctan\frac{\sin k_j-\lambda_h}{u},\quad j=1,...N_a.$$

Note that we added only 4 additional equations for defining the numbers k_h, λ_h. Other equations are exactly the Bethe Ansatz equations for N_a-2 particles. The sets J_α, I_j are the same as for the ground state of N_a particles.

We re-write the equations (3.59) and (3.60) for $N=N_a-2$,

$$\begin{aligned}\sigma_{N_a-2}(\lambda) &= \frac{1}{2\pi}\int_{-\pi}^{\pi} K_1(\lambda-\sin k)\rho_{N_a-2}(k)\,dk-\frac{1}{2\pi}\int_{-\infty}^{\infty}K_2(\lambda-\mu)\sigma_{N_a-2}(\mu)\,d\mu\\ &+\frac{1}{2\pi}\int_{-\pi}^{\pi} K_1(\lambda-\sin k)X^c_{N_a-2}(k)\,dk-\frac{1}{2\pi}\int_{-\infty}^{\infty}K_2(\lambda-\mu)X^s_{N_a-2}(\mu)\,d\mu\\ &-\frac{1}{2\pi N_a}\sum_{k_h}K_1(\lambda-\sin k_h)+\frac{1}{2\pi N_a}\sum_{\lambda_h}K_2(\lambda-\lambda_h),\end{aligned}\tag{3.73}$$

$$\begin{aligned}\rho_{N_a-2}(k) &= \frac{1}{2\pi}+\frac{1}{2\pi}\int_{-\infty}^{\infty}K_1(\sin k-\lambda)\sigma_{N_a-2}(\lambda)\cos k\,d\lambda\\ &+\frac{1}{2\pi}\int_{-\infty}^{\infty}K_1(\sin k-\lambda)X^s_{N_a-2}(\lambda)\,\cos k\,d\lambda-\frac{1}{2\pi N_a}\sum_{\lambda_h}K_1(\sin k-\lambda_h)\cos k,\end{aligned}\tag{3.74}$$

where the functions $X^{s,c}_{N_a-2}$ are given by

$$X^s_{N_a-2}(\lambda)=\frac{1}{N_a}\sum_{\alpha=1}^{N_a/2}\delta(\lambda-\lambda_\alpha)-\sigma_{N_a-2}(\lambda),\tag{3.75}$$

$$X^c_{N_a-2}(k)=\frac{1}{N_a}\sum_{j=1}^{N_a}\delta(k-k_j)-\rho_{N_a-2}(k),\tag{3.76}$$

where the summation over k_j, λ_α includes the additional numbers k_h, λ_h.

Then, in the thermodynamic limit we have for the densities of a system with N_a-2 particles

$$\begin{aligned}\sigma_{\infty,N_a-2} &= \sigma_{\infty,N_a}-\frac{1}{2\pi N_a}\sum_{k_h}\frac{\pi}{2u}\frac{1}{\cosh\frac{\pi}{2u}(\lambda-\sin k_h)}\\ &+\frac{1}{2\pi N_a}\sum_{\lambda_h}\int_0^\infty\frac{\cos\omega(\lambda-\lambda_h)}{\cosh\omega u}e^{-\omega u},\end{aligned}\tag{3.77}$$

$$\rho_{\infty,N_a-2} = \rho_{\infty,N_a} - \frac{\cos k}{2\pi N_a}\sum_{k_h}\int_0^\infty \frac{\cos\omega(\sin k-\sin k_h)}{\cosh\omega u}e^{-\omega u} - \frac{\cos k}{2\pi N_a}\sum_{\lambda_h}\frac{\pi}{2u}\frac{1}{\cosh\frac{\pi}{2u}(\sin k-\lambda_h)}, \tag{3.78}$$

and

$$Z^c_{N_a-2}(k) = Z^c_{N_a}(k) - \frac{1}{2\pi N_a}\sum_{k_h}\int_0^\infty \frac{\sin(\omega(\sin k-\sin k_h))e^{-\omega u}}{\omega\cosh\omega u}d\omega - \frac{1}{2\pi N_a}\sum_{\lambda_h} 2\arctan[\tanh(\frac{\pi}{4u}(\sin k-\lambda_h)]. \tag{3.79}$$

For calculating the finite size corrections we should find the differences between the densities $\rho_{N_a}(k)$, $\sigma_{N_a}(\lambda)$, $\sigma_{N_a-2}(\lambda)$, $\rho_{N_a-2}(k)$ and their thermodynamic limits values. Subtracting the equations of the thermodynamic limit from Eqs. (3.67) and (3.68) for the case $N = N_a$ we obtain:

$$\delta\sigma_{N_a}(\lambda) = \sigma_{N_a}(\lambda) - \sigma_{\infty,N_a}(\lambda) = \frac{1}{2\pi}\int_{-\pi}^{\pi} K_1(\lambda-\sin k)\delta\rho_{N_a}(k)\,dk - \frac{1}{2\pi}\int_{-\infty}^{\infty} K_2(\lambda-\mu)\delta\sigma_{N_a}(\mu)\,d\mu + \frac{1}{2\pi}\int_{-\pi}^{\pi} K_1(\lambda-\sin k)X^c_{N_a}(k)\,dk - \frac{1}{2\pi}\int_{-\infty}^{\infty} K_2(\lambda-\mu)X^s_{N_a}(\mu)\,d\mu, \tag{3.80}$$

$$\delta\rho_{N_a}(k) = \rho_{N_a}(k) - \rho_{\infty,N_a}(k) = \frac{1}{2\pi}\int_{-\infty}^{\infty} K_1(\sin k-\lambda)\cos k\;\delta\sigma_{N_a}(\lambda)\,d\lambda + \frac{1}{2\pi}\int_{-\infty}^{\infty}\cos k\;K_1(\sin k-\lambda)X^s_{N_a}(\lambda)\,d\lambda. \tag{3.81}$$

Equations (3.80) and (3.81) lead to algebraic equations for the Fourier transforms of $\delta\sigma_{N_a}(\lambda)$ and $\delta\rho_{N_a}(k)$, which yields:

$$\delta\sigma_{N_a}(\lambda) = \int_{-\pi}^{\pi}\frac{\pi}{2u}\frac{1}{\cosh\left[\pi(\lambda-\sin k)/2u\right]}X^c_{N_a}(k)\frac{dk}{2\pi} - \int_{-\infty}^{\infty}d\mu\int_0^\infty\frac{\cos[\omega(\lambda-\mu)]}{\cosh(\omega u)}\exp(-\omega u)X^s_{N_a}(\mu)\frac{d\omega}{2\pi}, \tag{3.82}$$

$$\delta\rho_{N_a}(k) = \cos k\int_0^\infty\frac{d\omega}{2\pi}\int_{-\pi}^{\pi}\frac{\exp(-\omega u)}{\cosh(\omega u)}\cos[\omega(\sin k-\sin q)]X^c_{N_a}(q)\,dq + \frac{\cos k}{2\pi}\int_{-\infty}^{\infty}\frac{\pi}{2u}\frac{1}{\cosh\left[\pi(\sin k-\lambda)/2u\right]}X^s_{N_a}(\lambda)\,d\lambda. \tag{3.83}$$

Equations for $\delta\sigma_{N_a-2}(\lambda)$ and $\delta\rho_{N_a-2}(k)$ are obtained in a similar way taking into account that in the thermodynamic limit $k_h = \pm\pi$ and $\lambda_h = \pm\infty$. This gives Eqs. (3.80), (3.81) and (3.82), (3.83) where N_a is replaced by $N_a - 2$ and $X^{s,c}$ by $\tilde{X}^{s,c}$. The quantity $\tilde{X}^s_{N_a-2}$ is given by Eq. (3.75) in which the values of λ_h are put equal to $+\infty$ and $-\infty$:

$$\tilde{X}^s_{N_a-2}(\lambda) = \frac{1}{N_a}\sum_{\alpha=1}^{N_a/2-2}\delta(\lambda-\lambda_\alpha) - \sigma_{N_a-2}(\lambda), \tag{3.84}$$

and $\tilde{X}^c_{N_a-2}$ by Eq. (3.76) where the values k_h are put equal to $+\pi$ and $-\pi$:

$$\tilde{X}^c_{N_a-2}(k) = \frac{1}{N_a}\left[\sum_{j=1}^{N_a-2}\delta(k-k_j) + \delta(k-\pi) + \delta(k+\pi)\right] - \rho_{N_a-2}(k). \tag{3.85}$$

In order to calculate the corrections to the energy of the gap we need to calculate the corrections to the ground state energies for the considered states, which are equal to

$$E_{N_a} = -2\sum_1^{N_a}\cos k_j, \quad E_{N_a-2} = -2\sum_1^{N_a}\cos k_j + 2\sum_{k_h}\cos k_h. \tag{3.86}$$

Using $X^c_{N_a}$ from Eq. (3.57) these relations can be rewritten in an integral form as

$$\frac{E_{N_a}}{N_a} = -2\int_{-\pi}^{\pi}\rho_{N_a}(k)\cos k\,dk - 2\int_{-\pi}^{\pi}X^c_{N_a}(k)\cos k\,dk, \tag{3.87}$$

$$\begin{aligned}\frac{E_{N_a-2}}{N_a} &= -2\int_{-\pi}^{\pi}\rho_{N_a-2}(k)\cos k dk - 2\int_{-\pi}^{\pi}X^c_{N_a-2}(k)\cos k\,dk + 2\sum_{k_h}\frac{\cos k_h}{N_a}\\ &= -2\int_{-\pi}^{\pi}\rho_{N_a-2}(k)\cos k\;dk - 2\int_{-\pi}^{\pi}\tilde{X}^c_{N_a-2}(k)\cos k\;dk - \frac{4}{N_a}.\end{aligned} \tag{3.88}$$

The finite size corrections to the ground state energy are given by (Eq. (3.61))

$$\delta E_N = E_N - E_{\infty,N}, \tag{3.89}$$

where the energies $E_{\infty,N}$ in the thermodynamic limit are

$$\frac{E_{\infty,N_a}}{N_a} = -2\int_{-\pi}^{\pi}\rho_{\infty,N_a}(k)\cos k\;dk, \tag{3.90}$$

$$\frac{E_{\infty,N_a-2}}{N_a} = -2\int_{\pi}^{\pi} \rho_{\infty,N_a-2}(k)\cos k\; dk - \frac{4}{N_a}, \tag{3.91}$$

with $\rho_{\infty,N_a}(k)$ given by Eq. (3.32) and $\rho_{\infty,N_a-2}(k)$ by Eq. (3.78) with $k_h = \pm\pi$ and $\lambda_h = \pm\infty$.

Using Eqs. (3.87), (3.88), (3.85), (3.83), and Eq. (3.91) with ρ_{∞,N_a} and ρ_{∞,N_a-2} following from Eqs. (3.32) and Eq. (3.78), we obtain

$$\frac{\delta E_{N_a}}{N_a} = -\int_{-\pi}^{\pi} \epsilon_c(k) X^c_{N_a}(k)\; dk - \int_{-\infty}^{\infty} \epsilon_s(\lambda) X^s_{N_a}(\lambda)\; d\lambda, \tag{3.92}$$

$$\frac{\delta E_{N_a-2}}{N_a} = -\int_{-\pi}^{\pi} \epsilon_c(k) \tilde{X}^c_{N_a-2}(k)\; dk - \int_{-\infty}^{\infty} \epsilon_s(\lambda) X^s_{N_a-2}(\lambda)\; d\lambda, \tag{3.93}$$

where

$$\epsilon_c(k) = 2\cos k + 2\int_0^{\infty} \frac{J_1(\omega)\exp(-\omega u)}{\omega\cosh(\omega u)}\cos(\omega\sin k)\; d\omega, \tag{3.94}$$

$$\epsilon_s(\lambda) = 2\int_0^{\infty} \frac{J_1(\omega)}{\omega\cosh(\omega u)}\cos(\omega\lambda)\; d\omega, \tag{3.95}$$

and we used the fact that $\epsilon_s(\pm\infty) = 0$, so that $\tilde{X}^s_{N_a-2}(\lambda)$ can be replaced by $X^s_{N_a-2}(\lambda)$ in Eq. (3.93).

For the repulsive Hubbard model at half filling, the gap is in the charge sector and the spin sector is gapless. Accordingly, the first term in the right-hand side of Eq. (3.92) describes the contribution of gapped charge excitations, and the second term is due to the contribution of gapless spin excitations.

We now return to the equation for the gap, Eq. (3.64), and using Eq. (3.92) we re-write the finite size corrections to the gap in the form

$$\delta\Delta = \delta E_{N_a-2} - \delta E_{N_a} = \delta\Delta_{ng} + \delta\Delta_g + \delta, \tag{3.96}$$

where

$$\delta\Delta_{ng}/N_a = \int_{-\infty}^{\infty} \epsilon_s(\lambda) X^s_{N_a}\; d\lambda - \int_{-\infty}^{\infty} \epsilon_s(\lambda) X^s_{N_a-2}\; d\lambda, \tag{3.97}$$

is the contribution of the gapless sector,

$$\delta\Delta_g/N_a = \int_{-\pi}^{\pi} \epsilon_c(k) X^c_{N_a}\; dk - \int_{-\pi}^{\pi} \epsilon_c(k) X^c_{N_a-2}\; dk, \tag{3.98}$$

is due to gapped excitations, and we used a relation

$$\tilde{X}^c_{N_a-2} = X^c_{N_a-2} - \frac{1}{N_a}\sum_{h=1}^{2}\delta(k-k_h) + \frac{1}{N_a}\left[\delta(k-\pi)+\delta(k+\pi)\right].$$

The term δ which is present in the gapped sector is given by

$$\delta = \sum_h \epsilon(k_h) - \epsilon(\pi) - \epsilon(-\pi) \tag{3.99}$$

and for $N_a\Delta_\infty \gtrsim 1$ it reduces to

$$\delta \approx \epsilon_c''(\pi)(k_h^+ - \pi)^2,$$

where k_h^+ is the value of k_h which is close to π at large N_a. This term behaves as $1/N_a^2$ for large N_a. In the limit of $u \ll 1$ the value of k_h^+ can be found from Eqs. (3.71) and (3.79) using the condition $Z_{N_a-2} = 1/2 - 1/2N_a$. We then obtain

$$\frac{\delta}{\Delta_\infty} = \frac{8\pi^2}{[\Delta_\infty N_a + (16/\pi)\ln 2]^2}, \tag{3.100}$$

where at half filling the gap of the thermodynamic limit Δ_∞ is given by

$$\Delta_\infty = 4u - 4 + 4\int_0^\infty \frac{\exp(-\omega u)J_1(\omega)}{\omega\cosh\omega u}d\omega \tag{3.101}$$

at any interaction strength. The origin of the term δ is related to the definition of the gap. The state with two additional or two missing spin up (or spin down) particles contains unpaired fermions with energies above the gap. gapped excitations of our model are $S = 1/2$ -solitons which appear only in pairs. We thus calculate the exact energy of the states with 2 solitons which have different nonzero momenta and energies near the bottom of the excitation band. The contribution (3.99) takes into account these nonzero kinetic energies of the solitons and is proportional to the curvature of the excitation spectrum.

Note that the contribution of the gapped charge excitations for the repulsive Hubbard model corresponds to the contribution of gapped spin excitations for the attractive model, and the contribution of gapless spin excitations corresponds to the contribution of gapless charge excitations in the attractive case.

3.2.3 Exponential corrections for half filling

In this Section we calculate the finite size corrections to the gap originating from the gapped sector and given by Eq. (3.98). Using the Poisson relation $\sum_n \delta(x-n) = \sum_m \exp[2\pi x m i]$ we reduce each of the terms in the right-hand side of Eq. (3.98) to the form

$$\int_{-\pi}^{\pi} dk \epsilon_c(k) X_N^c(k) = \tag{3.102}$$
$$- \int_{-\pi}^{\pi} dk \epsilon_c(k) \left[\frac{\rho_N(k)}{\exp[-2\pi i N_a Z_N^c(k+i0)]+1} + \frac{\rho_N(k)}{\exp[2\pi i N_a Z_N^c(k-i0)]+1} \right].$$

To lowest order, we take the functions $\rho_N(k)$ and $Z_N^c(k)$ equal to their values in the thermodynamic limit, they are given by Eq. (3.32) and Eq. (3.71) for the case $N = N_a$, and by Eq. (3.78) and Eq. (3.79) for $N = N_a - 2$, with $k_h = \pm\pi$ and $\lambda_h = \pm\infty$. One can show that the integral from $-\pi$ to π in the right-hand side of Eq. (3.102) is equal to the integral from $(-\pi + i\text{arcsinh}u)$ to $(\pi + i\text{arcsinh}u)$ for the first term of the integrand plus the integral from $(-\pi - i\text{arcsinh}u)$ to $(\pi - i\text{arcsinh}u)$ for the second term. The edge points of the integration ($k_0 = \pm\pi \pm i\text{arcsinh}u$) are the saddle points at which $\rho(k) = dZ/dk|_{k=k_0} = 0$. Equation (3.98) then reduces to

$$\frac{\delta\Delta_g}{N_a} = \int_{-\pi+i\gamma}^{\pi+i\gamma} \left[\frac{\rho_{N_a}(k)\epsilon_c(k)}{1+\exp\left[-2\pi i N_a Z_{N_a}^c(k)\right]} - \frac{\rho_{N_a-2}(k)\epsilon_c(k)}{1+\exp\left[-2\pi i N_a Z_{N_a-2}^c(k)\right]} \right] dk$$
$$+ c.c. = \frac{1}{2\pi i N_a} \int_{-\pi+i\gamma}^{\pi+i\gamma} \epsilon_c'(k) \ln\left(\frac{1+\exp[2\pi i N_a Z_{N_a}^c(k)]}{1+\exp[2\pi i N_a Z_{N_a-2}^c(k)]} \right) dk + c.c., \tag{3.103}$$

where $\gamma = \text{arcsinh}u$.

The edge points of the integration $k_0 = \pm\pi \pm i\text{arcsinh}u$ are the saddle points at which $\rho_{N_a}(k) = dZ_{N_a}/dk = 0$. For sufficiently large N_a we may use the saddle point approximation, and the expression for $\delta\Delta_g$ becomes

$$\delta\Delta_g \approx C \frac{|\epsilon_c'(k_0)|}{\pi\sqrt{N_a|\rho'(k_0)|}} \exp[-S_0], \tag{3.104}$$

where

$$\epsilon_c'(k_0) = i\left[2u - 2\sqrt{u^2+1} \int_0^\infty J_1(\omega) \tanh(\omega u) \exp(-\omega u)\, d\omega \right], \tag{3.105}$$

$$\rho'(k_0) = \frac{i}{2\pi}\left[\frac{u}{\sqrt{u^2+1}} + (u^2+1)\int_0^\infty \omega \tanh(\omega u)\, J_0(\omega)\exp(-\omega u)\, d\omega\right], \quad (3.106)$$

$$S_0 = -2\pi i(Z^c_{N_a}(k_0) - 1/2) = N_a\left[\gamma - \int_0^\infty \frac{\tanh(\omega u)\exp(-\omega u)}{\omega} J_0(\omega) d\omega\right], \quad (3.107)$$

$$C = \left[1 - \left(\frac{\Gamma(3/4)}{2\Gamma(5/4)}\right)^4\right], \quad (3.108)$$

and we used the relation

$$Z^c_{N_a-2}(k_0) = Z^c_{N_a}(k_0) + \frac{i}{\pi N_a}\int_0^\infty \frac{\tanh(\omega u)}{\omega}\exp(-\omega u)\, d\omega = Z^c_{N_a}(k_0) + \frac{2i}{\pi N_a}\ln\left[\frac{2\Gamma(5/4)}{\Gamma(3/4)}\right]. \quad (3.109)$$

The saddle point approximation assumes that the exponent in Eq. (3.104) is large:

$$S_0 \gg 1. \quad (3.110)$$

In the case of strong interaction, $u \gg 1$, Eq. (3.104) gives

$$\delta\Delta_g \approx \frac{1}{\sqrt{N_a}\, u^{N_a-1}}, \quad (3.111)$$

and one sees that in this limit the correction $\delta\Delta_g$ is negligible.

The situation changes for $u < 1$. In the limit of $u \ll 1$, from Eq. (3.104) we obtain:

$$\delta\Delta_g \approx C\sqrt{\frac{2}{\pi}}\frac{\Delta_\infty \exp[-\Delta_\infty N_a/4]}{\sqrt{\Delta_\infty N_a}} \approx 0.6\frac{\Delta_\infty \exp[-\Delta_\infty N_a/4]}{\sqrt{\Delta_\infty N_a}}, \quad (3.112)$$

where the gap in the thermodynamic limit, Δ_∞, is given by Eq. (3.43). The criterion (3.110) then becomes $N_a\Delta_\infty \gg 1$. The obtained relation (3.112) is in accordance with the universal scaling behavior of the gap in massive quantum field theories [102], which is expected for the Hubbard model at $u \ll 1$.

3.2.4 Power law corrections

In this section we rederive the correction to the gap, $\delta\Delta_{ng}$, provided by the gapless sector using the conformal field theory $1/N$ expansion for the energy [99, 100, 103], Eq. (3.50) and (3.49). For the half-filled case, and to the first order in $1/N$, we

have (Eq. (3.51)),

$$\delta\Delta_{ng} = \frac{2\pi}{N_a}\frac{I_1\left(\frac{\pi}{2u}\right)}{I_0\left(\frac{\pi}{2u}\right)}\left(1 - \frac{1}{2\ln[N_a I_0(\pi/2u)]}\right). \tag{3.113}$$

In the limit of strong coupling this expression becomes:

$$\delta\Delta_{ng} \simeq \frac{\pi^2}{2N_a u}; \qquad u \gg 1, \tag{3.114}$$

and the power law correction (3.114) always dominates over the negligible exponential correction (3.111). The situation is the same for $u \sim 1$. In the limit of weak coupling, from Eq. (3.113) we obtain:

$$\delta\Delta_{ng} = \frac{2\pi}{N_a}; \qquad u \ll 1. \tag{3.115}$$

Comparing Eq. (3.115) with Eq. (3.112) we see that there is a range of Δ_∞ and N_a where the exponential correction is important.

3.2.5 Numerical results

In this Section we present the numerical results for the gap of the Fermi-Hubbard model in the case of attractive interaction ($U < 0$). The gap was calculated directly from Eq. (3.63) (Eq. (3.64) for the half-filled case), where the energies E_{N_a} and E_{N_a-2} were calculated using Eq. (3.19) with momenta k_j following from the Bethe ansatz equations (3.26).

It is convenient to present the ratio $\delta\Delta_g/\Delta_\infty$ as a function of $N_a\Delta_\infty$. In Fig. (3.1) we show $\delta\Delta_g/\Delta_\infty$ versus $N_a\Delta_\infty$ for several values of u, and one clearly sees that for not very large $N_a\Delta_\infty$ this correction becomes significant.

The comparison of $\delta\Delta_{ng}/\Delta_\infty$ (3.113) for $u = 1$ with the result of exact calculations from Eq. (3.97) shows the validity of conformal results even for not very large N_a (see Fig. 3.2). For example, at $u = 1$ even for $N_a = 10$, ($N_a\Delta_\infty \approx 13$) the relative difference is $\sim 15\%$.

In the limit of strong coupling the power law correction (3.114) always dominates over the negligible exponential correction (3.111). The situation changes for $u < 1$. For not very large $\Delta_\infty N_a$, the non-conformal correction $\delta\Delta_g$ originating

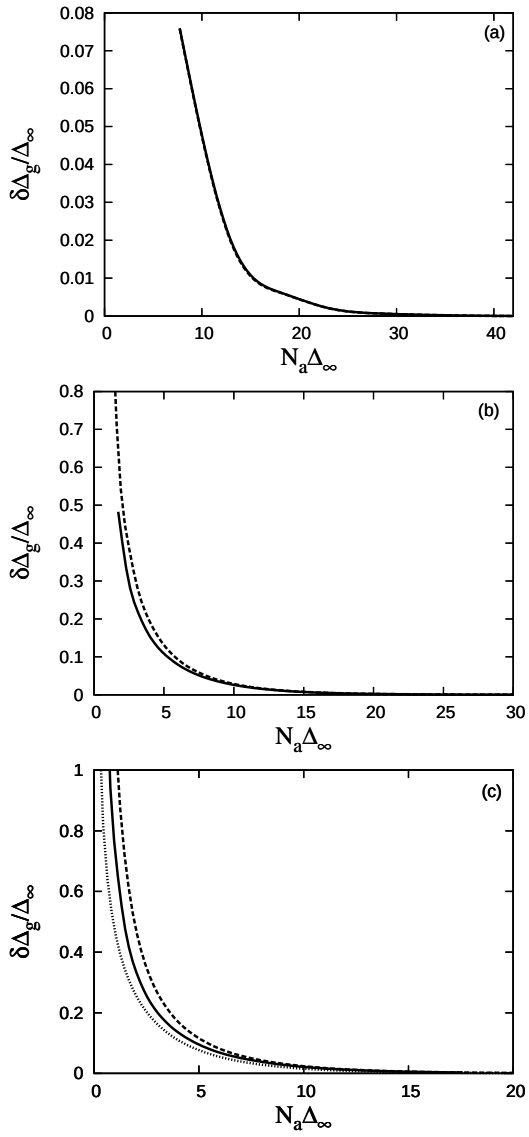

Figure 3.1: The correction $\delta\Delta_g/\Delta_\infty$ versus $N_a\Delta_\infty$. The solid curve is the result of exact calculations from Eq. (3.98), and the dashed curve represents the result of Eq. (3.103). In a) $u = 1$, in b) $u = 0.5$, and in c) $u = 0.25$ with the dotted curve showing the result of Eq. (3.112)

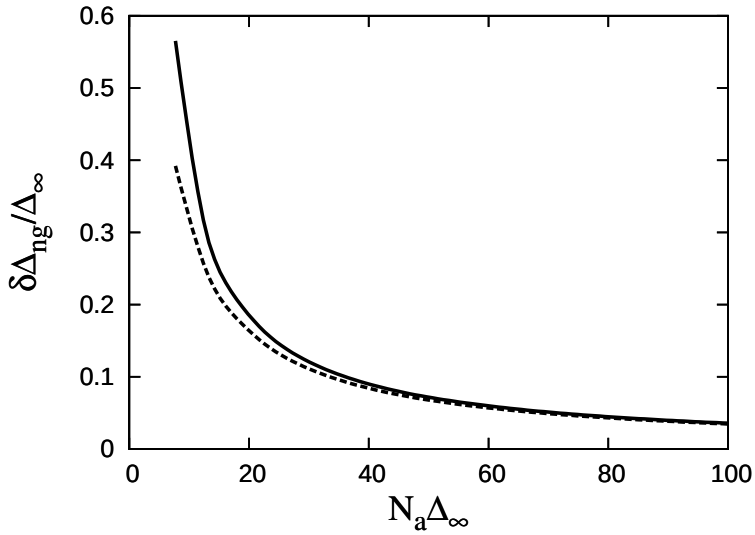

Figure 3.2: The correction $\delta\Delta_{ng}/\Delta_\infty$ versus $N_a\Delta_\infty$ for $u = 1$. The solid curve shows the result of exact calculation from Eq. (3.97) and the dashed curve shows the result of Eq. (3.113).

from gapped excitations becomes comparable with $\delta\Delta_{ng}$. This is seen from Fig. (3.3), where we present the two corrections for $u = 1$, $u = 0.5$ and $u = 0.25$. We also display the correction δ/Δ_∞ which turns out to be significant for $N_a\Delta_\infty$ not greatly exceeding unity.

In Fig. (3.4) we can see the comparison between the value of the gap calculated from formula (3.63) and its analytical expression. The crosses show the numerical results for Δ as a function of N_a at half filling and the solid curve shows the result of the relation

$$\Delta = \Delta_\infty + \delta\Delta_g + \delta\Delta_{ng} + \delta, \tag{3.116}$$

where the gap in the thermodynamic limit, Δ_∞, is given by Eq. (3.101) [90]. The conformal power law correction $\delta\Delta_{ng}$ is given by Eq. (3.113), and the non-conformal correction $\delta\Delta_g$ by Eqs. (3.112). A direct comparison of Δ with the gap of the thermodynamic limit Δ_∞ (3.101) shows that finite size corrections can be safely omitted for $N_a\Delta_\infty > 40$. On the other hand, already at $N_a\Delta_\infty < 10$,

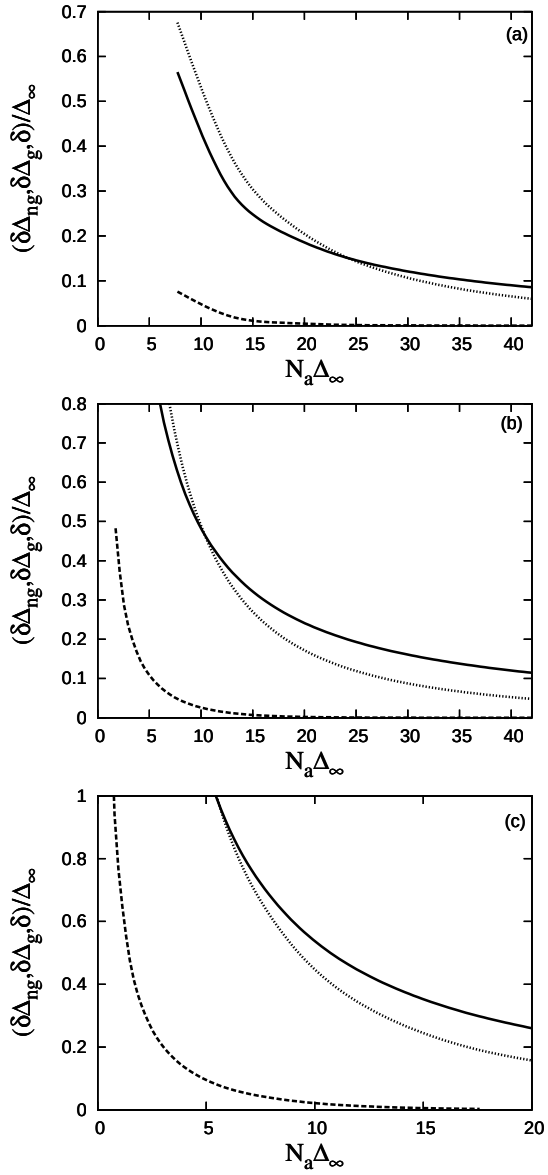

Figure 3.3: The result of exact calculations from Eqs. (3.97), (3.98) and (3.99) for $\delta\Delta_{ng}/\Delta_\infty$ (solid curve), $\delta\Delta_g/\Delta_\infty$ (dashed curve), and δ/Δ_∞ (dotted curve) versus $N_a\Delta_\infty$. In a) $u = 1$, in b) $u = 0.5$, and in c) $u = 0.25$.

they dominate the gap. For $u = 0.25$ where $\Delta_\infty = 5 \cdot 10^{-3}$ this occurs already at $N_a < 1.5 \cdot 10^3$. For $u = 1$ we have $\Delta_\infty = 1.28$ and finite size corrections are important only for $N_a < 30$.

It is important that for $N_a \Delta_\infty \sim 10$ or even somewhat large the non-conformal corrections originating from the gapped sector become comparable with conformal corrections. This is seen in Fig. (3.1). For $u = 1$ even the exponential correction $\delta\Delta_g$ is comparable with $\delta\Delta_{ng}$. For $u = 0.5$ and $u = 0.25$ this is the correction δ that remains comparable with $\delta\Delta_{ng}$, whereas the exponential correction $\delta\Delta_g$ is about 10% of $\delta\Delta_{ng}$.

Qualitatively, the dependence $\Delta(N_a)$ remains the same for smaller filling factors. This is seen from Fig. (3.5), where we present our numerical results for filling factor $n = 0.2$. For $u = 1.25$ finite size effects become important only at a very small number of lattice sites $N_a < 20$. For $u = 0.25$ the thermodynamic-limit gap is $\Delta_\infty \approx 5 \cdot 10^{-2}$ and finite size effects are already important for $N_a \approx 500$.

3.3 $N_a u \ll 1$ limit

The discussed results were related to the case where $N_a u \gg 1$. For example, the inequality (3.110) automatically requires the condition $N_a u \gg 1$, irrespective of weather u is large or small. In the opposite limit of $N_a u \ll 1$, which can be realised for $u \ll 1$, the energy spectrum of the attractive Hubbard Model shows no exponential gap and both charge and spin sectors are conformal. The analysis of Lieb-Wu equations for this case has been done in [104, 105], and found corrections $\sim u/N_a$. This can be understood from the conformal $1/N_a$ expansion as a consequence of the linear dependence of the velocities of elementary excitations on the interaction constant u [104, 106].

In this Section we consider the limit of $uN_a \ll 1$ for completeness and present first order corrections in u to the ground state energy and to the gap in the excitation spectrum. As in the previous sections, we calculate the energy for the Hubbard model in the repulsive case, where the Bethe Ansatz equations are easily solved, and then restore the energy for the attractive case using the particle-hole

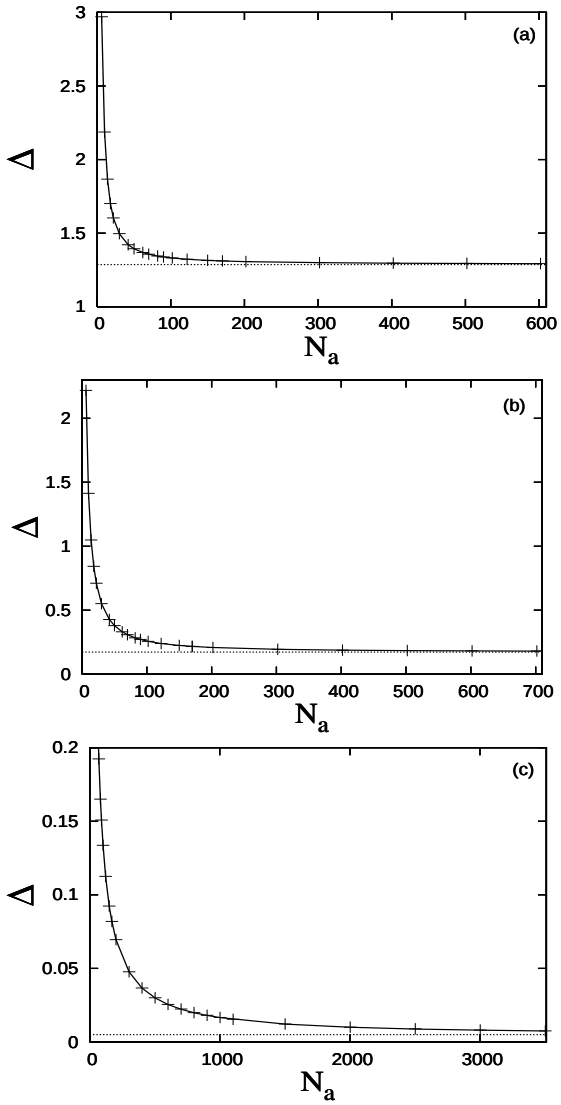

Figure 3.4: The gap Δ in units of t versus N_a at half filling for $u = 1$ in a), $u = 0.5$ in b), and $u = 0.25$ in c). The dotted line is the value of the gap in the thermodynamic limit. The sum $\delta\Delta_{ng} + \delta\Delta_g + \delta + \Delta_\infty$ (solid line) exactly coincides with the gap Δ calculated directly from the Bethe Ansatz equations (3.26) and (3.25) using Eqs. (3.19) and (3.64) (crosses).

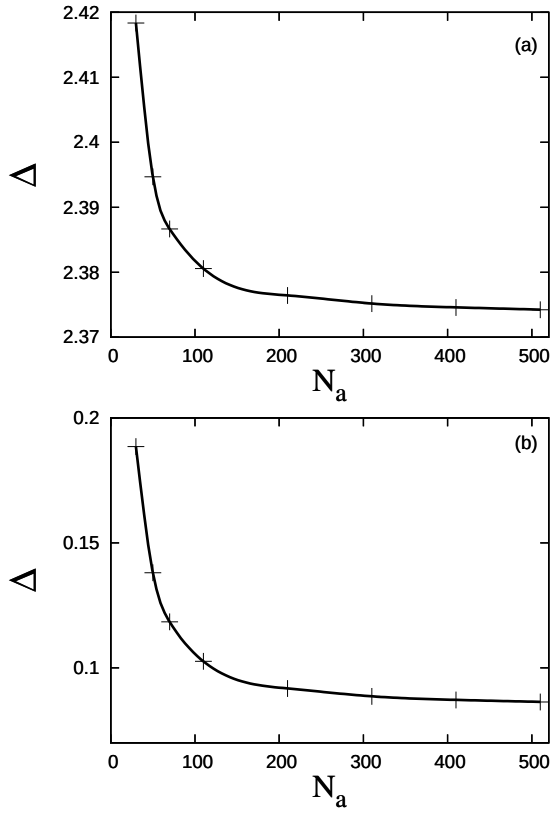

Figure 3.5: The gap Δ in units of t versus N_a, calculated numerically for $u = 1.25$ in a), and $u = 0.25$ in b) for the filling factor $n = 0.2$.

symmetry.

Consider a system of N particles ($N_\downarrow$ spin-down and $N - N_\downarrow$ spin-up) with repulsive interaction. From the Lieb-Wu equation (3.26) we obtain the momenta k_j to first order in u:

$$e^{ik_j N_a} = \prod_{\alpha=1}^{N_\downarrow} \frac{\sin k_j - \lambda_\alpha + iu}{\sin k_j - \lambda_\alpha - iu} \Rightarrow \delta k_j = k_j - k_j^0 = \frac{1}{N_a} \sum_{\alpha=1}^{N_\downarrow} \frac{2u}{\sin k_j^0 - \lambda_\alpha^0}, \quad (3.117)$$

where k^0 and λ^0 are the momenta and rapidities for $u \to 0$. The energy itself and

the interaction-induced change of the energy are given by

$$E = -2\sum_{j=1}^{N}\cos k_j \Rightarrow \delta E = E - E^0 = \frac{4u}{N_a}\sum_{j=1}^{N}\sum_{\alpha=1}^{N_\downarrow}\frac{\sin k_j^0}{\sin k_j^0 - \lambda_\alpha^0}, \tag{3.118}$$

where E_0 is the ground state energy for $u \to 0$.

We now calculate the densities of momenta k and rapidities λ in the thermodynamic limit from Eqs. (3.29) and (3.28). To the lowest order in u, using the definition of the Dirac delta function $\lim_{u\to 0}\frac{u}{x^2+u^2} = \pi\delta(x)$, we obtain:

$$\begin{aligned} 2\sigma(\lambda) &= \int_{-Q}^{Q}\delta(\lambda - \sin k)\rho(k)dk \\ \rho(k) &= \frac{1}{2\pi} + \cos k\int_{-B}^{B}\delta(\lambda - \sin k)\sigma(\lambda)d\lambda. \end{aligned} \tag{3.119}$$

The solution of Eq. (3.119) is

$$\begin{aligned} \sigma(\lambda) &= \frac{1}{2\pi}\frac{1}{\sqrt{1-\lambda^2}}, \\ \rho(k) &= \begin{cases} 1/\pi; & k \le \pi n_\downarrow \\ 1/2\pi; & \pi n_\downarrow < k \le \pi(n - n_\downarrow), \end{cases} \end{aligned} \tag{3.120}$$

where we took into account the two regimes $Q \le \pi/2$ and $Q > \pi/2$. Then, using Eq. (3.30) for the total number of particles and the number of spin-down particles we find an expression for the integration limits Q and B:

$$B = \sin(\pi n_\downarrow), \qquad Q = \pi(n - n_\downarrow). \tag{3.121}$$

Note that $B \le \sin Q$.

Using Eq. (3.120) we obtain the interaction-induced change of the energy to first order in u:

$$\begin{aligned} \frac{\delta E}{N_a} &= 4u\int_{-Q}^{Q}dk\int_{-B}^{B}d\lambda\frac{\sin k}{\sin k - \lambda}\sigma(\lambda)\rho(k) = \\ &= \frac{4u}{\pi^2}(\pi n_\downarrow)^2 + \frac{4u}{\pi^2}\int_{\pi n_\downarrow}^{\pi(n-n_\downarrow)}dk\int_0^{\pi n_\downarrow}dq\frac{\sin^2 k}{\sin^2 k - \sin^2 q}, \end{aligned} \tag{3.122}$$

where we made the change of variables $\lambda \Rightarrow \sin q$. For the case of attraction we should substitute $n_\uparrow \to 1 - n_\uparrow$, $n_\downarrow \to n_\downarrow$, in accordance with the symmetry properties (3.16), and integrating over dq we find:

$$\frac{\delta E(-u)}{N_a} = -4un_\downarrow + 4un_\downarrow^2 + \frac{2u}{\pi^2}\left(2\int_{\pi n_\downarrow}^{\pi/2} - \int_{\pi n_\downarrow}^{\pi n_\uparrow}\right) dk \tan k \ln\left(\frac{\tan k + \tan \pi n_\downarrow}{\tan k - \tan \pi n_\downarrow}\right). \tag{3.123}$$

Eq. (3.123) leads to the following result for the interaction-induced change of the energy to first order in $N_a u$:

$$\begin{aligned}\frac{\delta E(-u)}{N_a} &= 4un_\downarrow^2 - 4un_\downarrow + \frac{4u}{\pi}\arctan \pi n_\downarrow \\ &- \frac{u}{\pi^2}\ln\left(\frac{1+\tan^2 \pi n_\uparrow}{1+\tan^2 \pi n_\downarrow}\right)\ln\left(\frac{\tan \pi n_\uparrow + \tan \pi n_\downarrow}{\tan \pi n_\uparrow - \tan \pi n_\downarrow}\right) \\ &+ \frac{2u}{\pi^2}\left(-\mathrm{Re}Li_2\left(\frac{2\tan \pi n_\downarrow}{\tan \pi n_\downarrow - i}\right) - \mathrm{Re}Li_2\left(\frac{\tan \pi n_\uparrow + \tan \pi n_\downarrow}{\tan \pi n_\downarrow - i}\right)\right. \\ &+ \left.\mathrm{Re}Li_2\left(\frac{\tan \pi n_\uparrow - \tan \pi n_\downarrow}{-\tan \pi n_\downarrow - i}\right)\right),\end{aligned} \tag{3.124}$$

where $Li_2(z) = \sum_{k=1}^{\infty} z^k/k^2$ is a polylogarithmic function.

In the limit of small filling factors, $N_\uparrow \ll N_a$ and $N_\downarrow \ll N_a$, after a straightforward algebra we obtain:

$$\frac{\delta E}{N_a} \approx u(-4n_\downarrow - 4n_\uparrow n_\downarrow + 2n_\downarrow^2) \tag{3.125}$$

The limit of small filling factors in the Hubbard model corresponds to the gas phase of spin-1/2 fermions. For this case the ground state energy at $Nu \ll 1$ has been calculated in Refs. [107, 108, 109], and the result of Eq. (3.125) coincides with that of Refs. [107, 108, 109] in the attractive case.

Using Eq. (3.62) we then find a small interaction-induced correction to the gap in the excitation spectrum ($n_\uparrow = n_\downarrow = n/2$) of the attractive model to the lowest order in uN_a. For small filling factors we have: $\delta\Delta \approx 4u/N_a$, and in the considered limit of $N_a u \ll 1$ this correction is small compared to the level spacing $\sim 1/N_a$ in our finite size system.

3.4 Conclusions

In conclusion, in this chapter we have studied finite size effects for the gap in the excitation spectrum of the 1D Fermi Hubbard model with on-site attraction. The approach developed for the situation in which the thermodynamic-limit gap Δ_∞ greatly exceeds the level spacing (near the Fermi energy) of the finite size system leads to two types of finite size corrections. For large interactions ($u > 1$) the leading is a power law conformal correction to Δ_∞, which behaves as $1/N_a$ and originates from the gapless sector of the excitation spectrum. We also find a non-conformal exponential correction originating from the gapped branch of the spectrum. As found at half filling, in the weakly interacting regime ($u \ll 1$) the non-conformal correction can become of the same order of the conformal one.

For sufficiently small number of lattice sites (particles) the gap Δ is dominated by finite size effects. From a general point of view, this happens when $\Delta_\infty < 1/N_a$, i. e. Δ_∞ is smaller than the level spacing of the finite size system at energies close to the Fermi energy. Accordingly, for large interactions ($u \gg 1$) the finite size effects are not important as long as $N_a \gg 1$. However, in the weakly interacting regime ($u < 1$) they become dominant already at significantly larger N_a than a simple dimensional estimate $1/\Delta_\infty$. This is clearly seen from our results in Fig. (3.3) and Fig. (3.4) for $\Delta(N_a)$ at half filling.

Our findings are especially important for the studies of the 1D regime with cold atoms, where the number of particles in a 1D tube ranges from several tens to several hundreds [110, 111]. For such systems in the weakly interacting regime one cannot use the result of the thermodynamic limit for the gap.

Chapter 4

Parametric excitation of a 1D gas in integrable and non-integrable cases

4.1 Introduction

The field of ultracold gases has progressed enormously towards obtaining quantum systems with desired densities and types of constituent atoms, trapping geometries, and well controlled interparticle interactions [112]. In particular, by using either an optical potential or large magnetic field gradients, one can confine the motion of atoms to one dimension and create interacting 1D gases of bosons [43, 44, 113, 34, 114, 115] and fermions [46], which can be described by the integrable Lieb-Liniger [25] and Yang-Gaudin [116, 117] models respectively. The purity and isolation of such systems from the environment makes them ideal candidates for studies of fundamental differences between integrable and non-integrable many-body dynamics. A pioneering experiment on this subject has been performed recently by Kinoshita and co-workers [48]. They have shown that a 1D Bose gas initially prepared in a highly excited state does not equilibrate in the lifetime of the experiment, whereas essentially the same system with a weaker 1D confinement

thermalises much faster.

How do we decide whether a system is integrable or not? Let us put aside strict mathematical definitions of quantum integrability ([118, 119], see also [14]) and look at the problem phenomenologically. What measurement should we perform on a system in order to conclude on its integrability? The field of quantum chaos suggests to look at the spectrum of the system [120]. More specifically at its statistics. If energy levels are not correlated (the nearest neighbour spacing distribution is Poissonian), we are dealing with an integrable or regular system [121]. If, in contrast, levels repel each other, the system is not integrable [123, 122]. The problem with this criterion is that the density of levels grows exponentially with the number of atoms and it seems unrealistic to achieve such single level sensitivity in experiments with ultracold gases.

Another signature of integrability is the localization of eigenstates of a regular system in a certain physically meaningful basis [124]. Excitations initially localized in this basis will stay localized like an electron below the mobility edge of a disordered semiconductor. Moreover, one can probe the local density of states by acting on the system with a localized perturbation. The passage from integrable to non-integrable behaviour is similar to the localization-delocalisation transition. The idea of such a transition in the Fock space of many-electron states turned out to be very successful in understanding the structure of the spectrum of mesoscopic systems [125, 126]. In the case of the Lieb-Liniger and Yang-Gaudin models the eigenfunctions of excited states are localized in momentum space. This can be seen directly from their Fourier transform - in the non-interacting case the eigenfunctions are delta-peaks, and switching on the interaction only slightly delocalises them.

In this chapter we study the response of a highly excited 1D gas to a periodic modulation of the coupling constant. We calculate the corresponding dynamic structure factors and show that they are dramatically different in the two considered cases: the integrable Lieb-Liniger model and the non-integrable model of a single mobile impurity in a Fermi gas. The non-integrable system is sensitive to

excitations with frequencies as low as the mean level spacing, which is exponentially small, whereas the threshold frequency in the integrable case is much larger and scales polynomially with the size of the system. We argue that this is a clear manifestation of the localization of the many-particle wave functions of the integrable system in momentum space and is related to the fact that the modulation of the coupling constant is a localized perturbation in this space. This effect can be used as a probe of integrability for mesoscopic 1D systems and can be observed experimentally by measuring the heating rate of a parametrically excited gas.

The chapter is organized as follows. In Section 4.1.1 we briefly review the theoretical approach for studying the response of a generic system to a weak time-dependent perturbation. We derive the diffusion equation for the state population in the case of highly excited (classical) states, discuss how this equation can be used for calculating the energy absorption rate, and relate the corresponding diffusion constant to the dynamic structure factor. In Section 4.2 we introduce the 1D Hamiltonian and the perturbation that we are going to work with. The dynamic structure factor in the case of a single mobile impurity interacting with two or three fermionic atoms is calculated in Section 4.3. We also compute the spectrum and eigenstates of the system and discuss the evolution of the level statistics with an increase in the number of atoms. The integrable case is discussed in Section 4.4 where we study the spectrum and excitations of the Lieb-Liniger gas and calculate the dynamic structure factor for three and four bosons. In Section 4.5 we develop a theoretical model for calculating the dynamic structure factor of the Lieb-Liniger model in the case of an arbitrary number of atoms and compare the analytical results with the exact numerical calculation of Section 4.4. We conclude in Section 4.6.

4.1.1 Linear response

Consider a Hamiltonian which contains a time-independent part H_0 and a time-dependent perturbation $V(t)$. The evolution of the wavefunction is governed by

the Schrödinger equation

$$i\frac{\partial}{\partial t}|\Psi(t)\rangle = [H_0 + V(t)]|\Psi(t)\rangle, \tag{4.1}$$

and we look for its solution in the form $|\Psi(t)\rangle = \sum_\nu \alpha_\nu(t)\exp(-i\epsilon_\nu t)|\psi_\nu^0\rangle$, where $|\psi_\nu^0\rangle$ and ϵ_ν are the eigenfunctions and eigenenergies of H_0. Using the orthonormality of the set $\{|\psi_\nu^0\rangle\}$ we obtain the evolution equation for the coefficients $\alpha_\nu(t)$:

$$\dot{\alpha}_\nu(t) = -i\sum_\mu \langle\psi_\nu^0|V(t)|\psi_\mu^0\rangle\alpha_\mu(t)e^{-i(\epsilon_\mu-\epsilon_\nu)t}. \tag{4.2}$$

Assume that the system is initially in the state η of the unperturbed Hamiltonian. The initial condition then reads $|\Psi(0)\rangle = |\psi_\eta^0\rangle$ or, equivalently, $\alpha_\nu(0) = \delta_{\nu\eta}$, and Eq. (4.2) to the first order in $V(t)$ reduces to

$$\dot{\alpha}_\nu^{(1)}(t) = -i\langle\psi_\nu^0|V(t)|\psi_\eta^0\rangle e^{-i(\epsilon_\eta-\epsilon_\nu)t}. \tag{4.3}$$

Without loss of generality we can now consider the perturbation in the form

$$V(t) = Fe^{-i\omega t} + F^\dagger e^{i\omega t}, \tag{4.4}$$

where the operator F is time independent. The solution of Eq. (4.3) for $\nu \neq \eta$ with the initial condition $\alpha_\nu(0) = 0$ reads

$$\alpha_\nu(t) = -\frac{F_{\nu\eta}(e^{i(\epsilon_\nu-\epsilon_\eta-\omega)t}-1)}{(\epsilon_\nu-\epsilon_\eta-\omega)} - \frac{F_{\eta\nu}^*(e^{i(\epsilon_\nu-\epsilon_\eta+\omega)t}-1)}{(\epsilon_\nu-\epsilon_\eta+\omega)}, \tag{4.5}$$

where $F_{\nu\eta} = \langle\psi_\nu^0|F|\psi_\eta^0\rangle$. As we expect, $\alpha_\nu(t)$ is peaked for the states which are in resonance with the perturbation: $\epsilon_\nu \approx \epsilon_\eta \pm \omega$. The modulus squared of the coefficient α_ν determines the probability of diffusion into the state ν. Neglecting fast oscillating terms it is given by

$$|\alpha_\nu(t)|^2 = |F_{\nu\eta}|^2\frac{4\sin^2\left(\frac{\epsilon_\nu-\epsilon_\eta-\omega}{2}t\right)}{(\epsilon_\nu-\epsilon_\eta-\omega)^2} + |F_{\eta\nu}^*|^2\frac{4\sin^2\left(\frac{\epsilon_\nu-\epsilon_\eta+\omega}{2}t\right)}{(\epsilon_\nu-\epsilon_\eta+\omega)^2}. \tag{4.6}$$

Accordingly, the probability for the system to remain in the state η decreases with the rate

$$\Omega = \frac{d}{dt}\sum_{\nu\neq\eta}|\alpha_\nu(t)|^2 = 2\pi\left[S(\epsilon_\eta,\omega) + S(\epsilon_\eta,-\omega)\right]. \tag{4.7}$$

In Eq. (4.7) we replaced summation over ν by integration over energy and introduced the dynamic structure factor

$$S(\epsilon_\eta, \omega) = \sum_\nu \delta(\omega - \epsilon_\nu + \epsilon_\eta)|F_{\nu\eta}|^2, \tag{4.8}$$

which should be understood as the average of $|F_{\nu\eta}|^2$ over (many) final states ν in a narrow energy interval around $\epsilon_\eta + \omega$ multiplied by the density of states at this energy $\rho(\epsilon_\eta + \omega)$.

We can now generalize these results to the case where the initial state distribution is given by the probability density $f(\epsilon)$. The kinetic equation then reads

$$\begin{aligned} \frac{\partial f(\epsilon)}{\partial t} &= 2\pi S(\epsilon - \omega, \omega) f(\epsilon - \omega) + 2\pi S(\epsilon + \omega, -\omega) f(\epsilon + \omega) \\ &- 2\pi S(\epsilon, \omega) f(\epsilon) - 2\pi S(\epsilon, -\omega) f(\epsilon), \end{aligned} \tag{4.9}$$

which can be further simplified assuming that f and S are smooth functions of ϵ on the scale ω. We then arrive to the diffusion equation for the state population

$$\frac{\partial f}{\partial t} = D(\epsilon, \omega) \frac{\partial^2 f}{\partial \epsilon^2}, \tag{4.10}$$

where the diffusion constant equals

$$D(\epsilon, \omega) = 2\pi S(\epsilon, \omega)\omega^2. \tag{4.11}$$

Equation (4.10) gives the energy transfer per unit time from the external field (4.4) to the system

$$\frac{dE}{dt} = \int \epsilon \frac{df(\epsilon)}{dt} d\epsilon = 2\pi\omega^2 \int \epsilon S(\epsilon, \omega) \frac{\partial^2 f(\epsilon)}{\partial \epsilon^2} d\epsilon. \tag{4.12}$$

In the same manner one can write down expressions for the rate of change of other thermodynamic quantities such as entropy or temperature (for systems close to the thermodynamic equilibrium).

Another fundamental issue that naturally arises from the above discussion is the question of adiabaticity. Indeed, the asymptotic behaviour of $S(\epsilon, \omega)$ at small ω gives the dissipative part of the response of the system to a slow variation

of its Hamiltonian and, therefore, measures the degree at which this variation can be assumed adiabatic. Clearly, the more the diffusion constant in Eq. (4.10) is suppressed at small ω the more adiabatic the passage is. In this chapter we show that this low-frequency behaviour strongly depends on whether we consider integrable or non-integrable system.

4.2 Presentation of the problem

Let us consider a system of atoms with short-range interactions on a quasi-1D ring. If the kinetic energie of the atoms is much smaller than the level spacing in the direction of tight confinement, then the gas is kinematically one-dimensional (see Section 1.4). In the case of equal masses of the atoms the corresponding 1D coupling constant is given by Eq. (1.23) [49]

$$g_{1D} = \frac{2}{ma_{1D}} = \frac{2a_{3D}}{ma_{\perp}^2}\left(1 - C\frac{a_{3D}}{a_{\perp}}\right)^{-1}, \tag{4.13}$$

where a_{3D} is the 3D s-wave scattering length, $a_{\perp}$ is the oscillator length of the transversal confinement, and $C = 1.0326...$ is the numerical constant. In the general case we write the 1D Hamiltonian as

$$H = -\sum_{j=1}^{N} \frac{1}{2m_j}\frac{\partial^2}{\partial x_j^2} + \sum_{i<j} g_{1D}^{ij}\delta(x_i - x_j), \tag{4.14}$$

where the interaction strengths g_{1D}^{ij} are related to the one-dimensional scattering lengths by $g_{1D}^{ij} = 1/\mu_{ij}a_{1D}^{ij}$, and the reduced mass is $\mu_{ij} = m_i m_j/(m_i + m_j)$. We consider the case of repulsive interactions only, for which $g_{1D}^{ij} > 0$.

We are interested in the dynamics of the gas under a periodic modulation of the one-dimensional scattering length:

$$a_{1D}^{ij}(t) = a_{1D}^{ij} + A^{ij}\cos(\omega t). \tag{4.15}$$

This perturbation can be realised by modulating the 3D scattering length by using, for example, its dependence on the magnetic field near a Feshbach resonance.

Alternatively, a_{1D} can be modified by changing the oscillator length of the tight confinement (see Eq. (1.23)). A similar approach for a 3D elongated BEC has been demonstrated in [127].

In the limit of a weak perturbation, $A \ll a_{1D}$, the Hamiltonian (4.14) can be written in the form $H = H_0 + V(t)$, where $V(t)$ is defined by Eq. (4.4) with

$$F = -\sum_{j<k}^{N} \frac{A^{jk}}{2(a_{1D}^{jk})^2 \mu_{jk}} \delta(x_j - x_k). \tag{4.16}$$

In the following we will consider two models: (*i*) a single mobile impurity interacting with a gas of polarised non-interacting fermions and (*ii*) the Lieb-Liniger gas. The former is not integrable if the masses of the impurity and fermions are different. We will focus on this non-integrable model in the next section and calculate the dynamic structure factor $S(\epsilon, \omega)$ with respect to the modulation of a_{1D} in the three- and four-body cases.

4.3 Non-integrable case

The Hamiltonian of a heavy mobile impurity interacting with two light fermions is written as

$$H = -\frac{1}{2M}\frac{\partial^2}{\partial x_1^2} - \sum_{j=2}^{3} \frac{1}{2m}\frac{\partial^2}{\partial x_j^2} + \sum_{j=2,3} \frac{1}{\mu a_{1D}} \delta(x_1 - x_j), \tag{4.17}$$

where M is the mass of the heavy atom, m is the fermion mass, and $\mu = Mm/(M+m)$ is the reduced mass. We use the word "heavy" only for presentation purposes - the ratio M/m is formally allowed to be smaller than one.

We perform the following change of variables for the coordinates of the three atoms on the ring,

$$\begin{aligned} X &= (Mx_1 + mx_2 + mx_3)/(M + 2m), \\ x &= (x_2 + x_3 - 2x_1)/\tan\theta, \\ y &= x_3 - x_2, \end{aligned} \tag{4.18}$$

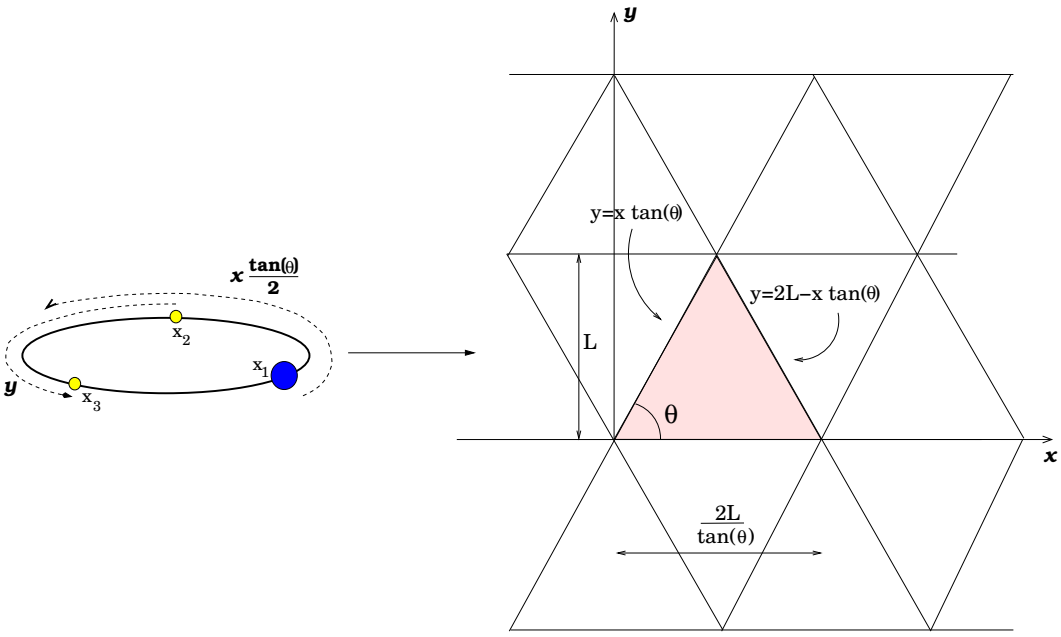

Figure 4.1: Mapping of the 1D three-body problem onto a 2D one-body problem. The shaded triangle corresponds to the region $x_1 < x_2 < x_3 < x_1 + L$.

where $\theta = \arctan\sqrt{1+2m/M}$. In this new coordinates the Schrödinger equation reads

$$\left(-\nabla_X^2 - \nabla_x^2 - \nabla_y^2 - mE + \frac{2m}{\mu a_{1D}} \sum_{n=-\infty}^{\infty} \sum_{\pm} \delta(y \pm x\tan\theta + 2nL)\right) \Psi(x,y,X) = 0, \tag{4.19}$$

where L is the length of the ring and the summation over n takes into account the periodicity of the ring. The motion of the centre of mass integrates out and we will not consider it further. This results in a 2D problem in the xy plane, divided into triangles by three families of lines,

$$y = mL, \quad y = \pm x\tan(\theta) + 2nL, \qquad m,n \text{ integers.} \tag{4.20}$$

The shaded triangle in Fig. (4.1) corresponds to the domain $x_1 < x_2 < x_3 < x_1 + L$. The knowledge of $\Psi(x,y)$ inside this triangle unambiguously determines the wavefunction in all other domains (triangles) because of the periodic boundary

conditions and the symmetry relations:

$$\begin{aligned}
&\Psi(x,y) \overset{x_2\to x_2+L}{=} \Psi(x+L/\tan\theta, y+L),\\
&\Psi(x,y) \overset{x_3\to x_3+L}{=} \Psi(x+L/\tan\theta, y-L),\\
&\Psi(x,y) = -\Psi(x,-y).
\end{aligned} \tag{4.21}$$

In order to diagonalize the Hamiltonian (4.17) and calculate the matrix elements $F_{\nu\eta}$ it is convenient to introduce an auxiliary function

$$f(x) = \Psi(x, x\tan\theta). \tag{4.22}$$

Then the Schrödinger equation (4.19) can be rewritten in the form (we assume that the centre of mass energy is zero):

$$(-\nabla_x^2 - \nabla_y^2 - mE)\Psi = \frac{2m}{a_{1D}\mu}\sum_{n=-\infty}^{\infty}\sum_{\pm} \pm f(x)\delta(y \pm x\tan\theta + 2nL), \tag{4.23}$$

which we can solve for Ψ using the Green function of the Euler equation

$$(-\nabla_x^2 - \nabla_y^2 - mE)G_E(x,y) = \delta(x)\delta(y). \tag{4.24}$$

For the function Ψ we get

$$\Psi(x,y) = \sum_{n=-\infty}^{\infty}\frac{2m}{a_{1D}\mu}\int_{x'}dx'\sum_{\pm}\mp G_E\left(\sqrt{(x-x')^2 + (y \pm x'\tan\theta + 2nL)^2}\right) f(x'). \tag{4.25}$$

Finally, by setting $y = x\tan\theta$ in Eq. (4.25) and using Eq. (4.22) we arrive at the integral equation for the function $f(x)$

$$f(x) = \sum_{n=-\infty}^{\infty}\frac{2m}{a_{1D}\mu}\int_{x'}dx'\sum_{\pm}\mp G_E\left(\sqrt{(x-x')^2 + (\tan\theta(x \pm x') + 2nL)^2}\right) f(x'). \tag{4.26}$$

Equations (4.26) and (4.19) are equivalent, but the former is more convenient for numerical calculation because of the smaller dimension of the configuration space (1D instead of 2D). We can in principle obtain the wavefunction Ψ from the calculated f by using Eq. (4.25). However, for computing $F_{\nu\eta}$ the total information

on Ψ_ν and Ψ_η is not necessary. Indeed, the perturbation F given by Eq. (4.16) is not zero only when the heavy atom is on top of one of the light fermions, the amplitude of which is nothing else than f (see Eqs. (4.22) and (4.18)). Our numerical procedure based on the momentum-space equivalent of Eq. (4.26) allows us to calculate the spectrum and eigenfunctions of the three-body problem for up to ten thousand levels with a very good accuracy.

It is straightforward to generalize the procedure described above to the case of one heavy atom and three light fermions. In this case the function f depends on two spatial coordinates and the size of the configuration space still allows an accurate calculation of several thousand of states.

As we mentioned in the introduction the degree of integrability or chaoticity of a quantum system can be understood from the statistics of its energy levels [121, 122]. Namely, for an integrable system one expects the Poisson distribution, $P(s) = \exp(-s)$, of the nearest neighbour spacings [121]. On the other hand, the Bohigas-Giannoni-Schmit conjecture [122] suggests that (after a proper rescaling) the level fluctuations of any chaotic system with time reversal invariance coincide with the eigenvalue fluctuations of the Gaussian Orthogonal Ensemble (GOE) of random matrices. The nearest neighbour spacing distribution in this case is well fitted by the Wigner surmise, $P(s) = (\pi/2)s\exp(-\pi s^2/4)$.

In order to perform this test and compare the spectral fluctuations of our systems with the Poisson or GOE fluctuations we first unfold the spectrum by the mapping $\{\epsilon_\nu\} \to \left\{\int_0^{\epsilon_\nu} \rho(\epsilon)d\epsilon\right\}$, where $\rho(\epsilon)$ is the mean density of states. The mean level spacing of the unfolded (or rectified) spectrum is equal to unity, $d = 1$.

In Fig. (4.2) we show the nearest neighbour spacing distribution for a system consisting of a single bosonic Rb atom and two fermionic K atoms ($M/m = 87/40$). We calculated 7 000 energy levels starting from the state number 500 and used $a_{1D} = 0.0023\, L$. We can clearly see the level repulsion, meaning that the system is not integrable. On the other hand, the nearest neighbour spacing distribution is rather far from the random matrix result. We find that it can be well fitted by the semi-Poisson distribution, typical for pseudo-integrable systems such as

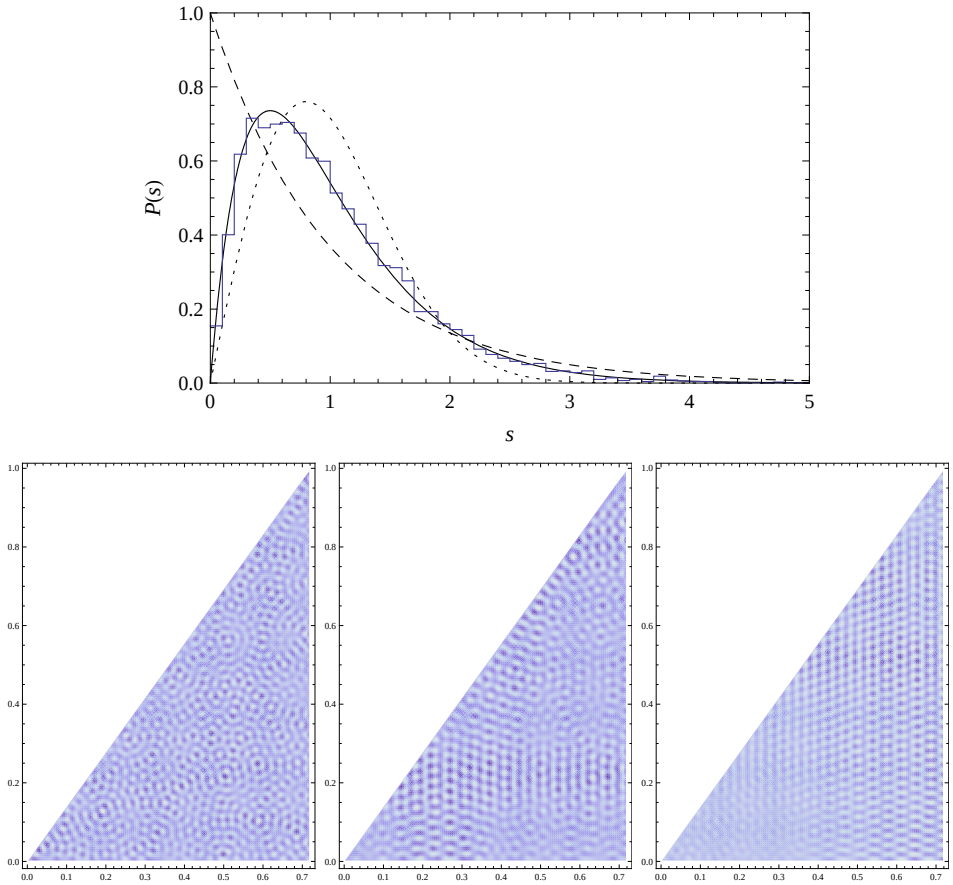

Figure 4.2: Top: nearest neighbour spacing distribution for 7 000 states starting from the state 500 for the system of two fermionic Potassium atoms and one Rubidium atom ($M/m = 87/40$). The dotted line corresponds to the GOE ensemble, the dashed line to the uncorrelated distribution of levels (Poisson), and the solid line to the semi-Poisson distribution. Bottom: density plot of the wave function for three different eigenstates in the xy-plane. On the left: wave function corresponding to the state number 1 835, it displays chaotic behaviour. In the middle: wave function for the state number 1 296, in it different regions of the xy plane show regular and chaotic behaviour. On the right: wave function for the state 1 676, it displays a regular behaviour.

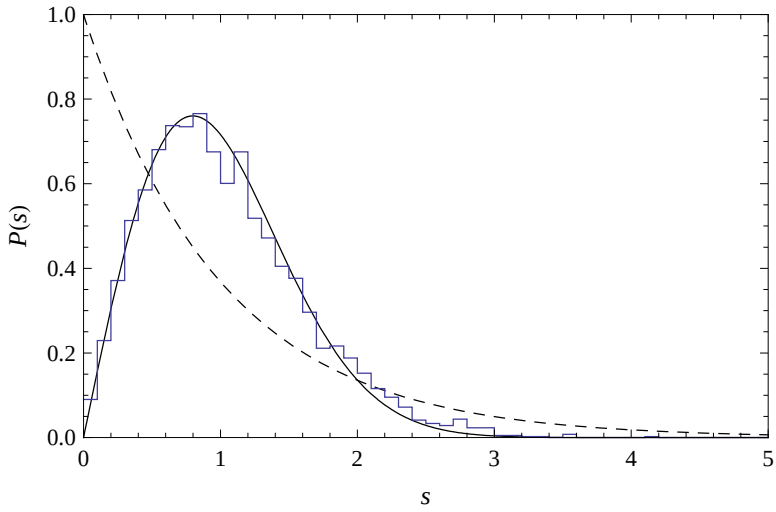

Figure 4.3: Nearest neighbour spacing distribution for 3 879 states starting from the state 122 for the system of three fermionic Potassium atoms and one Rubidium atom. The solid line corresponds to the GOE ensemble and the dashed line to the Poisson distribution.

triangular billiards [128]. The fact that the system belongs to the intermediate regime is also confirmed by looking at its wave functions - some of them look rather regular while others behave chaotically. In Fig (4.2, bottom) we show three eigenfunctions for different eigenstates, they display chaotic behaviour (left), regular behaviour (right), or exhibit simultaneously regular and chaotic properties in different regions of space (middle). The whole area in this figure is the left half of the shaded triangle in Fig. (4.1). In Fig. (4.3) we show the nearest neighbour spacing distribution for the rectified spectrum of a system containing a Rubidium atom and three fermionic Potassium atoms. Here we calculated 3879 levels starting from the state number 122 and used $a_{1D} = 0.0064\,L$. The GOE curve fits the data with much better accuracy, which allows us to conclude that the four-body system is closer to the chaotic limit.

Let us now turn to the dynamical properties of these two non-integrable systems and discuss their response to the periodic modulation of a_{1D} given by

Eq. (4.15). In order to calculate the dynamic structure factor $S(\epsilon,\omega)$ we numerically compute the matrix elements of the perturbation $F_{\nu\eta}$ and average them over the initial and final states in narrow energy windows around $\epsilon_\eta \approx \epsilon$ and $\epsilon_\nu \approx \epsilon_\eta+\omega$. We should then multiply this average by the density of states at the final energy $\rho(\epsilon+\omega)$. In Fig. (4.4) we plot $S(\epsilon,\omega)$ in arbitrary units for the three-atom case (top) and the four-atom case (bottom). The energy ϵ corresponds to the level number $\eta \approx 7\,000$ in the three-body case and $\eta \approx 2\,000$ in the four-body case. The values of a_{1D} are $0.0023\,L$ and $0.0064\,L$ respectively. We observe that $S(\epsilon,\omega)$ never vanishes, which means that on average all states are coupled by the perturbation. In fact, the singularity at small ω reflects the fact that states separated by the energy of the order of the mean level spacing, $d = 1/\rho(\epsilon)$, are strongly coupled by the perturbation.

The structure of $S(\epsilon,\omega)$ at large ω is attributed to periodic two-particle orbits accumulated near the frequency $\omega \approx (2\pi/L)\sqrt{2\epsilon/\mu}$ in both three- and four-body cases. We postpone the discussion of the effect of the periodic orbits until Section 4.5.

4.4 Integrable case

Let us consider N identical bosons on a ring of length L. Equation (4.14) then takes the form of the Lieb-Liniger Hamiltonian

$$H = \frac{1}{2}\sum_{j=1}^{N}\frac{\partial^2}{\partial x_j^2} + \frac{2}{a_{1D}}\sum_{j<k}\delta(x_j - x_k), \tag{4.27}$$

which is solvable by the Bethe ansatz [25] (see Section 1.3). Here, we set $m = 1$. The equations for the momenta of the N atoms are given by

$$Lk_j = 2\pi n_j - 2\sum_{i=1}^{N}\arctan[(k_j - k_i)/c], \quad j = 1,\ldots,N, \tag{4.28}$$

where $c = 2/a_{1D}$ and $\{n_j\}$ is a set of N quantum numbers, which are integers in the case of odd N and half-integers for even N. Each different set $\{n_j\}$ determines

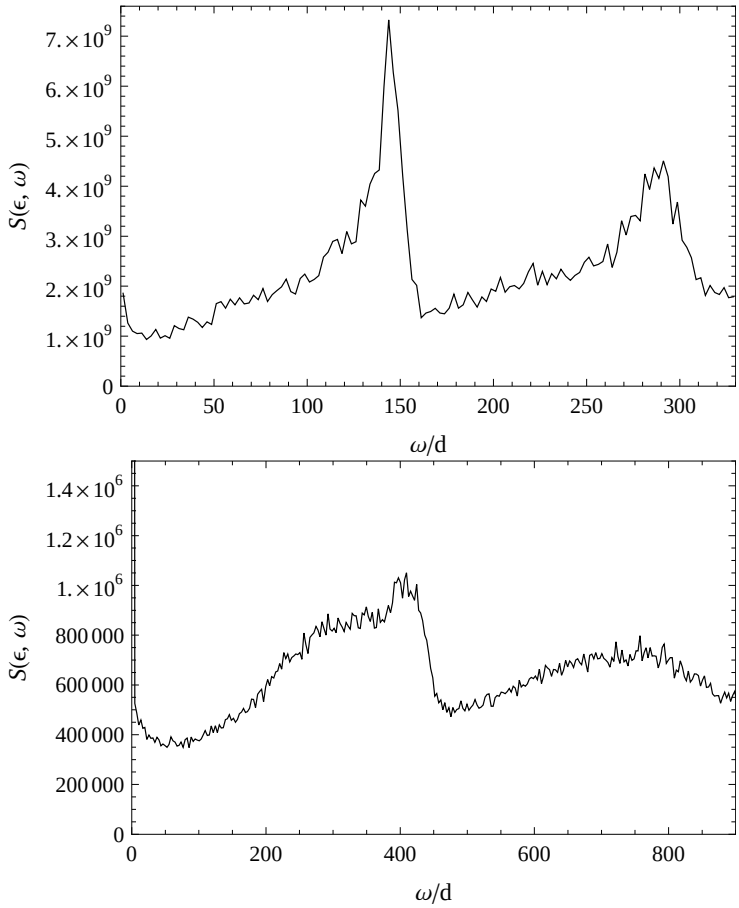

Figure 4.4: Top: $S(\epsilon, \omega)$ for the system of two fermionic Potassium atoms and one Rubidium atom ($M/m = 87/40$) at the energy ϵ corresponding to the level number 6 850. Bottom: $S(\epsilon, \omega)$ for three fermionic Potassium atoms and one Rubidium atom and state number 1500.

a distinct excited state of the system [129]. The total energy and momentum are

$$E = \frac{1}{2}\sum_{j=1}^{N} k_j^2; \qquad K = \sum_{j=1}^{N} k_j = \frac{2\pi}{L}\sum_{j=1}^{N} n_j. \tag{4.29}$$

We will be interested in the states with zero total momentum, i.e. $\sum_{j=1}^{N} n_j = 0$.

In Fig. (4.5) we plot the nearest neighbour spacing distributions for the rectified

spectra of $N = 3$ (top) and $N = 4$ (bottom) bosons calculated by using Eqs. (4.28) and (4.29). We counted the first 50 000 states and used $a_{1D} = 0.0014\, L$ in the former case and 50 000 states and $a_{1D} = 0.012\, L$ in the latter. Visible regular deviations from the Poisson distribution originate from the fact that for both very low and very high energies (Tonks gas and ideal gas limit, respectively) the spectrum is degeneracy dominated and the distances between the levels are integer multiples of $2\pi^2$. For $N = 3$ these regularities are more visible because in this case to rectify the spectrum means to multiply it by the constant density of states.

Let us now discuss the response of these systems to the modulation of a_{1D}. In this case the operator F which enters in the perturbation $V(t)$ (see Eq. (4.4)) is written as

$$F = -\frac{A}{a_{1D}^2} \sum_{j<k} \delta(x_j - x_k). \tag{4.30}$$

In order to calculate the dynamic structure factor with respect to F we use the explicit expression for the (unnormalised) eigenfunctions of the Lieb-Liniger Hamiltonian (4.27) [129, 118]

$$\psi_\nu(x_1, ..., x_N) = \sum_P (-1)^{[P]} e^{i \sum_{j=1}^N x_j k_{Pj}} \prod_{j>m} (k_{Pj} - k_{Pm} - ic), \tag{4.31}$$

where ν denotes the set $\{n_j\}$, momenta k_j are obtained from Eq. (4.28), and $[P]$ is the parity of the permutation P. The wavefunction (4.31) is defined in the spatial domain $x_1 < x_2 < \cdots < x_N < x_1 + L$ and can be continued by symmetry to the whole space.

To normalise the eigenfunction (4.31) we multiply it by the normalisation coefficient $\mathcal{N}_\nu$ satisfying the equation

$$\frac{\partial \epsilon_\nu}{\partial a_{1D}} = \mathcal{N}_\nu^2 \langle \psi_\nu | \frac{\partial H}{\partial a_{1D}} | \psi_\nu \rangle, \tag{4.32}$$

where $\partial H / \partial a_{1D} = 2F/A$. The left hand side of Eq. (4.32) can be easily calculated from the Bethe ansatz equations (4.28) and the matrix element on the right hand side in the case $N = 3$ and $N = 4$ is a bulky but manageable analytic function of momenta and a_{1D}. The same holds for the matrix element $F_{\nu\mu} = \langle \psi_\nu | F | \psi_\mu \rangle$ which we can now straightforwardly calculate using the normalised ψ_ν and ψ_μ.

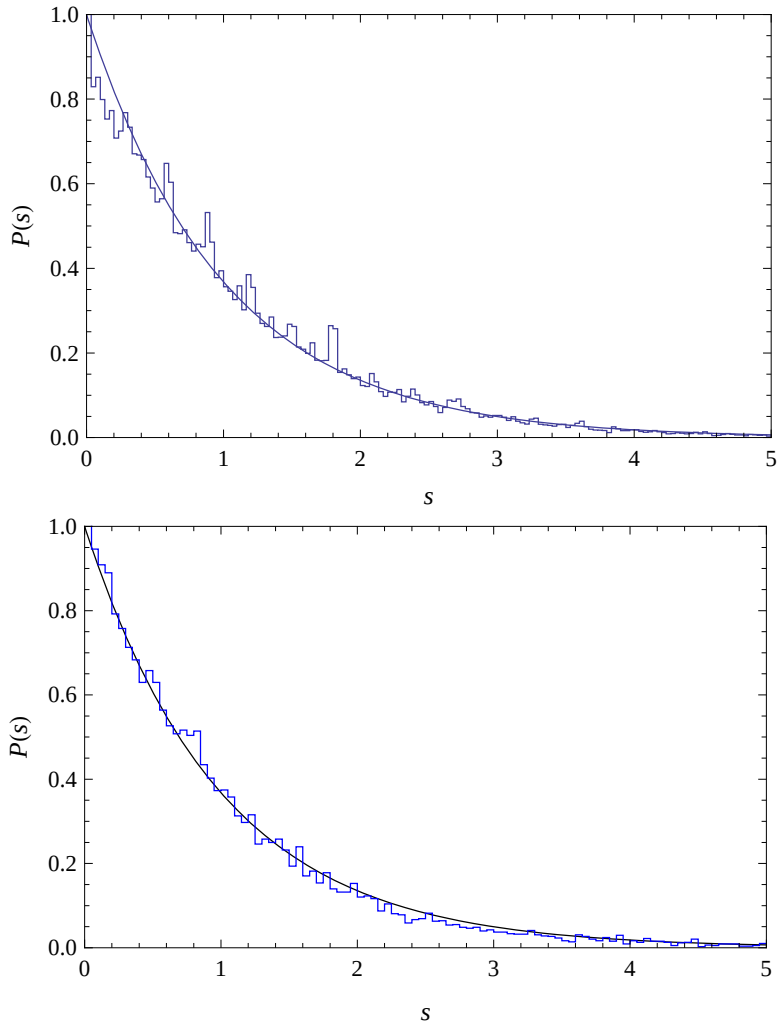

Figure 4.5: Nearest neighbour spacing distribution for rectified spectra of three (top) and four (bottom) identical bosons. Solid line is the Poisson distribution.

In Fig. (4.6) we plot the dynamic structure factor $S(\epsilon, \omega)$ for three (top) and four (bottom) identical bosons. The energy ϵ corresponds to the state number 4 000 in the three-body case and 40 000 in the four-body case, d denotes the three- and four-body mean level spacings at these energies, and $a_{1D} = 0.0014\, L$ and $0.012\, L$ respectively. We see that at large ω the dynamic structure factor

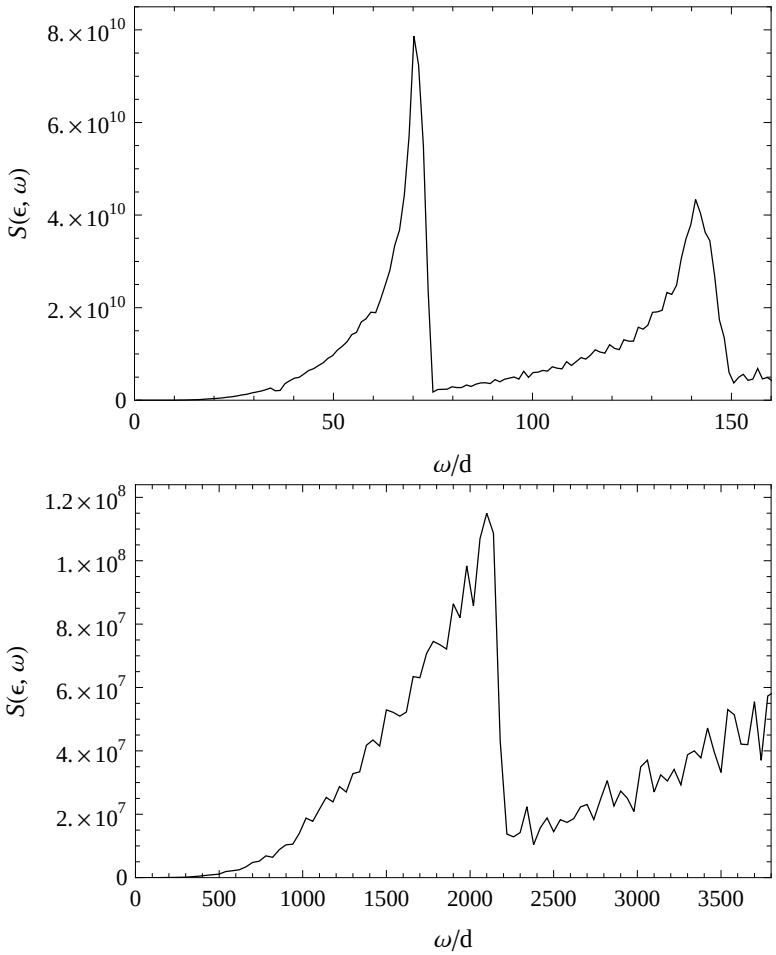

Figure 4.6: Top: $S(\epsilon, \omega)$ versus ω for three identical bosons on a ring. Here ϵ corresponds to the excited state number 4 000, and $d = 24\sqrt{3}\pi/L^2$ is the mean level spacing. Bottom: the same for four bosons, ϵ corresponds to the state number 40 000, the mean level spacing $d = 48\sqrt{2}\pi^2/\sqrt{\epsilon}L^3$.

has more or less the same structure as in the non-integrable case (compare with Fig. 4.4). In contrast, for small ω we see a remarkable suppression of $S(\epsilon, \omega)$ for the integrable systems. This means that $F_{\nu\mu}$ is suppressed for pairs of states with close energies. This behaviour is different from the non-integrable cases where

neighbouring states are strongly coupled by the perturbation.

4.5 Theoretical model for arbitrary N

It is instructive to discuss the asymmetric resonance-like features in the dynamic structure factor dependence on ω, which are visible in both non-integrable (Fig. 4.4) and integrable (Fig. 4.6) cases. Let us first assume that there is no interaction between the atoms and consider a pair of them having relative velocity v. This pair can be excited by the modulation of the coupling constant with the angular frequency $\omega = 2\pi l v/L$, where l is an integer. When we calculate $S(\epsilon, \omega)$ we average over all possible N-body states with the total energy ϵ, and the upper bound for v is reached when this energy is concentrated in the relative motion of the two atoms. This explains the abrupt jumps of $S(\epsilon, \omega)$ at the frequencies $\omega_l^* = (2\pi l/L)\sqrt{2\epsilon/\mu}$, where μ is the reduced mass of the two atoms. The threshold law for $\omega < \omega^*$ is governed by the density of states of all other particles ($N-2$ degrees of freedom) which share the energy $\omega^* - \omega$. In particular, in the three-body case $S(\epsilon, \omega) \propto 1/\sqrt{\omega^* - \omega}$ and in the four-body case it has a finite discontinuity at ω^*.

The above picture is based on two assumptions: (*i*) the modulation of the two-body interaction potential can excite only two particles at a time, i.e. it cannot simultaneously change three or more momenta, and (*ii*) the excited particles go around the ring without exchanging momenta with the other particles. The former is obvious from the classical viewpoint and the latter is actually not correct in the non-integrable case. Indeed, the heavy atom "forgets" its initial momentum after several collisions with the light atoms. However, the rate of this diffusion is not universal and can be quite small compared to ω^*. It depends on the number of particles in the system, their interaction, and the mass ratios.

To see a more universal signature of chaoticity we should give the heavy particle more time for diffusion, i.e. we should look at the low-frequency behaviour of $S(\epsilon, \omega)$. Indeed, the dynamic structure factor has dramatically different asymptotes in the non-integrable and integrable situations (compare Figs. 4.4 and 4.6).

We find that in the non-integrable case $S(\epsilon,\omega) \propto 1/\sqrt{\omega}$, which is consistent with the result of Wilkinson [130] based on the Random Matrix Theory.

In order to understand the asymptotic behaviour of the dynamic structure factor in the integrable case let us translate the semiclassical picture of N atoms moving along the ring with constant velocities into the language of the Lieb-Liniger model, where the state of the system is given by the collection of N quantum numbers, $\{n_j\}$. Being consistent with the assumptions (i) and (ii), our calculations in the cases $N = 3$ and $N = 4$ show that the matrix elements $F_{\nu\mu}$ are the largest for the pairs of states which differ by two quantum numbers: $\nu = \{n_1, ..., n_i, ..., n_j, ..., n_N\}$ and $\mu = \{n_1, ..., n_i - l, ..., n_j + l, ..., n_N\}$. We see that the perturbation F changes the state of two atoms to a large extent irrespective of the other particles. Let us now continue this line of reasoning and solve the N-body problem by separating it into two-body independent pieces: consider a pair of atoms with coordinates x_1 and x_2 and calculate the matrix elements of the perturbation (4.30) between the states $\{n_i, n_j\}$ and $\{n_i - l, n_j + l\}$. In the case $|n_j - n_i| \gg 1$ the wavefunction of the state $\{n_i, n_j\}$ is given by

$$\Psi_{n_i,n_j}(x_1,x_2) = \frac{1}{\sqrt{2L}}\left(e^{ik_ix_1+ik_jx_2} - \frac{1-ia_{1D}(k_j-k_i)/2}{1+ia_{1D}(k_j-k_i)/2}e^{ik_ix_2+ik_jx_1}\right), \quad (4.33)$$

where $k_i \approx 2\pi n_i/L$ and $k_j \approx 2\pi n_j/L$. The matrix element $\langle\Psi_{n_i,n_j}|F|\Psi_{n_i-l,n_j+l}\rangle$ then reads

$$\begin{aligned} F_{\{n_i,n_j\},\{n_i-l,n_j+l\}} &= -\frac{A}{La_{1D}^2}\frac{(k_j-k_i)(k_j'-k_i')a_{1D}^2}{(1+ia_{1D}(k_j-k_i)/2)(1-ia_{1D}(k_j'-k_i')/2)} \quad (4.34)\\ &\approx -\frac{(2\pi)^2A}{L^3}\frac{(n_j-n_i)(n_j-n_i+2l)}{(1+i\pi(n_j-n_i)a_{1D}/L)(1-i\pi(n_j-n_i+2l)a_{1D}/L)}, \end{aligned}$$

where $k_i' \approx 2\pi(n_i - l)/L$ and $k_j' \approx 2\pi(n_j + l)/L$. The corresponding energy difference is

$$\omega = \Delta E_{\{n_i,n_j\}\to\{n_i-l,n_j+l\}} \approx (2\pi)^2[(n_j-n_i)l + l^2]/L^2. \quad (4.35)$$

From Eq. (4.34) we observe that the matrix element $F_{\{n_i,n_j\},\{n_i-l,n_j+l\}}$ rapidly grows with $n_j - n_i$ until it reaches saturation at $n_j - n_i \sim L/\pi a_{1D}$. Assuming

that a_{1D} is sufficiently small, the most important contribution to the dynamic structure factor comes from exciting pairs of atoms with large relative momenta. Indeed, the perturbation (4.30) probes the local density-density correlations, which are suppressed at small momenta - a manifestation of the "fermionisation" of 1D interacting bosons. On the other hand, Eq. (4.35) imposes that the distance $n_j - n_i$ can never exceed $\omega L^2/(2\pi)^2$. Otherwise, the resonant condition cannot be satisfied. It is then easy to see that the largest contribution to $S(\epsilon, \omega)$ comes from the pairs of states $\{n_i, n_j\}$ and $\{n_i - l, n_j + l\}$ with a large difference $n_j - n_i$ and small l. Then, if $\omega \ll 4\pi/a_{1D}L$, we can approximate

$$|F_{\{n_i,n_j\},\{n_i-l,n_j+l\}}|^2 \approx \frac{(2\pi)^4 A^2}{L^6}(n_j - n_i)^4. \tag{4.36}$$

In the present case the definition of the dynamic structure factor (4.8) can be written as

$$S(\epsilon,\omega) = \frac{1}{\rho(\epsilon)}\frac{\partial^2}{\partial\epsilon\partial\omega} \sum_{\nu:\epsilon_\nu<\epsilon} \sum_{j>i} \sum_{l=1}^{\left\lfloor \frac{\omega L^2}{(2\pi)^2(n_j-n_i)} \right\rfloor} |F_{\{n_i,n_j\},\{n_i-l,n_j+l\}}|^2, \tag{4.37}$$

where

$$\rho(\epsilon) = \frac{\partial}{\partial\epsilon} \sum_{\nu:\epsilon_\nu<\epsilon} 1 \tag{4.38}$$

is the density of states, index ν stands for the set of quantum numbers $\{n_1, ..., n_N\}$, and $\lfloor x \rfloor$ denotes the integer part of x.

In the limit $(2\pi)^2/L^2 \ll \omega \ll \epsilon$ the sums in Eqs. (4.37) and (4.38) can be substituted by integrals. Using Eq. (4.36) and the asymptotic formula $\int_0^\infty x^4 \lfloor \xi/x \rfloor \mathrm{d}x \approx \xi^5\zeta(5)/5$ valid for large ξ we get

$$S(\epsilon,\omega) = \frac{\zeta(5)}{2^{15/2}\pi^6}\frac{1}{(N-2)!}\frac{A^2\omega^4L^4}{\rho(\epsilon)}\frac{\partial}{\partial\epsilon}V_{N-1}\left(\frac{L\sqrt{\epsilon}}{\pi\sqrt{2}}\right), \tag{4.39}$$

and

$$\rho(\epsilon) = \frac{1}{N!}\frac{\partial}{\partial\epsilon}V_N\left(\frac{L\sqrt{\epsilon}}{\pi\sqrt{2}}\right). \tag{4.40}$$

The function $V_N(R)$ in Eqs. (4.39) and (4.40) denotes the volume of an N-dimensional hypersphere of radius R:

$$V_N(R) = \frac{\pi^{N/2} R^N}{\Gamma\left(\frac{N}{2}+1\right)}. \tag{4.41}$$

Finally, putting together Eqs. (4.39) and (4.40) we obtain the dynamic structure factor

$$S(\epsilon,\omega) = \frac{\zeta(5)}{2^7\pi^{11/2}} \frac{(N-1)^2\Gamma(N/2+1)}{\Gamma(N/2+1/2)} \frac{A^2\omega^4 L^3}{\sqrt{\epsilon}}. \tag{4.42}$$

Equation (4.42) is derived without restricting the centre of mass momentum K to be zero. Following the same calculation with the restriction $n_1 + ... + n_N = 0$ we get

$$S_{K=0}(\epsilon,\omega) = \frac{\zeta(5)}{2^7\pi^{11/2}} \frac{N(N-2)\Gamma(N/2+1/2)}{\Gamma(N/2)} \frac{A^2\omega^4 L^3}{\sqrt{\epsilon}}. \tag{4.43}$$

In Figs. (4.7) and (4.8) we compare our numerical results for the dynamic structure factor with the asymptote (4.43) in the cases $N = 3$ and $N = 4$. As we see, Eq. (4.43) works perfectly in the region of its validity, $(2\pi)^2/L^2 \ll \omega \ll 4\pi/a_{1D}L$. This confirms our initial assumption that pairs of atoms are excited independently of other atoms. Deviations of the exact $S(\epsilon,\omega)$ from the expression (4.43) are expected at frequencies larger than $4\pi/a_{1D}L$ and smaller than $(2\pi)^2/L^2$. Indeed, in the former case Eq. (4.43) overestimates the exact result because of the breakdown of Eq. (4.36) at $n_j - n_i \sim L/\pi a_{1D}$ corresponding to frequencies $\omega \sim 4\pi/a_{1D}L$. In Fig. (4.8) we plot $S(\epsilon,\omega)$ in the case $N = 4$ for different values of a_{1D} to demonstrate this effect. Concerning the low-frequency limit, from Eq. (4.35) we see that the lowest possible excitation energy of an atom pair is $\Delta E \sim (2\pi)^2/L^2$, and, therefore, perturbations with lower frequencies are never resonant. Note, that for $N > 3$ this gives a gap which is much larger than the mean level spacing of the many-body problem (with the centre of mass motion integrated out).

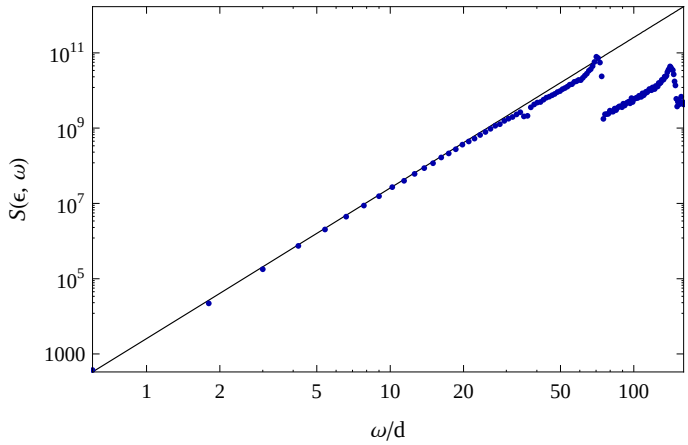

Figure 4.7: $S(\epsilon, \omega)$ versus ω for three identical bosons on a ring. The solid line is given by Eq. (4.43). The energy ϵ corresponds to the excited state number 4 000, and the mean level spacing is $d = 4\sqrt{2}\pi/L^2$.

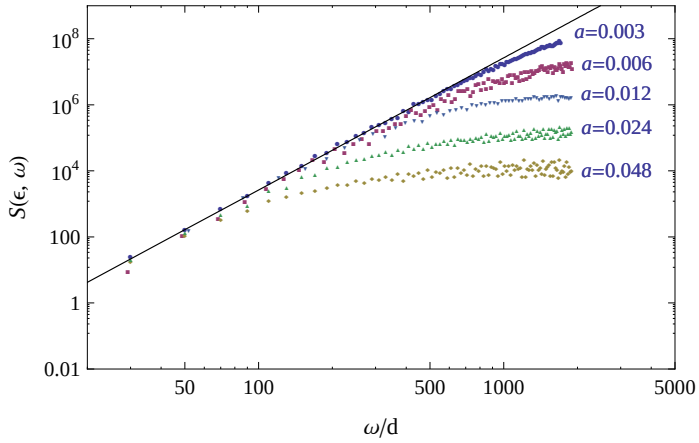

Figure 4.8: $S(\epsilon, \omega)$ versus ω in the case $N = 4$ plotted for five different values of the 1D scattering length a_{1D}. We clearly observe the saturation of $S(\epsilon, \omega)$ at $\omega \sim 4\pi/a_{1D}L$. The energy ϵ corresponds to the state number 40 000, and $d = 48\sqrt{2}\pi^2/\sqrt{\epsilon}L^3$.

4.6 Concluding remarks

Validity of Eqs. (4.42) and (4.43) in the case $N > 4$ seems to be a reasonable assumption, although it has yet to be confirmed. Nevertheless, let us take it as a conjecture and discuss its consequences. The most remarkable is, of course, the frequency dependence of the dynamic structure factor. It is proportional to ω^4, which leads to the strong frequency dependence of the diffusion constant $D(\epsilon, \omega) \propto \omega^6$ (see Eq. (4.11)). This scaling significantly differs from the usual law, $D \propto \omega^2$, which originates from the Kubo formula [131], and suggests a straightforward experiment on measuring the heating rate of a 1D gas as a function of the perturbation frequency.

Related to this is the question of adiabaticity. We note that Eqs. (4.42) and (4.43) are valid for frequencies smaller than $4\pi/a_{1D}L$, and therefore, a discussion of the thermodynamic limit would not make much sense. However, the dynamic structure factor grows only polynomially with L and N [132], which is still surprising. Indeed, consider a very high-energy eigenstate of N atoms and monitor its evolution under a slow variation of the coupling constant. In a generic situation the probability to find the system in the same microscopic state in the end of the experiment is exponentially small since the density of states grows exponentially with L and N. In our case, however, the polynomial dependence of the dynamic structure factor on L and N substituted into Eq. (4.7) gives a polynomial law for the rate of the diffusion, i.e. it requires only polynomially slow variation of the parameter to remain in the same state. To emphasize the importance of the difference between exponential and polynomial dependencies we can make parallels with currently popular topic of adiabatic quantum computing [133], where the main problem is to change a parameter in the Hamiltonian of a many-body system keeping the entropy low. If one can do this with a polynomial rate, a number of NP-complete problems could be solved in a polynomial time.

Microscopic states of the Lieb-Liniger gas which are very close in energy are very far from each other in the space of quantum numbers and in momentum space, as can be seen from the shape of the wave functions (Eq. 4.31). On the

other hand, the perturbation is localized in this space (it can only change the relative momentum of two atoms). Therefore, it does not couple states with close energies. In this sense, by perturbing the system we probe the local density of states which scales only polynomially with the size of the system. In the non-integrable case the states are delocalized in any space and the perturbation, no matter localized or not, couples all of them.

Appendix A

Two-body problems

A.1 Two-body scattering

For a generic two-body problem, the Schrödinger equation takes the form

$$-\frac{1}{2}\left(\frac{\partial^2}{\partial x_1^2}+\frac{\partial^2}{\partial x_2^2}\right)\Psi(x_1,x_2)+V(x_2-x_1)\Psi(x_1,x_2)=E\Psi(x_1,x_2). \tag{A.1}$$

Here, we put $m_1 = m_2 = 1$, $\hbar = 1$ and the coordinates are taken such that x_1 is the coordinate of particle 1 and x_2 the coordinate of particle 2. In the asymptotic region the momenta are $k_1 > k_2$. In the centre of mass reference frame,

$$\begin{aligned} R &= x_1 + x_2, \qquad r = x_2 - x_1, \\ K &= k_1 + k_2, \qquad k = k_1 - k_2, \end{aligned} \tag{A.2}$$

the Schrödinger equation becomes

$$-\frac{\partial^2}{\partial r^2}\Psi(r)+V(r)\Psi(r)=\left(\frac{k}{2}\right)^2\Psi(r), \tag{A.3}$$

where we integrated out the centre of mass motion described by the wave function $\Psi(x_1, x_2) = e^{iKR/2}\Psi(r)$. The energy reads

$$E=\frac{k_1^2+k_2^2}{2}=\frac{K^2+k^2}{2}. \tag{A.4}$$

We consider only symmetric potentials such that $V(r) = V(-r)$, so we will have symmetric and antisymmetric solutions $\Psi_\pm(-r) = \pm\Psi_\pm(r)$. After a scattering process the wave function can be written in the asymptotic region as a superposition of an incoming and an outgoing wave, with a phase shift between the two of them, $-\theta_\pm(k)$, which depends on the scattering potential $V(r)$:

$$\Psi_\pm(r) \to \begin{cases} e^{-i\frac{kr}{2}} - e^{i\frac{kr}{2}-i\theta_\pm(k)},\ r \to +\infty \\ \pm\left(e^{i\frac{kr}{2}} - e^{-i\frac{kr}{2}-i\theta_\pm(k)}\right),\ r \to -\infty \end{cases}. \tag{A.5}$$

The $\pm$ sign in front of the negative asymptotic region takes into account the symmetry or antisymmetry of the wave function, and the minus sign in front of the phase shift is taken for convention. The phase shift is an odd ($\theta_\pm(-k) = \theta_\pm(k)$) and real ($\theta^*_\pm(k) = \theta_\pm(k^*)$) function of k.

In the case of distinguishable particles we can give them identities and introducing the reflection R and transmission T coefficients we have:

$$\frac{\Psi_+(r) + \Psi_-(r)}{2} \to \begin{cases} e^{-i\frac{kr}{2}} + R(k)e^{i\frac{kr}{2}},\ r \to +\infty \\ T(k)e^{-i\frac{kr}{2}},\ r \to -\infty \end{cases}, \tag{A.6}$$

where the scattering coefficients are defined as

$$R(k) = -\frac{e^{-i\theta_+} + e^{-i\theta_-}}{2}, \qquad T(k) = \frac{e^{-i\theta_-} - e^{-i\theta_+}}{2}. \tag{A.7}$$

In terms of the coefficients of the Bethe ansatz wave function, Eq. (1.6), we get the following relation for the transmission and reflection coefficients:

$$\begin{aligned} \Psi(12|21) &= R(k)\Psi(12|12) + T(k)\Psi(21|12), \\ \Psi(21|21) &= R(k)\Psi(21|12) + T(k)\Psi(12|12). \end{aligned} \tag{A.8}$$

Such a process is sketched in Fig. (A.1). In the matrix form we have

$$\Psi(21) = \begin{pmatrix} \Psi(12|21) \\ \Psi(21|21) \end{pmatrix} = \begin{pmatrix} R(k)\ T(k) \\ T(k)\ R(k) \end{pmatrix} \begin{pmatrix} \Psi(12|12) \\ \Psi(21|12) \end{pmatrix} = S^r(k)\Psi(12), \tag{A.9}$$

where $S^r(k)$ is the scattering operator in the reflection-diagonal representation. In the transmission-diagonal representation we have a similar expression:

$$\Phi(21) = \begin{pmatrix} \Psi(21|21) \\ \Psi(12|21) \end{pmatrix} = \begin{pmatrix} T(k)\ R(k) \\ R(k)\ T(k) \end{pmatrix} \begin{pmatrix} \Psi(12|12) \\ \Psi(21|12) \end{pmatrix} = S^t(k)\Psi(12). \tag{A.10}$$

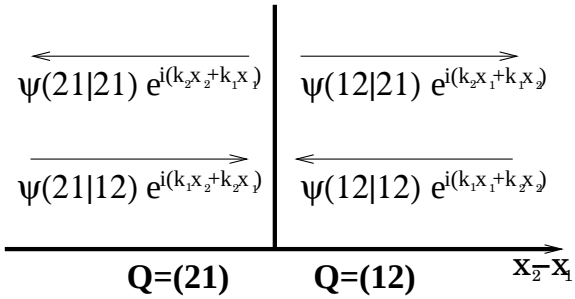

Figure A.1: Picture of the scattering of two particles with $k_1 > k_2$. The two different regions in space, $Q = (12)$ for $x_2 > x_1$ and $Q = (21)$ for $x_1 > x_2$ are indicated, as well as the incoming and outgoing waves.

Defining the permutation operator $\hat{P}$

$$\hat{P} = \begin{pmatrix} 0 & 1 \\ 1 & 0 \end{pmatrix}, \tag{A.11}$$

we can write these operators as

$$S^r(k) = R(k) + \hat{P}T(k), \qquad S^t(k) = T(k) + \hat{P}R(k). \tag{A.12}$$

In the case where the particles are identical we have $\hat{P} = \pm 1$, the plus sign for bosons and the minus sign for fermions. Thus, exchanging bosons to fermions is equivalent to conjugating the representation of the permutation group, $\hat{P} \to \bar{\hat{P}} = -\hat{P}$.

Finally we consider the Yang-Baxter consistency conditions. For the scattering operator in the reflection-diagonal representation, the conditions Eq. (1.8):

$$S_1(k_2, k_3)S_2(k_1, k_3)S_1(k_1, k_2) = S_2(k_1, k_2)S_1(k_1, k_3)S_2(k_2, k_3) \tag{A.13}$$

can be written in the following way:

$$T_{23}R_{13}R_{12} + R_{23}R_{13}T_{12} - R_{12}T_{13}R_{23} = 0, \tag{A.14}$$

where the subscript ij means $(k_i - k_j)$.

A.2 The δ-function potential

The potential we wish to consider is

$$V = c\delta(x). \tag{A.15}$$

Since the particles can be considered as being free on both sides of the barrier, we write the wave-function as:

$$\Psi(x) = 2i\sin(kx + \phi). \tag{A.16}$$

The antisymmetric wave-function vanishes at the origin and so the potential has no effect there, therefore $\Psi_-(x) = -2i\sin\left(\frac{kx}{2}\right)$ and $\theta_-(k) = 0$.

For the symmetric case the wave function is continuous at the origin and has a discontinuity in the derivative across the origin,

$$\Psi_+(0^-) = \Psi_+(0^+), \quad \left.\frac{\Psi'_+(r)}{\Psi(r)}\right|_{r=0} = \frac{c}{2}. \tag{A.17}$$

The δ-function potential is a point-like interaction, therefore the asymptotic region is everywhere except at the origin; we have for the symmetric wave function

$$\Psi_+(r) = -2i\sin\left(\frac{k|r|}{2} - \frac{\theta_+}{2}\right). \tag{A.18}$$

The phase-shift is in this case

$$\theta_+(k) = -2\arctan\left(\frac{k}{c}\right). \tag{A.19}$$

Using the identity $\ln\left(\frac{1+ix}{1-ix}\right) = 2i\arctan(x)$ we write

$$e^{-i\theta_+(k)} = \frac{c+ik}{c-ik}. \tag{A.20}$$

A bound state appears for the attractive case $c < 0$ with wave function $\Psi_+(r) = \exp(-|cr|)$.

For the case of identical particles this phase shift is all that is needed. For fermions we have an antisymmetric wave function whereas for bosons the wave function is symmetric.

For different particles we calculate the reflection and transmission coefficients, Eq. (A.7),

$$R(k) = \frac{-ic}{k+ic},\ T(k) = \frac{k}{k+ic} \longrightarrow S^t(k) = \frac{k-ic\hat{P}}{k+ic}. \tag{A.21}$$

A.3 The Hubbard model

We wish here to calculate the scattering matrix for the Hubbard model, with Hamiltonian

$$H = -\sum_{\sigma=\uparrow,\downarrow;j=1}^{N_a} (c^\dagger_{\sigma,j} c_{\sigma,j+1} + c^\dagger_{\sigma,j+1} c_{\sigma,j}) + U \sum_{j=1}^{N_a} n_{j,\uparrow} n_{j,\downarrow}. \tag{A.22}$$

This model is a lattice model, and double occupancy of lattice sites by fermions with different spin is allowed. The Schrödinger equation reads

$$\begin{aligned} E\Psi(Q|x_1,\cdots,x_N) = &-\sum_{j=1}^{N} (\Psi(Q|\cdots,x+1,\cdots) + \Psi(Q|\cdots,x-1,\cdots)) + \\ &+ U \sum_{j<l} \delta(x_j - x_l)\Psi(Q|x_1,\cdots,x_N), \end{aligned} \tag{A.23}$$

where the interaction terms only appear if two atoms sit on the same lattice site.

In the absence of multiple occupation of lattice sites we have only kinetic energy. The Schrödinger equation for the Hubbard Hamiltonian then reads

$$E\Psi(Q|x) = -\sum_{j=1}^{N} \left(\Psi(Q|\cdots,x_j+1,\cdots) + \Psi(Q|\cdots,x_j-1,\cdots)\right). \tag{A.24}$$

Since we consider the wave function of the Bethe ansatz form Eq. (1.6):

$$\Psi(Q_1,\ldots,Q_N|x_1,\ldots,x_N) = \sum_P \psi(Q|P) e^{i\sum_{j=1} N x_j k_{Pj}}, \tag{A.25}$$

the energy and momentum are

$$E = -2\sum_{j=1}^{N} \cos k_j, \qquad K = \sum_{j=1}^{N} k_j. \tag{A.26}$$

We consider now the case with doubly occupied sites: a site x is occupied by particles q and q', so that $x_j = x_{j+1} = x$. In this case the ordering of the particles is ambiguous, it can be either $Q = (\ldots, Qj = q, Qj+1 = q', \ldots)$ or $Q = (\ldots, Qj = q', Qj+1 = q, \ldots)$. Two adjacent sectors have now a common part, and the continuity requires

$$\Psi(Q = \cdots, q, q', \cdots | \cdots, x, x, \cdots) = \Psi(Q' = \cdots, q', q, \cdots | \cdots, x, x, \cdots). \quad \text{(A.27)}$$

The Schrödinger equation reads for this doubly occupied site

$$\begin{aligned} E\Psi(Q|\cdots, x, x\cdots) = U\Psi(Q|\cdots, x, x, \cdots) &- \Psi(Q|\cdots, x, x+1, \cdots) \\ - \Psi(Q|\cdots, x-1, x, \cdots) &- \Psi(Q'|\cdots, x+1, x, \cdots) \\ - \Psi(Q'|\cdots, x, x-1, \cdots) &+ \cdots \end{aligned} \quad \text{(A.28)}$$

where the dots account for all the other processes involving the rest of the particles in other sites, that are linearly independent. Note that the third and forth terms in the right-hand-side belong to a different sector Q'. We will subtract from Eq. (A.28) the following relation

$$\begin{aligned} E\Psi(Q|\cdots, x, x\cdots) = &-\Psi(Q|\cdots, x+1, x, \cdots) - \Psi(Q|\cdots, x-1, x, \cdots) \\ - \Psi(Q|\cdots, x, x+1, \cdots) &- \Psi(Q|\cdots, x, x-1, \cdots) + \cdots, \end{aligned} \quad \text{(A.29)}$$

which is fulfilled for every amplitude in a given sector, here Q. We then obtain

$$\begin{aligned} U\Psi(Q|\cdots, x, x\cdots) = &-\Psi(Q'|\cdots, x+1, x, \cdots) + \Psi(Q|\cdots, x+1, x, \cdots) \\ - \Psi(Q'|\cdots, x, x-1, \cdots) &+ \Psi(Q|\cdots, x, x-1, \cdots). \end{aligned} \quad \text{(A.30)}$$

Substituting the value for the wave function, Eq. (A.25), and grouping terms we obtain the following relation between the amplitudes:

$$(\psi(Q'|P) - \psi(Q|P'))i(\sin k - \sin k') + \frac{U}{2}(\psi(Q|P) + \psi(Q|P')) = 0, \quad \text{(A.31)}$$

where the permutations are $P = (k, k')$ and $P' = (k', k)$. We obtain for the amplitude in the sector P':

$$\psi(Q|P') = \frac{-i(\sin k - \sin k')}{U/2 - i(\sin k - \sin k')}\psi(Q'|P) + \frac{-U/2}{U/2 - i(\sin k - \sin k')}\psi(Q|P). \quad \text{(A.32)}$$

Therefore, we can write for the reflection and transmission amplitudes

$$R(k,k') = \frac{U/2}{i(\sin k - \sin k') - U/2} \quad , \quad T(k,k') = \frac{i(\sin k - \sin k')}{i(\sin k - \sin k') - U/2},$$
$$\longrightarrow S^t(k,k') = \frac{\frac{U}{2}\hat{P} + i(\sin k - \sin k')}{i(\sin k - \sin k') - U/2}. \tag{A.33}$$

Appendix B

Continuum limit for the Hubbard model

The system of fermions interacting via a δ-function potential can be obtained from the Hubbard model taking the continuum limit. This limit corresponds to take the site separation $a \to 0$ and the filling $\nu \to 0$ while keeping the density finite.It is also called dilute limit. In this limit, the lattice site index i will be replaced by the space coordinate x. The number of particles in the system is conserved. In the Hubbard model we have

$$N = \sum_j c_j^\dagger c_j, \tag{B.1}$$

while in the continuum case, using the continuum operators for the creation and annihilation of fermions,

$$N = \int dx\ \Psi^\dagger(x)\Psi(x). \tag{B.2}$$

The conversion from sum to integral is done in the general way $\sum_j \longrightarrow \frac{1}{a}\int dx$ and it gives us the correct dimensionality of the operators,

$$c_j = \sqrt{a}\Psi(x). \tag{B.3}$$

In this limit, the length of the system is given by

$$L = aN_a. \tag{B.4}$$

We will see how we can convert the Hamiltonian of the Hubbard model

$$H_{\mathrm{HM}} = -t \sum_{\sigma=\uparrow,\downarrow;j=1}^{N_a} (c^\dagger_{\sigma,j} c_{\sigma,j+1} + c^\dagger_{\sigma,j+1} c_{\sigma,j}) + U \sum_{j=1}^{N_a} n_{j,\uparrow} n_{j,\downarrow} \tag{B.5}$$

into the one of electrons in the continuum

$$H_{\mathrm{continuum}} = \frac{\hbar^2}{2m} \left(-\sum_{i=1}^{N} \frac{\partial^2}{\partial x_i^2} + 2c \sum_{i<j} \delta(x_i - x_j) \right), \tag{B.6}$$

using the transformations (B.3).

We start by looking at the kinetic energy part, where we first rearrange the terms in the following way

$$\begin{aligned} H_k &= -t \sum_{\sigma,j} (c^\dagger_{\sigma,j} c_{\sigma,j+1} + c^\dagger_{\sigma,j+1} c_{\sigma,j}) = \\ &= -t \sum_{\sigma,j} (c^\dagger_{\sigma,j} c_{\sigma,j+1} + c^\dagger_{\sigma,j+1} c_{\sigma,j} + c^\dagger_{\sigma,j} c_{\sigma,j-1} + c^\dagger_{\sigma,j-1} c_{\sigma,j}) = \\ &= -t \sum_{\sigma,j} (c^\dagger_{\sigma,j} (c_{\sigma,j+1} + c_{\sigma,j-1}) + c_{\sigma,j} (c^\dagger_{\sigma,j+1} + c^\dagger_{\sigma,j-1})). \end{aligned} \tag{B.7}$$

Then we perform the transformations Eq. (B.3), for $c_{j\pm1}$ we have

$$c_{j\pm1} = \sqrt{a} \left(\Psi(x) \pm a\Psi'(x) + \frac{a^2}{2} \Psi''(x) \right), \tag{B.8}$$

and so the kinetic part of the Hamiltonian transforms

$$\begin{aligned} H_k &= -t \int \frac{dx}{a} \left(\Psi^\dagger_\sigma(x) \left(2\Psi_\sigma(x) + a^2 \Psi''_\sigma(x) \right) + \Psi_\sigma(x) \left(2\Psi^\dagger_\sigma(x) + a^2 \Psi''^\dagger_\sigma(x) \right) \right) a = \\ &= -4tN - ta^2 \int \Psi^\dagger_\sigma \frac{\partial^2}{\partial x^2} \Psi_\sigma dx. \end{aligned} \tag{B.9}$$

The first term is a constant and will be absorbed into the chemical potential, while the second term corresponds to the kinetic energy term in the Hamiltonian for the fermions in the continuum.

For the interaction part of the Hamiltonian, we have the following straightforward transformation:

$$\begin{aligned} H_{int} &= U \sum_j n_{j,\uparrow} n_{j,\downarrow} = U \sum_j c^\dagger_{j,\uparrow} c^\dagger_{j,\downarrow} c_{j,\downarrow} c_{j,\uparrow} = \\ &= Ua \int dx \Psi^\dagger_\uparrow(x) \Psi^\dagger_\downarrow(x) \Psi_\downarrow(x) \Psi_\uparrow(x) \end{aligned} \tag{B.10}$$

Comparing Eq. (B.9) and Eq. (B.10) to Eq. (B.6) we find the equivalences:

$$\begin{aligned} \frac{\hbar^2}{2m} &= ta^2, \\ \frac{c\hbar^2}{m} = g_{1\mathrm{D}} &= Ua. \end{aligned} \tag{B.11}$$

Appendix C

Local density approximation

In most experimental set-ups the system is confined in a spatially inhomogeneous trapping potential. If the system was exactly solvable in the homogeneous case, it would not in general be exactly solvable any more when trapped. In general, the homogeneous solution for a model is no longer valid when we consider the trapped configuration. However, normally the trapping potentials tend to be very shallow, such that the variation of the potential in space is smaller than the typical length of the system. In this case the system can be considered as being "locally uniform", and if its equation of state is known in the homogeneous configuration we can solve it for the trapped situation. In practical set-ups, when the trapping potential is normally approximated to a harmonic oscillator, $V_{\text{trap}}(\vec{r}) = \frac{1}{2}m\omega^2 r^2$, we want the size of the cloud to be much bigger than the harmonic oscillator length, $R \gg a_z$, implying that $E_F \gg \hbar\omega_z$ and $N \gg 1$.

Suppose that we have the expression of the energy of a system as a function of the total number of particles $E = E(N)$, or the density of particles $E = E(n)$, where $n = N/L$ and L is the size of the system. The energy density is $\epsilon(N) = E(N)/N$ and the chemical potential is defined by

$$\mu(n) = \frac{\partial}{\partial N}E(N) = \frac{\partial}{\partial N}\left(N\epsilon(N)\right) = \left(1 + N\frac{\partial}{\partial N}\right)\epsilon(N) = \left(1 + n\frac{\partial}{\partial n}\right)\epsilon(n). \tag{C.1}$$

The equation $\mu = \mu(n)$ (Eq. C.1) is the equation of state of the system.

Let us suppose now that we have a slowly varying external potential $V(r)$, and we want to minimize the energy of the system

$$E(n) = \int (nV(r) + n\epsilon(n) - \mu_o n)\, dr, \tag{C.2}$$

where the density now depends on the coordinates, $n = n(r)$, and μ_o is a Lagrangian multiplier used to fix the total number of particles, $\int n(r)\ dr = N$. Minimizing the energy we get the relation

$$\frac{\delta E}{\delta n} = 0 \Rightarrow \mu(n) = \mu_o - V(r), \tag{C.3}$$

which is physically equivalent to impose a chemical potential that depends on the position, i.e. a local chemical potential $\mu_o - V(r)$.

Take the harmonic potential $V(r) = \frac{1}{2}m\omega^2 r^2$ as an example. The chemical potential in this case reads

$$\mu(n) = \mu_o - \frac{1}{2}m\omega^2 r^2 = \mu_o \left(1 - \frac{r^2}{R^2}\right), \tag{C.4}$$

where $R^2 = 2\mu_o/m\omega^2$. Inverting equation (C.4) the density and the total number of particles can be written as

$$n(r) = \mu^{-1}\left(\mu_o\left(1 - \frac{r^2}{R^2}\right)\right) \rightarrow N = \int n(r)dr = R\int_{-1}^{1} \mu^{-1}(\mu_o(1-\xi^2))d\xi, \tag{C.5}$$

where $\xi = r/R$, and we find an equation for μ_o:

$$N\sqrt{\frac{m}{2}}\omega = \mu_o^{1/2}\int_{-1}^{1} \mu^{-1}(\mu_o(1-\xi^2))d\xi \equiv f(\mu_o). \tag{C.6}$$

Solving $f(\mu_o)$ for a given N we find the chemical potential for the system in the inhomogeneous configuration.

For a system with two different components the situation is a bit more complicated. The total energy and the density depend now on the number of particles in each component: $E(N_1, N_2) = (N_1 + N_2)\ \epsilon(n_1, n_2)$; and so we have two equations

of state, one for each component:

$$\mu_1 = \frac{\partial E(N_1,N_2)}{\partial N_1} = \frac{\partial}{\partial N_1}[(N_1+N_2)\ \epsilon(N_1,N_2)] = \left(1 + n\frac{\partial}{\partial n_1}\right)\epsilon(n_1,n_2)$$
$$\mu_2 = \frac{\partial E(N_1,N_2)}{\partial N_2} = \frac{\partial}{\partial N_2}[(N_1+N_2)\ \epsilon(N_1,N_2)] = \left(1 + n\frac{\partial}{\partial n_2}\right)\epsilon(n_1,n_2). \quad \text{(C.7)}$$

Applying an external potential, that can interact differently with each of the components, the equations for the minimisation of the energy are ($i = (1,2)$):

$$\frac{\delta E(n_1,n_2)}{\delta n_i} = \frac{\delta}{\delta n_i}\int [n_1 V_1(r) + n_2 V_2(r) + (n_1+n_2)\ \epsilon(n_1,n_2) - \mu_1^o n_1 - \mu_2^o n_2]dr = 0. \quad \text{(C.8)}$$

We obtain here two "local chemical potentials", one for each component, but both of them depending on the densities of all the components:

$$\mu_1(n_1,n_2) = \mu_1^o - V_1(r) \qquad \text{and} \qquad \mu_2(n_1,n_2) = \mu_2^o - V_2(r). \quad \text{(C.9)}$$

We have thus in this case two radii R_1 and R_2, similar to Eq. (C.5), for each of the given components. Fixing the number of particles in each component we calculate the value of the two parameters μ_1^o and μ_2^o, in a similar way of that in equation (C.6):

$$N_1 = \int_{-R_1}^{R_1} n_1(r)dr \qquad \text{and} \qquad N_2 = \int_{-R_2}^{R_2} n_2(r)dr \quad \text{(C.10)}$$

Bibliography

[1] A.O. Gogolin, A.A. Nersesyan and A.M. Tsvelik, *Bosonisation and strongly correlated systems*, Cambridge University Press (1998).

[2] T. Giamarchi, "Quantum physics in one dimension", Oxford University Press (2003).

[3] Z. Phys. **71**, 205 (1931).

[4] S. White, Phys. Rev. Lett. **69**, 2863 (1992).

[5] U. Schollwöck, Rev. Mod. Phys **77**, 259 (2005).

[6] S. Biermann, A. Georges, T. Giamarchi, A. Lichtenstein, "Quasi-one-dimensional organic conductors: dimensional crossover and some puzzles", Proceedings of the NATO ASI "Field Theory of Strongly Correlated Fermions and Bosons in Low - Dimensional Disordered Systems", Windsor, August, 2001 (also preprint arXiv:cond-mat/0201542v1).

[7] T. Giamarchi, Chem. Rev. **104**, 5037 (2004).

[8] D. Jérome, Chem. Rev. **104**, 5565 (2004).

[9] S. Ijima, T. Ichihashi, Nature **363**, 603 (1993).

[10] D. S. Bethune, C. H. Klang, M. S. de Vries, G. Gorman, R. Savoy, J. Vazquez, R. Beyers, Nature **363**, 605 (1993).

[11] C. Dekker, Phys. Today, **52**, 22 (1999).

[12] C. W. J. Beenakker and H. von Houten, Solid State Physics **44**, 1 (1991).

[13] V.A. Yurovsky, M. Olshanii, D.S. Weiss, Advances in atomic, molecular, and optical physics **55**, Book Series: Advances in atomic, molecular, and optical physics, Pages: 61-138, (2008).

[14] B. Sutherland, *Beautiful models*, World Scientific Publishing Co., (2004).

[15] F. Calogero, O. Ragnisco and C. Marchioro, Lett. Nuovo Cimento **13**, 383 (1975).

[16] F. Calogero, Lett. Nuovo Cimento **13**, 411 (1975).

[17] F. Calogero J. Math. Phys. **10**, 2197 (1969).

[18] F. Calogero J. Math. Phys **10**, 2191 (1969).

[19] F. Calogero J. Math. Phys **12**, 419 (1971).

[20] C Marchioro and E Presutti Lett. Nuovo Cimento **4**, 488 1970.

[21] A.M. Perelomov Theor. Math. Phys. **6**, 263 1971.

[22] B. Surtherland Phys. Rev. A **4**, 2019 (1971).

[23] B. Sutherland J. Math. Phys **12**, 246 (1971).

[24] B. Sutherland J. Math. Phys. **12**, 251 (1971), Phys. Rev. A, **5** 1372 (1972).

[25] E.H. Lieb and W. Liniger Phys. Rev. **130**, 1605 (1963).

[26] McGuire J. Math. Phys. **5**, 622 (1964).

[27] D.E. Pritchard, Phys. Rev. Lett. **51**, 1336 (1983).

[28] H.A. Hänsel, J. Reichel, P. Hommelhoff and T.W. Hänsch, Phys. Rev. A **64**, 063607 (2001).

[29] R. Folman, P. Krueger, J. Schmiedmayer, J. Denschlag and C. Henkel, Adv. At. Mol. Opt. Phys. vol. **48**, Academic Press, New York, pp.263-356 (2002).

[30] M. Boyd, E.W. Streed, P. Medley, G.K. Campbell, J. Mun, W. Ketterle and D.E. Pritchard, Phys. Rev. A **76**, 043624 (2007).

[31] S. Burger, K. Bongs, S. Dettmer, W. Ertmer, K. Sengstock, A. Sanpera, G.V. Shlyapnikov and M. Lewenstein, Phys. Rev. Lett. **83**, 5198 (1999).

[32] L. Khaykovich, F. Schreck, G. Ferrari, T. Bourdel, J. Cubizolles, L.D. Carr, Y. Castin and C. Salomon, Science **296**, 1290 (2002).

[33] K.E. Strecker, G.B. Partridge, A.G. Tuscot and R.G. Hulet, Nature **417**, 150 (2002).

[34] F. Schreck, L. Khaykovich, K.L. Corwin, G. Ferrari, T. Bourdel, J. Cubizolles and C. Salomon Phys. Rev. Lett. **87**, 080403 (2001).

[35] S. Richard, F. Gerbier, J.H. Thywissen, M. Hugbart, P. Bouyer and A. Aspect, Phys. Rev. Lett. **91**, 010405 (2003).

[36] D. Clement, A.F. Varon, M. Hugbart, J.A. Retter, P. Bouyer, L. Sanchez-Palencia, D.M. Gangardt, G.V. Shlyapnikov and A. Aspect Phys. Rev. Lett. **95**, 170409 (2005).

[37] M. Hugbart, J. A. Retter, F. Gerbier, A.F. Varon, S. Richard, J.H. Thywissen, D. Clement, P. Bouyer and A. Aspect, Eur. Phys. J. D **35**, 155 (2005).

[38] J. Esteve, J.-B. Trebbia, T. Schumm, A. Aspect, C.I. Westbrook, I. Bouchoule Phys. Rev. Lett. **96**, 130403 (2006).

[39] M. Greiner, I. Bloch, O. Mandel, T. W. Hï¿$\frac{1}{2}$nsch, and T. Esslinger, Phys. Rev. Lett. **87**, 160405 (2001).

[40] M. Greiner, I. Bloch, O. Mandel, T.W. Hänsch and T. Esslinger, Phys. Rev. Lett. **87** 160405 (2001).

[41] T. Kinoshita, T. Wenger and D. S. Weiss, Phys. Rev. Lett. **95**, 190406 (2005).

[42] B.L. Tolra, K.M. O'Hara, J.H. Huckans, W.D. Phillips, S.L. Rolston and J.V. Porto, Phys. Rev. Lett **92**, 190401 (2004).

[43] B. Paredes, A. Widera, V. Murg, O. Mandel, S. Fölling, I. Cirac, G. V. Shlyapnikov, T. W. Hänsch and I. Bloch, Nature **429**, 277, (2004).

[44] T. Kinoshita, T. Wenger and D. S. Weiss, Science **305**, 1125 (2004).

[45] C.D. Fertig, K.M. O'Hara, J.H. Huckans, S.L. Rolston, W.D. Phillips and J.V. Porto, Phys. Rev. Lett. **94**, 120403 (2005).

[46] H. Moritz, T. Stöferle, K. Günter, M. Köhl and T. Esslinger, Phys. Rev. Lett. **94**, 210401 (2005).

[47] K. Gunter, T. Stoferle, H. Moritz, M. Kohl and T. Esslinger, Phys. Rev. Lett. **95**, 230401 (2005).

[48] T. Kinoshita, T. Wenger and D. S. Weiss, Nature **440**, 900 (2006).

[49] M. Olshanii Phys. Rev. Lett. **81**, 938 (1998).

[50] H. Feshbach, Ann. Phys. **5**, 357 (1958).

[51] U. Fano, Phys. Rev. **124**, 1866 (1961).

[52] S. Inouye, M. R. Andrews, J. Stenger, H.-J. Miesner, D. M. Stamper-Kurn and W. Ketterle, Nature (London) **392**, 151 (1998).

[53] S. L. Cornish, N. R. Claussen, J. L. Roberts, E. A. Cornell and C. E. Wieman, Phys. Rev. Lett. **85**, 1795 (2000).

[54] T. Weber, J. Herbig, M. Mark, H.-C. Nägerl and R. Grimm, Science **299**, 232 (2003).

[55] M. Colomé-Tatché, Phys. Rev. A **78**, 033612 (2008).

[56] T. Bergeman, M. G. Moore and M. Olshanii, Phys. Rev. Lett. **91**, 163201 (2003).

[57] F.D.M. Haldane, J. Phys. C: Solid State Phys. **14**, 2585 (1981).

[58] O.M. Auslaender, H. Steinberg, A. Yacoby, Y Tserkovnyak, B.I Halperin, K.W. Baldwin, L.N. Pfeiffer and K.W. West Sicence **308**, 88 (2005).

[59] A. Recati, P.O Fedichev, W. Zwerger, J. van Delft and P. Zoller, Phys. Rev. Lett. **94**, 040404, (2003).

[60] C. Kollath, U. Schollwöck and W. Zwerger, Phys. Rev. Lett. **95** (2005).

[61] A. Luther and V. J. Emery, Phys. Rev. Lett. **33**, 589 (1974).

[62] M. W. Zwierlein, C. A. Stan, C. H. Schunck, S. M. F. Raupach, S. Gupta, Z. Hadzibabic and W. Ketterle, Phys. Rev. Lett. **91**, 250401 (2003).

[63] S. Jochim, M. Bartenstein, A. Altmeyer, G. Hendl, S. Riedl, C. Chin, J. Hecker Denschlag and R. Grimm, Science **302**, 2101 (2003).

[64] C. A. Regal, C. Ticknor, J. L. Bohn and D. S. Jin, Nature **424**, 47 (2003); C. Chin, A. J. Kerman, V. Vuletić and S. Chu, Phys. Rev. Lett. **90**, 033201 (2003).

[65] K. E. Strecker, G. B. Partridge, and R. G. Hulet, Phys. Rev. Lett. **91**, 080406 (2003).

[66] J. Cubizolles, T. Bourdel, S. J. J. M. F. Kokkelmans, G. V. Shlyapnikov and C. Salomon, Phys. Rev. Lett. **91**, 240401 (2003).

[67] J. N. Fuchs, A. Recati and W. Zwerger, Phys. Rev. Lett. **93**, 090408 (2004).

[68] I.V. Tokatly, Phys. Rev. Lett. **93**, 090405 (2004).

[69] D. S. Petrov and G. V. Shlyapnikov, Phys. Rev. A **64**, 012706 (2001).

[70] C. A. Regal, C. Ticknor, J. L. Bohn and D. S. Jin, Nature **424**, 47 (2003).

[71] M. Takahashi, Prog. Theor. Phys. **46**, No 5, 1388 (1971).

[72] G. Orso, Phys. Rev. Lett. **98**, 070402 (2007)

[73] Hui Hu, Xia-Ji Liu, and Peter D. Drummond, Phys. Rev. Lett. **98**, 070403 (2007).

[74] A.M. Clogston, 1962, Phys. Rev. Lett. **9**, 266.

[75] B.S. Chandrasekhar, Appl. Phys. Lett. **1**, 7 (1962).

[76] P. Fulde and R. A. Ferrel, Phys. Rev. **135**, A550 (1964).

[77] A. I. Larkin and Y. N. Ovchinnikov, Zh. Eks. Teor. Fiz. **47**, 1136 (1964) [Sov. Phys. JETP **20**, 762 (1965)].

[78] C.N. Yang, Phys. Rev. Lett. **19**, 1312 (1967).

[79] J. M. McGuire, J. Math. Phys. 6, 432 (1965).

[80] M. Flicker and E.H. Lieb, Phys. Rev. **161**, 179 (1967).

[81] B. Sutherland, Phys. Rev. B, **12**, 3795 (1975).

[82] M. Amoruso, I. Meccoli, A. Minguzzi and M.P. Tosi, Eur. Phys. J. D **8**, 361 (1999).

[83] M. Girardeau, J. Math. Phys. **1**, 516 (1960).

[84] M.D. Girardeau and A. Minguzzi, Phys. Rev. Lett. **99**, 230402 (2007).

[85] B. DeMarco and D.S. Jin, Science **285**, 1703 (1999).

[86] S. R. Granade, M. E. Gehm, K. M. OH́ara and J. E. Thomas, Phys. Rev. Lett. **88** 120405 (2002).

[87] K. M. OH́ara, S. L. Hemmer, M. E. Gehm, S. R. Granade and J. E. Thomas, Science **298**, 2179 (2002).

[88] M. Takahashi, *Thermodynamics of one-dimensional solvable models* (Cambridge University Press, 1999).

[89] F. H. L. Essler, H. Frahm, F. Gohmann, A. Klumper and V. Korepin, *The One-Dimensional Hubbard Model* (Cambridge University Press, Cambridge, 2005).

[90] E. H. Lieb and F.Y. Wu, Phys. Rev. Lett. **20**, 1445 (1968).

[91] F. Woynarovich, J. Phys. C: Solid State Phys., **16** 6593 (1983).

[92] V. Ya. Krivnov and A. A. Ovchinnikov, Sov. Phys. JETP **40**, 781 (1974).

[93] A. I. Larkin and J. Sak, Phys. Rev. Lett. **39**, 1025 (1977).

[94] A. A. Belavin, A. M. Polyakov and A. B. Zamolodchikov, Nuclear Physics B **241**, 333 (1984).

[95] J. L. Cardy, J. Phys. A: Math. Gen. **17**, L385 (1984).

[96] H. W. J. Blöte, J. L. Cardy, M. P. Nightingale, Phys. Rev. Lett **56**, 742 (1986).

[97] I. Affleck, Phys. Rev. Lett. **56**, 746 (1986).

[98] P. Di Francesco, Pierre Mathieu and D. Sénéchal "Conformal Field Theory", Springer (1996).

[99] F. Woynarovich and H.-P. Eckle , J. Phys. A: Math. Gen. **20**, L443 (1987).

[100] F. Woynarovich, J. Phys. A: Math. Gen.. **22**, 4243 (1989).

[101] H. J. de Vega and F. Woynarovich, Nuclear Physics B **251** [**FS13**], 439 (1985).

[102] M. Luscher, Commun. Math. Phys. **104**, 177 (1986).

[103] H. Frahm, V. E. Korepin, Phys. Rev. B **42** 10553 (1990).

[104] H. Frahm and M.P. Pfannmüller, Phys. Lett. A **204**, 347 (1995).

[105] L. Amico, A. Mastellone and A. Osterloh, Phys. Rev. B **73**, 214513 (2006).

[106] A.V. Chubukov, D.L. Maslov and F.H.L. Essler, arXiv:0801.1837.

[107] G. E. Astrakharchik, D. Blume, S. Giorgini and L. P. Pitaevskii, Phys. Rev. Lett. **93**, 050402 (2004).

[108] J. N. Fuchs, A. Recati and W. Zwerger, Phys. Rev. Lett. **93**, 090408 (2004).

[109] M. T. Batchelor, M. Bortz, X. W. Guan and N. Oelkers, J. Phys. Conf. Ser. **42**, 5 (2006).

[110] I. Bloch, J. Dalibard and W. Zwerger, Rev. Mod. Phys. **10** 885 (2008).

[111] S. Giorgini, L. P. Pitaevskii, and S. Stringari, Rev. Mod. Phys. (2008).

[112] I. Bloch, J. Dalibard, and W. Zwerger, Rev. Mod. Phys. **80**, 885 (2008).

[113] A. Görlitz, J. M. Vogels, A. E. Leanhardt, C. Raman, T. L. Gustavson, J. R. Abo-Shaeer, A. P. Chikkatur, S. Gupta, S. Inouye, T. Rosenband and W. Ketterle, Phys. Rev. Lett. **87**, 130402 (2001).

[114] K. E. Strecker, G. B. Partridge, A. G. Truscott and R. G. Hulet, Nature (London) **417**, 150 (2002).

[115] M. Köhl, T. Stöferle, H. Moritz, C. Schori and T. Esslinger, Appl. Phys. B **79**, 1009 (2004). B. L. Tolra, K. M. OH́ara, J. H. Huckans, W. D. Phillips, S. L. Rolston, and J. V. Porto, Phys. Rev. Lett. **92**, 190401 (2004)

[116] C. N. Yang, Phys. Rev. Lett. **19**, 1312 (1967).

[117] M. Gaudin, Phys. Lett. **24**A (1967) 55.

[118] V.E. Korepin, N.M. Bogoliubov and A.G. Izergin, "Quantum inverse scattering method and correlation functions", Cambridge University Press, (1993).

[119] A. B. Zamolodchikov and Al. B. Zamolodchikov, JETP Lett. **26**, 457 (1977).

[120] I.C. Percival, J. Phys. B: Atom. Molec. Phys. **6**, L229 (1973).

[121] M.V. Berry and M. Tabor, Proc. R. Soc. Lond. A **356**, 375 (1977).

[122] O. Bohigas, M. J. Giannoni, and C. Schmit, Phys. Rev. Lett. **52**, 1 (1984).

[123] C. F. Porter, "Statistical theory of spectra: fluctuations". New York, London: Academic Press (1965).

[124] M.V. Berry, J. Phys. A: Math. Gen. **10**, 2083 (1977).

[125] B.L. Altshuler, Y. Gefen, A. Kamenev and L. Levitov, Phys. Rev. Lett. **78**, 2803 (1997).

[126] M. Pascaud and G. Montambaux, Ann. Phys. **7**, 406, (1998)

[127] F. Chevy, V. Bretin, P. Rosenbusch, K. W. Madison, and J. Dalibard, Phys. Rev. Lett. **88**, 250402 (2002).

[128] E. B. Bogomolny, U. Gerland and C. Schmit, Phys. Rev. E **59**, R1315 (1999).

[129] E.H. Lieb, Phys. Rev. **130**, 1616 (1963).

[130] M. Wilkinson, Phys. Rev. A **41**, 4645 (1989).

[131] R. Kubo, Can. J. Phys. **34** 1274 (1956).

[132] The polynomial scaling is consistent with the results of A. Polkovnikov and V. Gritsev, Nature Physics **4**, 477 (2008).

[133] E. Farhi, J. Goldstone, S. Gutmann and M. Sipser, arXiv:quant-ph/0001106v1.